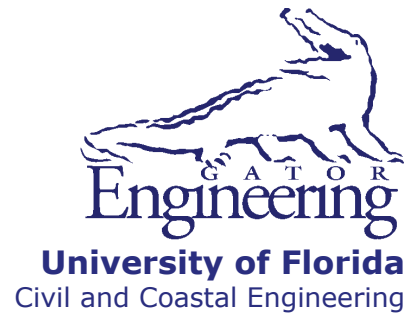


**UF**

**University of Florida  
Civil and Coastal Engineering**



---

**Final Report**

**December 2009**

**DETERMINATION OF SERVICE  
STRESSES IN PRETENSIONED  
BEAMS**

*Principal investigator:*  
H. R. Hamilton

*Research assistant:*  
Christina O'Neill

---

Department of Civil and Coastal Engineering  
University of Florida  
P.O. Box 116580  
Gainesville, Florida 32611

**Sponsor:**  
Florida Department of Transportation (FDOT)  
Marcus H. Ansley, P.E. – Project Manager

**Contract:**  
UF Project No. 00066037  
FDOT Contract No. BD 545-78

## **DISCLAIMER**

The opinions, findings, and conclusions expressed in this publication are those of the authors and not necessarily those of the State of Florida Department of Transportation.

1. Report No.		2. Government Accession No.		3. Recipient's Catalog No.	
4. Title and Subtitle Determination of Service Stresses in Pretensioned Beams			5. Report Date December 2009		
			6. Performing Organization Code		
7. Author(s) O'Neill, C. M. and Hamilton, H. R.			8. Performing Organization Report No. 00063967		
9. Performing Organization Name and Address University of Florida Department of Civil & Coastal Engineering P.O. Box 116580 Gainesville, FL 32611-6580			10. Work Unit No. (TRAIS)		
			11. Contract or Grant No. BD 545-78		
12. Sponsoring Agency Name and Address Florida Department of Transportation Research Management Center 605 Suwannee Street, MS 30 Tallahassee, FL 32399-0450			13. Type of Report and Period Covered Final Report 3/26/07-12/31/09		
			14. Sponsoring Agency Code		
15. Supplementary Notes					
16. Abstract <p>This report presents research on the evaluation of service flexural stresses and cracking moment in prestressed concrete members and on the minimum reinforcement requirements that are currently controlled by the flexural cracking moment. In prestressed concrete girders, the cracking moment changes when prestressing steel quantities are adjusted. If bonded prestressing steel is considered to contribute to the minimum reinforcement, then a single minimum reinforcement quantity is not possible. Furthermore, as bonded prestressing steel quantities are increased to satisfy the minimum reinforcement, the minimum steel requirement increases proportionately. A parametric study was conducted on hollow core, Florida bulb tee, and segmental box girders to evaluate the current minimum steel provisions. New minimum reinforcement provisions were then derived based on recommendations by Leonhardt 1964. These reinforcement provisions were then compared to the existing American Concrete Institute (ACI) 318 and American Association of State Highway and Transportation Officials (AASHTO) provisions using the sections from the parametric study.</p> <p>Ten precast, pretensioned pile cut offs from an FDOT construction project were salvaged and tested to determine cracking moment and to evaluate cracking behavior. Half of the piles were loaded monotonically to cracking and half were loaded cyclically to cracking. Cyclic loading was used in conjunction with AE monitoring and strain gage data to determine the initiation of microcracking. Structural cracking was determined using visual identification combined with interpolation from the load deflection plot.</p> <p>Six precast, pretensioned I-girders were also constructed and tested cyclically to determine cracking moment and evaluate cracking behavior. As both the piles and girders were loaded, microcracking and structural cracking were found to occur at lower stresses than would be calculated from the measured modulus of rupture and precompression. The stress range between the initiation of microcracking and the formation of a structural crack was found to increase with the prestress level. The current AASHTO provisions limiting tensile stress in harsh environments appear to be adequate in light of the girder test results.</p>					
G17. Key Word prestressed concrete, service stresses, cracking moment, minimum reinforcement, microcracking			18. Distribution Statement No restrictions. This document is available to the public through the National Technical Information Service, Springfield, VA, 22161		
19. Security Classif. (of this report) Unclassified		20. Security Classif. (of this page) Unclassified		21. No. of Pages 102	22. Price

## **ACKNOWLEDGMENTS**

The experimental research reported herein was conducted at the Florida Department of Transportation (FDOT) Structures Research Center. The authors thank the project manager, Marcus Ansley for his technical support and suggestions during the course of this project. We also acknowledge and thank the Structures Research Center staff including David Allen, Steven Eudy, Anthony Hobbs, William Potter, Paul Tighe, David Wagner, and Chris Weigly for their outstanding efforts in testing. The authors would also like to thank the FDOT State Materials Office and Charles Ishee and Richard Delorenzo for their support in materials testing.

Thanks are also offered to the staff and construction crew at Dura-stress as well as the FDOT quality control staff for helping to make the girder design and construction go as smoothly and efficiently as possible.

## EXECUTIVE SUMMARY

American Association of State Highway and Transportation Officials (AASHTO) LRFD Bridge Design Specification requires that the service level concrete stresses be used to determine minimum reinforcement requirements and to limit tensile stresses in harsh service conditions. This report presents research on the evaluation of service flexural stresses and cracking moment in prestressed concrete members and on the minimum reinforcement requirements that are currently controlled by the flexural cracking moment.

In prestressed concrete girders, the cracking moment changes when prestressing steel quantities are adjusted. If bonded prestressing steel is considered to contribute to the minimum reinforcement, then a single minimum reinforcement quantity is not possible. Furthermore, as bonded prestressing steel quantities are increased to satisfy the minimum reinforcement, the minimum steel requirement increases proportionately. A parametric study was conducted on hollow core, Florida bulb tee, and segmental box girders to evaluate the current minimum steel provisions. New minimum reinforcement provisions were then derived based on recommendations by Leonhardt 1964. These reinforcement provisions were then compared to the existing American Concrete Institute (ACI) 318 and AASHTO provisions using the sections from the parametric study.

Ten precast, pretensioned pile cut offs from an FDOT construction project were salvaged and tested to determine cracking moment and to evaluate cracking behavior. Half of the piles were loaded monotonically to cracking and half were loaded cyclically to cracking. Cyclic loading was used in conjunction with AE monitoring and strain gage data to determine the initiation of microcracking. Structural cracking was determined using visual identification combined with interpolation from the load deflection plot. Six precast, pretensioned I-girders were also constructed and tested cyclically to determine cracking moment and evaluate cracking behavior. As both the piles and girders were loaded, microcracking and structural cracking was found to occur at lower stresses than would be calculated from the measured modulus of rupture and precompression. The stress range between the initiation of microcracking and the formation of a structural crack was found to increase with the prestress level. The current AASHTO provisions limiting tensile stress in harsh environments appear to be adequate in light of the girder test results.

# TABLE OF CONTENTS

<b>1</b>	<b>INTRODUCTION.....</b>	<b>1</b>
<b>2</b>	<b>RESEARCH OBJECTIVES AND REPORT ORGANIZATION .....</b>	<b>2</b>
<b>3</b>	<b>LITERATURE REVIEW.....</b>	<b>3</b>
3.1	CONCRETE IN TENSION.....	3
3.2	FLEXURAL TENSION.....	5
3.3	PRESTRESSED CONCRETE AND MICROCRACKING.....	7
3.4	ACOUSTIC EMISSION (AE) .....	8
<b>4</b>	<b>MINIMUM REINFORCEMENT REQUIREMENTS: EXISTING AND PROPOSED .....</b>	<b>12</b>
4.1	HISTORICAL PERSPECTIVE.....	12
4.2	CURRENT AASHTO PROVISIONS.....	14
4.3	CURRENT ACI PROVISIONS .....	16
4.4	PARAMETRIC STUDY .....	16
4.5	PROPOSED PROVISIONS .....	18
4.6	COMPARISON BETWEEN PROPOSED AND CURRENT PROVISIONS.....	22
<b>5</b>	<b>INVERTED TEE TESTS .....</b>	<b>26</b>
5.1	DESIGN.....	26
5.2	CONSTRUCTION AND MATERIAL PROPERTIES .....	28
5.3	TEST SETUP AND PROCEDURES .....	29
5.4	INSTRUMENTATION .....	31
5.5	RESULTS AND DISCUSSION.....	31
5.6	EFFECTIVE PRESTRESS .....	33
5.7	STRAIN AND AE RESULTS .....	34
5.8	CRACKING MOMENT .....	35
<b>6</b>	<b>PILE TESTS.....</b>	<b>37</b>
6.1	DESIGN.....	37
6.2	CONSTRUCTION AND MATERIAL PROPERTIES .....	38
6.3	TEST SETUP AND PROCEDURES .....	39
6.4	INSTRUMENTATION .....	40
6.5	RESULTS AND DISCUSSION.....	41
6.6	EFFECTIVE PRESTRESS .....	43
6.7	STRAIN AND AE RESULTS .....	44
<b>7</b>	<b>PRETENSIONED GIRDER TESTS.....</b>	<b>46</b>
7.1	DESIGN.....	46
7.2	CONSTRUCTION AND MATERIAL PROPERTIES .....	47
7.3	TEST SETUP AND PROCEDURES .....	52
7.4	INSTRUMENTATION .....	53
7.5	RESULTS AND DISCUSSION.....	56
7.6	EFFECTIVE PRESTRESS .....	58
7.7	STRAIN AND AE RESULTS .....	61
<b>8</b>	<b>MICROCRACK ACCUMULATION .....</b>	<b>63</b>
<b>9</b>	<b>SUMMARY AND CONCLUSIONS.....</b>	<b>73</b>
<b>10</b>	<b>RECOMMENDATIONS.....</b>	<b>75</b>
<b>11</b>	<b>FUTURE RESEARCH.....</b>	<b>77</b>
<b>12</b>	<b>REFERENCES.....</b>	<b>78</b>
	<b>APPENDIX A – INVERTED TEE DATA.....</b>	<b>81</b>
	<b>APPENDIX B – PILE DATA .....</b>	<b>84</b>
	<b>APPENDIX C – GIRDER DATA.....</b>	<b>89</b>
	<b>APPENDIX D – ACCUMULATED DAMAGE ANALYSIS.....</b>	<b>98</b>

## LIST OF FIGURES

FIGURE 1. COMPLETE LOAD STRAIN CURVE FOR CONCRETE (EVANS AND MARATHE 1968).	4
FIGURE 2. STRAIN GAGE BEHAVIOR ON A DIRECT TENSION SPECIMEN (GUO AND ZHANG 1987).	5
FIGURE 3. LOAD STRAIN RELATIONSHIP ON MODULUS OF RUPTURE BEAM TESTS (KAPLAN 1963).	6
FIGURE 4. EFFECT OF COARSE AGGREGATE VOLUME ON MICROCRACKING AND ULTIMATE STRENGTH OF CONCRETE IN FLEXURAL TENSION (KAPLAN 1963)	7
FIGURE 5. FLEXURAL TENSILE BEHAVIOR OF PRESTRESSED CONCRETE AS POSITED BY ABELS AND HU 1971	8
FIGURE 6. WAVEFORM GENERATED BY A SENSOR HIT	9
FIGURE 7. PLOT ILLUSTRATING CYCLIC LOADING AND BREAKDOWN OF THE KAISER EFFECT	10
FIGURE 8. RESULTS FROM PARAMETRIC STUDY	18
FIGURE 9. STRESS STATE OF SECTION AT DECOMPRESSION	19
FIGURE 10. COMPARISON OF PROPOSED MINIMUM REINFORCEMENT REQUIREMENT FOR FBT	23
FIGURE 11. COMPARISON OF PROPOSED AND CURRENT MINIMUM REQUIREMENT FOR HC	24
FIGURE 12. COMPARISON OF PROPOSED AND CURRENT MINIMUM REQUIREMENT FOR SB UNDER NEGATIVE BENDING	24
FIGURE 13. CROSS SECTION DIMENSIONS FOR INVERTED TEES	27
FIGURE 14. PRESTRESSED STEEL LAYOUT FOR INVERTED TEES	27
FIGURE 15. PRESTRESSING STRAND AND REINFORCEMENT CAGE DURING FORM PLACEMENT. CASTING BED FOR INVERTED TEES	28
FIGURE 16. MONOSTRAND JACK USED TO POST-TENSION ITO	29
FIGURE 17. LOAD CELL TO VERIFY APPLIED PRESSURE	29
FIGURE 18. ANCHORAGES FOR ITO (A) LIVE END (B) DEAD END	29
FIGURE 19. TEST SETUP FOR INVERTED TEE TEST.	30
FIGURE 20. GAGES PLACED ADJACENT TO FIRST VISIBLE CRACK	30
FIGURE 21. LAYOUT OF STRAIN GAGES AND AE SENSORS	31
FIGURE 22. LOAD-DEFLECTION OF ITS FOR INITIAL AND FINAL LOADINGS	32
FIGURE 23. FAILURE OF THE COMPRESSION ZONE FOR ITS	32
FIGURE 24. LOAD-DEFLECTION OF ITO FOR INITIAL AND FINAL LOADINGS	33
FIGURE 25. STRAIN/LOAD DATA FROM GAGES PLACED ADJACENT TO FIRST VISIBLE CRACK	34
FIGURE 26. AE AND STRAIN RESULTS FOR ITS	35
FIGURE 27. AE AND STRAIN RESULTS FOR ITO	35
FIGURE 28. CROSS SECTION OF PILES	38
FIGURE 29. EVIDENCE OF PILE DAMAGE A)END VIEW B)SIDE VIEW	39
FIGURE 30. TEST SETUP FOR PILE	40
FIGURE 31. STRAIN GAGE AND SENSOR LAYOUT AT MIDSPAN ALONG THE A) BOTTOM OF THE PILE B) TOP OF THE PILE AND C) ELEVATION OF THE PILE.	41

FIGURE 32. PHOTOGRAPHS OF STRAIN GAGE AND SENSOR LAYOUT AT MIDSPAN ALONG THE A) BOTTOM OF THE PILE B) TOP OF THE PILE AND C) ELEVATION OF THE PILE.....	41
FIGURE 33. TYPICAL LOAD-DEFLECTION BEHAVIOR OF PILES LOADED MONOTONICALLY.....	42
FIGURE 34. TYPICAL LOAD-DEFLECTION BEHAVIOR OF PILES LOADED CYCLICALLY.....	42
FIGURE 35. MEASURED CRACKING MOMENT FROM LOAD-DEFLECTION DATA.....	43
FIGURE 36. MEASURED PERCENT PRESTRESS LOSS.....	44
FIGURE 37. GAGE AND SENSORS UTILIZED FOR DATA ANALYSIS.....	45
FIGURE 38. FELICITY EFFECT AND DISTRIBUTED MICROCRACKING IN SPECIMEN MET.....	45
FIGURE 39. CROSS SECTION DIMENSIONS OF ALL TEST GIRDERS.....	47
FIGURE 40. STRAND LAYOUTS FOR GIRDERS CONTAINING 0.5-IN. AND 0.6-IN STRAND.....	47
FIGURE 41. GIRDER CONSTRUCTION.....	48
FIGURE 42. DECK DIMENSIONS AND REINFORCEMENT LAYOUT.....	50
FIGURE 43. BRIDGE DECK REINFORCEMENT PRIOR TO CASTING.....	50
FIGURE 44. DECK CONSTRUCTION A) STEEL FORMS, AND B) WOOD BULKHEAD.....	51
FIGURE 45. DECK CONCRETE PLACEMENT AND VIBRATION.....	51
FIGURE 46. FINISHED GIRDER SPECIMENS READY FOR TESTING.....	52
FIGURE 47. PRETENSIONED GIRDERS TEST SETUP.....	53
FIGURE 48. CENTROID OF PRESTRESSING STEEL AND CORRESPONDING VWSG SETUP.....	54
FIGURE 49. VWSG PLACEMENT SETUP.....	54
FIGURE 50. VWSG INSTALLATION AT MIDSPAN (ARROW) OF GIRDER.....	54
FIGURE 51. VWSG CABLE COIL AT MIDSPAN.....	55
FIGURE 52. VWSG A) READOUT BOX B) DATA LOGGER.....	55
FIGURE 53. STRAIN GAGE AND AE SENSOR LAYOUT ALONG GIRDER BOTTOM.....	56
FIGURE 54. TYPICAL LOAD-DEFLECTION BEHAVIOR (B5S).....	56
FIGURE 55. TYPICAL LOAD-DEFLECTION BEHAVIOR (B6S).....	57
FIGURE 56. MEASURED CRACKING MOMENT FROM LOAD-DEFLECTION DATA AND VISUAL DOCUMENTATION.....	58
FIGURE 57. VWSG READINGS DURING PRESTRESS TRANSFER TO GIRDERS PRESTRESSED WITH 0.6-IN. STRAND.....	59
FIGURE 58. MEASURED TOTAL PRESTRESS LOSS AS A PERCENTAGE OF THE INITIAL PRESTRESS.....	60
FIGURE 59. ESTIMATE LOSSES USING PCI METHOD.....	61
FIGURE 60. MICROSTRAIN AND AE ENERGY VS APPLIED LOAD FOR B5S.....	62
FIGURE 61. MICROSTRAIN AND AE ENERGY VS. APPLIED LOAD FOR B6S.....	62
FIGURE 62. PLOT TO SHOW HOW ONSET OF MATERIAL DAMAGE WAS DETERMINED (B5S).....	64
FIGURE 63. STRESS RANGE OF MATERIAL DAMAGE THROUGH STRUCTURAL CRACKING (B5S).....	66
FIGURE 64. STRESS RANGE OVER WHICH MICROCRACKING OCCURS PRIOR TO STRUCTURAL CRACKING.....	67
FIGURE 65. EFFECT OF STRAIN GRADIENT ON CRACKING MOMENT.....	71

## LIST OF TABLES

TABLE 1. SUMMARY OF CRACKING, CAPACITY, AND DUCTILITY RESULTS FOR IT TESTS. ....	36
TABLE 2. SUMMARY OF MATERIALS TESTING RESULTS .....	38
TABLE 3. CONSTRUCTION AND TESTING SCHEDULE. ....	48
TABLE 4. RESULTS FOR COMPRESSIVE STRENGTH AND MODULUS OF RUPTURE TESTS (PSI). ....	49
TABLE 5. MEASURED SHORT-TERM PRESTRESS LOSS FROM VW SG (% OF INITIAL PRESTRESS) .....	59
TABLE 6. RESULTS OF MICROCRACKING AND STRUCTURAL CRACKING ANALYSIS ON GIRDERS AND PILES ( $F_T/\sqrt{F'_c}$ (PSI)). ....	67
TABLE 7. COEFFICIENTS FOR MODULUS OF RUPTURE AND CYLINDER TESTS FROM GIRDER CONCRETE. ....	71

## 1 INTRODUCTION

Service level concrete stresses are an integral part of the American Association of State Highway and Transportation Officials AASHTO LRFD Bridge Design Specification (AASHTO 2007). Service stresses are typically checked to avoid overstressing the section during prestressing and to determine the classification of the member under service load conditions. In addition, tensile stresses are further limited for members placed in a harsh environment. These limits are based on the modulus of rupture of concrete, which is estimated from the specified compressive strength of the concrete. Concrete in tension can begin to crack at stresses well below those associated with the formation of a visible structural crack. As concrete hardens and cures, small microcracks form at the interface of the aggregate and paste. As the concrete is loaded, tensile stresses activate these microcracks at stresses below those associated with the macroscale cracking related to the modulus of rupture. If sufficiently widespread, this microcracking may impair the long-term durability of the concrete.

Service stress checks also include calculating the cracking moment based on the modulus of rupture. The flexural cracking moment must be calculated under service loads for three reasons. One is for use in determining effective moment of inertia for deflections. Another is to determine the minimum reinforcement requirements. The third is for use in calculating the concrete contribution to shear capacity in the simplified shear provisions.

Stresses and cracking moment are calculated based on the assumption of linear elastic tensile and compressive behavior of concrete. The tensile strength of concrete is based on the modulus of rupture equation, which relates the square root of the concrete compressive strength to the tensile strength. A better understanding of how the concrete parameters typically affect the cracking moment is needed. Furthermore, an understanding of the effect of other parameters such as the prestress level on the cracking moment is important to understanding service load behavior.

## **2 RESEARCH OBJECTIVES AND REPORT ORGANIZATION**

This research project had two major objectives. The first was to determine the cracking behavior in prestressed concrete girders at or near the calculated cracking moment. The second objective was to evaluate and recommend improvements in the current minimum reinforcement provisions. Chapter 3 covers literature relevant to the behavior of concrete in tension, microcracking and its effect on beam behavior, and acoustic emission (AE). Chapter 4 covers minimum reinforcement requirements including an historical perspective on the current code requirements. In addition an alternative method of calculating minimum reinforcement is derived that is valid for both prestressed and nonprestressed concrete and yet does not rely explicitly on the calculation of cracking moment. Inverted tee tests, which were used to evaluate cracking moment are presented in Chapter 5. Chapter 6 covers pretensioned pile cut-offs preserved from a recent construction project that were tested in flexure to evaluate microcracking behavior. Chapter 7 covers pretensioned girder tests also used to evaluate microcracking behavior. Finally the microcracking behavior is further analyzed and compiled in Chapter 8 followed by summary and conclusions in Chapter 9 and recommendations in Chapter 10.

### 3 LITERATURE REVIEW

#### 3.1 CONCRETE IN TENSION

Concrete is composed primarily of aggregate and portland cement paste sometimes supplemented with cementitious materials. This mixture is a highly heterogeneous combination that responds to tensile and compressive stress as a composite. Of particular concern for tensile stress, however, is the bond between the aggregate and paste at the interfacial transition zone (ITZ). ITZ refers to the weakened cement paste in the immediate vicinity of the coarse aggregate surface. This weakened layer is caused by the accumulation of free water at the surface of the aggregate before the paste hardens. In addition, drying shrinkage, carbonation shrinkage, and differential thermal movement may contribute to preexisting microcracks at the interface of the aggregate and paste (Hsu et al. 1963).

Smadi and Slate 1989 investigated the effect of short and long term loads on microcracking in normal and high-strength concrete by taking x-rays of slices of concrete specimens. The cracks were categorized into bond cracks, mortar cracks, and combined cracks. Bond cracks are cracks in the ITZ while mortar cracks occur in the paste. The combined cracks are defined as a combination connected bond cracks or mortar cracks, or both. This same categorization is also presented in (Carrasquillo et al. 1981 and Shah and Chandra 1968). Of interest from this study is the cracking that exists prior to application of stress. It was found that, during curing, preexisting cracks were exclusively interfacial bond (ITZ) cracks. The total crack lengths, however, were lower in high-strength concrete (8500-10,000psi) than they were in the normal strength concrete (5000-6000psi). Drying shrinkage cracking was measured at 30 and 60 days of drying. As with curing, the cracks were mostly interfacial bond cracks and occurred less frequently in high strength concrete than in normal strength concrete.

Sturman et al. 1964 also studied internal microcracking directly. They observed bond cracks at the interface between the coarse aggregate and mortar on thin slices from strained specimens using X-ray and microscope techniques. The cracks were thought to be partly due to the stress at the interface caused by changes in volume of the mortar. At stress levels of one-quarter to one-third of the ultimate strength, the bond cracks began to propagate and the stress-strain curve was observed to deviate from linear. Furthermore, applied stress levels between 70

and 90 percent of ultimate resulted in the onset of mortar cracks and bridging of the bond and mortar cracks.

Evans and Marathe 1968 conducted direct tension tests using a stiff testing machine so that the descending branch of the load strain curve could be captured (Figure 1). They found that microcracking initiated in the range of 90 to 140 microstrain at a stress of 68 to 89% of the ultimate strength. The researchers used a microscope to detect microcracking in the specimen during testing rather than relying on the proportionality of the load strain curve. Although, examination of the plots shown below indicate that the proportional limit has been exceeded in all three specimens prior to reaching the peak stress.

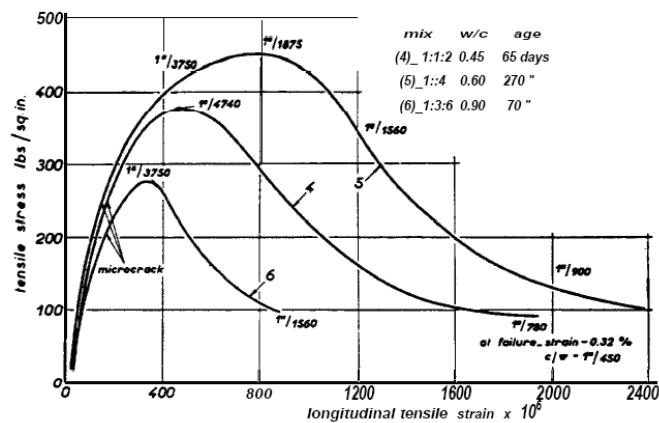


Figure 1. Complete load strain curve for concrete (Evans and Marathe 1968).

Guo and Zhang 1987 conducted direct tension testing to develop the full stress-deformation curve for concrete (Figure 2). The direct tension specimen was fitted with electrical resistance strain gages 40 mm in length. Although not noted by the original authors, the ascending branches of the curves indicate that the proportional limit was reached at approximately 60 microstrain. At this point the plots diverge, indicating the initiation of microcracking. The peak indicates the coalescence of a crack that passes through strain gage three. That strain gage continues to show increased strain as the specimen unloads. Gages 1 and 2, however, show decreasing strain indicating that the crack has formed away from the gages.

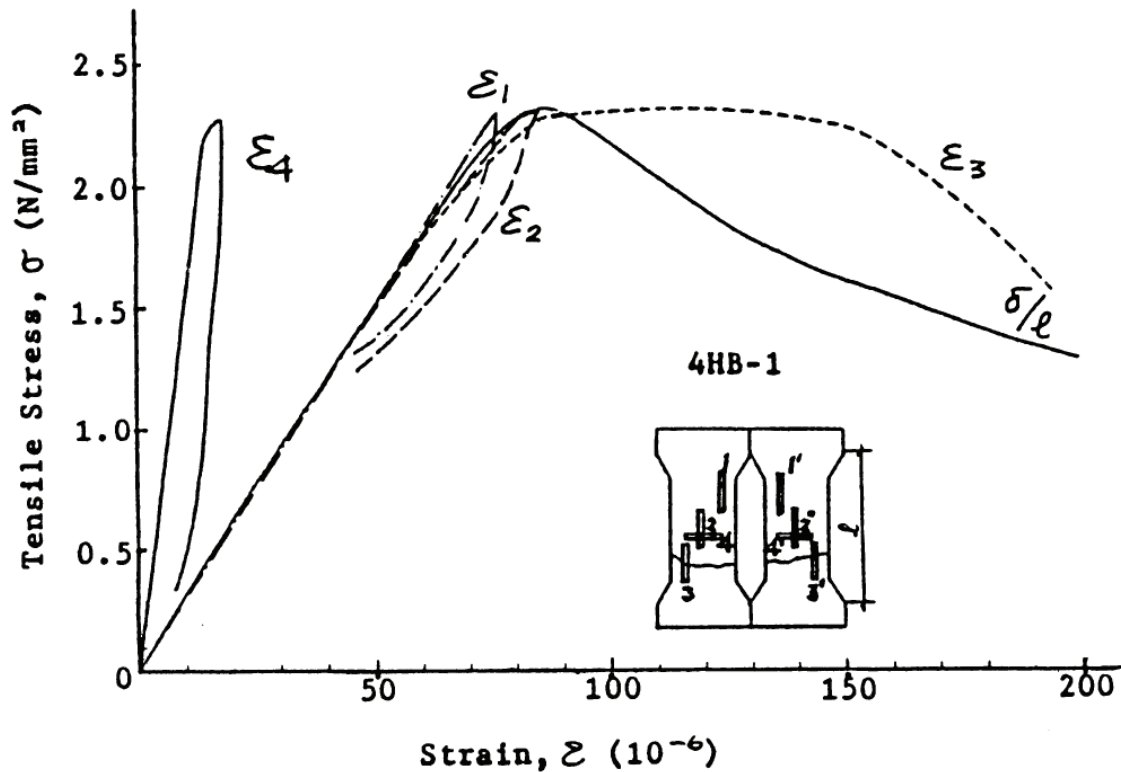


Figure 2. Strain gage behavior on a direct tension specimen (Guo and Zhang 1987).

### 3.2 FLEXURAL TENSION

Kaplan 1963 conducted flexure tests to determine the tensile strength of concrete with particular attention given to the initiation of cracking and to examine the effect of aggregate volume. It is indicated that by 1963, microcracking in concrete in tension and compression at loads less than ultimate was well established. He also indicates that initiation of microcracking is associated with the proportional limit of the load-strain measurements on beams in flexure. They conclude that, no matter the stress state, microcracking occurs at considerably less load than ultimate. Figure 3 shows the results of tests conducted on 6 x 6 x 20in. beams under four point bending. The plots are load-strain data from electrical resistance strain gages placed on the extreme tension fiber of the beam. The proportional limit of the two plots indicates that microcracking is occurring in the concrete prior to reaching the ultimate capacity.

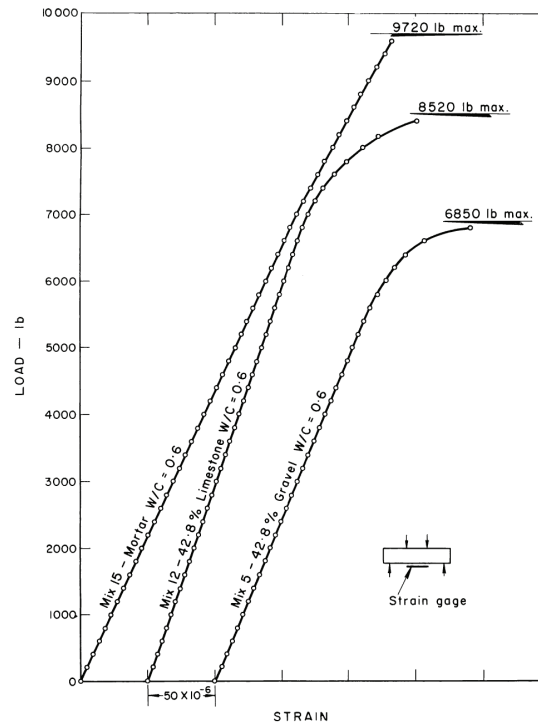


Figure 3. Load strain relationship on modulus of rupture beam tests (Kaplan 1963)

Tensile strains at cracking were found to be independent of aggregate type, but increased as the aggregate volume decreased. Figure 4 shows the variation in initiation of microcracking as determined by the end of the proportional limit of the load strain plot. In addition, the strain near the ultimate capacity is shown. For typical aggregate volumes (40 to 55%) the strain values were found to be from 110 to 85 microstrain for initiation of microcracking and approximately 160 microstrain near failure. Under direct tension, however, for the same coarse aggregate range, microcracking ranged from 55 to 40 microstrain with the associated ultimate strains from 95 to 75 microstrain. As expected, the concrete flexural tensile stress at ultimate, as calculated assuming linear elastic materials, varied with aggregate type and water/cement ratio suggesting that strain is the controlling factor in the concrete capacity rather than stress.

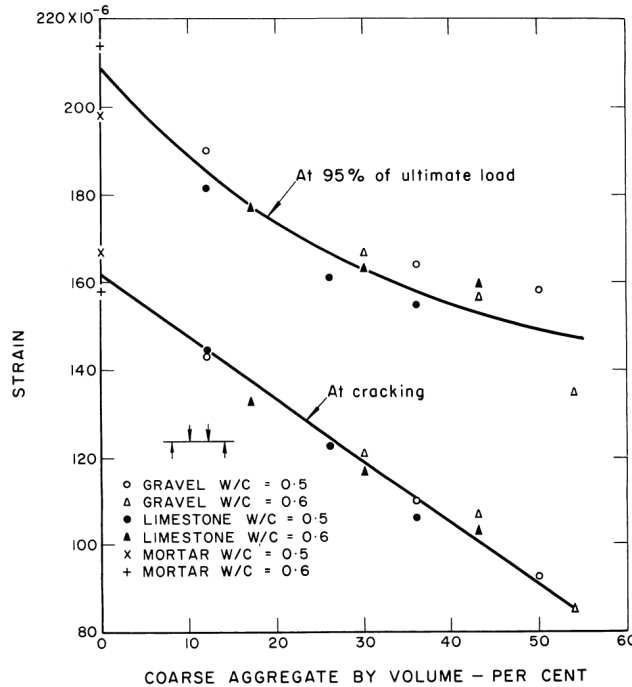


Figure 4. Effect of coarse aggregate volume on microcracking and ultimate strength of concrete in flexural tension (Kaplan 1963)

McNeely and Lash 1963 investigated the tensile strength of concrete using the modulus of rupture test on 3 x 3 x 14.5 in. beam specimens. They found that precompression values of 1000 and 2000 psi sustained for 7 and 28 days did not change the tensile strength of concrete but did find that higher loading rates increased the tensile capacity of the concrete.

### 3.3 PRESTRESSED CONCRETE AND MICROCRACKING

Abels and Hu 1971 suggested that microcracking occurs in reinforced and prestressed concrete beams prior to visible cracking (Figure 5). As the load is increased, the stress-deflection plot remains linear until microcracks develop. The departure from linear indicates that microcracking is forming in the extreme fiber in tension. To test their hypothesis, the researchers constructed small beams and used photoelastic coatings to detect microcracking.

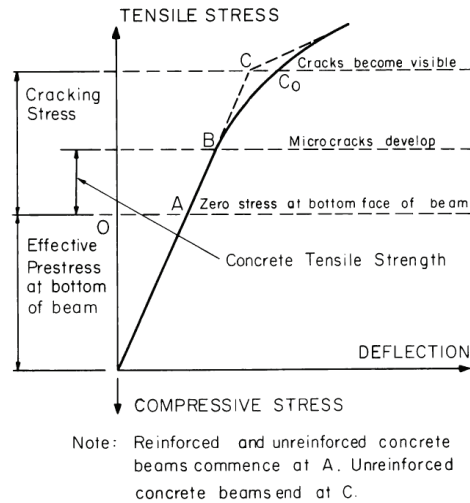


Figure 5. Flexural tensile behavior of prestressed concrete as posited by Abels and Hu 1971

### 3.4 ACOUSTIC EMISSION (AE)

When stress or deformation is applied to a material transient stress waves are typically generated which are termed acoustic emission (AE). A change of state of the material - such as a crack formation in concrete - is generally the cause of the energy release. The elastic wave travels through the material and can be detected by piezoelectric sensors mounted to the surface. These sensors generate an electrical signal (Figure 6) in response to the stress wave. Certain characteristics of the signal are used to distinguish the source of the emissions whether they are spurious signals (i.e. caused by friction) or credible signals (i.e. caused by crack progression or yielding). Characteristics commonly analyzed include amplitude, energy, duration, rise time, and count as detailed in the figure. A hit is considered to have occurred when the amplitude of the signal rises above a predetermined threshold. The threshold is set to eliminate noise caused by sources other than a structural defect, such as electrical interference.

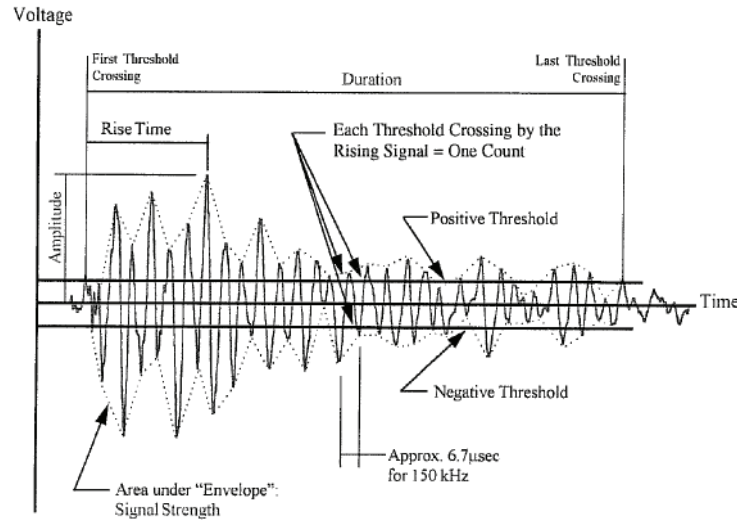


Figure 6. Waveform generated by a sensor hit

An event is defined as a local material change giving rise to AE (ASTM E-1316). It is distinct from a hit, which is simply the process of detecting and measuring an AE signal on a channel. To record events, hit data from at least two channels must be utilized. Interpolation or triangulation can be performed between multiple sensors to identify an event.

The Kaiser effect, which is generally observed in most materials using AE, can be used to evaluate damage. The ASTM definition of the Kaiser effect is “the absence of detectable AE at a fixed sensitivity level [threshold], until previous applied stress levels are exceeded,” (ASTM E1316 2009). Figure 7 illustrates this phenomenon in terms of the applied load and resulting cumulative event energy. In the first load cycle AE is detected and quantified as event energy. The plot shows the cumulative event energy over time, which also coincides with an increase in load. During the load hold and release, however, AE ceases. During the second load cycle, AE does not begin until the peak load reached in the first cycle is exceeded. As the load increases beyond this point, AE continues to accumulate. In some cases, the Kaiser effect can be used to determine the peak loads previously applied to the structure.

The Felicity Effect is the breakdown of the Kaiser Effect and is defined by ASTM as “the presence of AE, detectable at a fixed predetermined sensitivity level [threshold] at stress levels below those previous applied,” (ASTM E1316 2009). The Felicity Ratio is defined as the ratio between the load at the onset of AE during a reload and maximum load applied during the previous load cycle. Before the breakdown of the Kaiser Effect, this value is unity. As this ratio

becomes less than unity it is an indication structural damage has occurred. For example, during the third loading cycle AE event energy begins to accumulate at  $P_{begin}$  before the previous maximum load ( $P_{max}$ ) from the second load cycle. The ratio of  $P_{begin}$  to  $P_{max}$  is the Felicity Ratio.

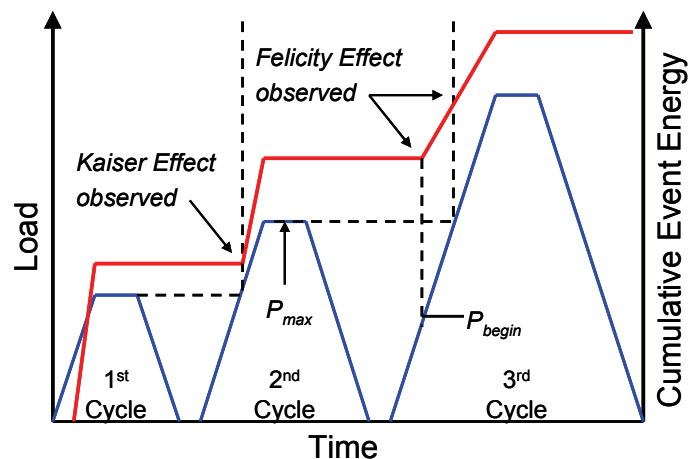


Figure 7. Plot illustrating cyclic loading and breakdown of the Kaiser Effect

Nielsen and Griffin 1977 were among the first to apply AE technology to concrete. Their focus was primarily on plain concrete. In these early tests, it was found that Kaiser Effect could be temporary in plain concrete (Nielsen and Griffin 1977). One possible explanation was that over time concrete experiences autogenous healing (the ability of cement to heal cracks in fractured concrete). More recent testing, however, has shown that the Kaiser Effect is present in both ordinary reinforced and prestressed concrete beams (Hearn and Shield 1997).

Oh et al. 2000 used AE to monitor concrete in flexure in an attempt to identify the characteristics of the AE feature data per the type of damage occurring in the section. Oh discusses the cracking mechanism in concrete and correlates the AE energy and duration data with particular percentages of ultimate load that are associated with different aspects of the cracking mechanism. At 30% of the ultimate load, deformation increases linearly when microcracks are forming randomly in a distributed manner. AE energy and duration data at 30% of ultimate was found to be relatively low and short compared to later results. At 50% of the ultimate load the quantity, length and width of microcracks within the ITZ increase. In addition, the microcracks were primarily bond cracks that had occurred along the boundary of the matrix and aggregate. At this state, AE energy and duration was observed to increase and was speculated to signal the slow development of bond cracks. Upon reaching 80% of the ultimate

load, bond cracks between the matrix and aggregate grew through the matrix. In addition, AE energy and duration greatly increased relative to the feature data from 50% of the ultimate load. At the ultimate load, cracks in the ITZ and matrix combine and the section fails when the crack reaches its critical length.

Labuz et al. 2001 used AE to map microcracking during load testing of modulus of rupture beams. The results indicated that the microcracking occurred progressively in a distributed manner.

Hearn and Shield 1997 applied AE to both reinforced and prestressed concrete beams under flexural monotonic and cyclic loading conditions. The reinforced concrete beams were 203 mm deep x 305 mm wide x 2.44 m long. The prestressed concrete beams were precast hollow core sections that were 203 mm deep x 610 mm wide x 3.66 m long. The beams were loaded at midspan cyclically with gradually increasing loads and a four channel AE system was used. They noted that the AE results did not follow the Kaiser effect in a strict sense. It was suggested that several cycles may have been needed to eliminate the AE from the lower load cycles. Because AE was detected at loads lower than the previous cycle, the Felicity ratio could be calculated. For the prestressed girders they found that the Felicity ratio decreased from 0.99 to approximately 0.46 as the load was decreased. One of the girders had a felicity ratio near 0.19 under the last load cycle.

Ridge and Ziehl 2006 found diminishing values of the Felicity Ratio as they applied cyclically increasing loads to strengthened reinforced concrete beams.

## 4 MINIMUM REINFORCEMENT REQUIREMENTS: EXISTING AND PROPOSED

### 4.1 HISTORICAL PERSPECTIVE

The earliest mention of minimum reinforcement found in the ACI code is in 1936 in which a minimum area of steel satisfying the following equation was required (ACI Committee 501 1936).

$$A_{s,\min} = 0.005b'd \quad \text{Equation 1}$$

where  $b'$  is the width of web in I- or T-shaped sections, and  $d$  is the distance from compression face of beam or slab to center of longitudinal tensile reinforcement. Slabs with uniform thickness were exempt from this requirement. ACI committee 323 published recommendations for design of prestressed concrete in 1958 (ACI-ASCE Committee 323 2004). In addition, the Bureau of Public Roads issued requirements for design of prestressed concrete bridges (Bureau of Public Roads 1954). Neither of these documents, however, contained minimum reinforcement requirements for prestressed concrete.

In 1963 the minimum reinforcement requirement for nonprestressed concrete was changed so that it was expressed in terms of reinforcement ratio,  $p$ , and was limited to no less than  $200/f_y$  (ACI 318-63 1963). If the area of reinforcement was 1/3 greater than required by analysis, however, then the limit was considered satisfied. This appears to be the first time that the basis of the minimum code provision (for nonprestressed concrete) was articulated in the commentary:

*Section 911(a) is concerned with beams, which for architectural or other reasons, are much larger in cross section than required by strength considerations. With very small reinforcement ratios the computed ultimate bending moment as [sic] a reinforced concrete section becomes less than that of the corresponding plain concrete section computed from its modulus of rupture. Failure in such a case is quite sudden.*

*To prevent such failure, there is required a minimum steel ratio,  $p = 200/f_y$ , which for 40,000 and 60,000 psi yield point steels becomes 0.5 percent and 0.33 percent respectively.*

*The  $200/f_y$  value was derived by equating the ultimate strength computed by the modulus of rupture of the plain concrete section to the ultimate strength computed as a reinforced section and solving for  $p$ . This minimum reinforcement must be provided wherever positive reinforcement is needed except where the reinforcement is one-third greater than required by analysis. This exception provides sufficient extra reinforcement for safety in large members where  $200 bd/f_y$  would be excessive.*

*In Section 911(b), the minimum reinforcement required for slabs is a little less than that required for beams, since an overload would be distributed laterally and a sudden failure would be less likely. The structural reinforcement should, however, be at least equal to the shrinkage and temperature reinforcement.*

A prestressed concrete design chapter was introduced in 1963 with separate requirements for minimum reinforcement. The minimum reinforcement (both prestressed and nonprestressed) were required to be adequate to develop an ultimate load capacity greater than 1.2 times the cracking load. The cracking load was to be based on a modulus of rupture of  $7.5\sqrt{f'_c}$  (psi). The commentary for this provision is as follows:

*No provision for minimum amount of tensile steel appeared in previous design recommendations in this country. The provision is a precaution against abrupt flexural failure resulting from rupture of the prestressing steel when ultimate capacity is reached immediately after cracking. The usual member requires considerable additional load beyond cracking to reach ultimate capacity. Thus, considerable deflection warns that the ultimate capacity is being approached. However, if ultimate capacity occurs shortly after cracking the warning deflection may not occur.*

Based on the behavior cited in this commentary section, it appears that minimum reinforcement was considered necessary for prestressed concrete for the same reasons it was considered necessary for nonprestressed concrete. The provisions for minimum reinforcement come from PCI Standard Building Code for Prestressed Concrete developed by TAC in 1959.

*Sec. 309(b) A minimum percentage of steel should be used in a member so that ultimate failure will not immediately occur at the instant of cracking of concrete.*

In 1983 (ACI 318-83 1986) an exclusion was added for flexural members with shear and flexural strength at least twice that required by specified load. The minimum requirements for nonprestressed concrete remained unchanged for this code cycle. The commentary indicates that this exclusion was added to avoid requirements for excessive reinforcement that might be needed to meet the requirement of 1.2 times the cracking load. This exception is similar to the 4/3 factor allowed for nonprestressed members where the minimum reinforcement provisions are considered satisfied when the reinforcement provides at least 1/3 more capacity than that required by the loads. The factor of 2 was derived by modifying the minimum tensile strength/minimum yield strength by the 4/3 ratio. For grade 60 steel this gives  $90/60 \times 4/3 = 2.0$ .

In 1995 (ACI 318-95 1995), the minimum reinforcement requirements for nonprestressed concrete were revised to include the specified concrete and reinforcement strengths. Equation 2 gives the typical requirement (with a lower limit of  $200b_wd/f_y$ ):

$$A_{s,\min} = \frac{3\sqrt{f'_c}}{f_y} b_w d \quad \text{Equation 2}$$

The commentary indicates that these provisions provide the same fundamental protection against sudden failure for large cross sections that are lightly reinforced. The new provisions were added to address concrete strengths higher than approximately 5000 psi. The prestressed minimum reinforcement requirement remained unchanged in this version of the code.

In 2008 (ACI 318-08 2008), another exception was added to the prestressed minimum provisions. The requirement for minimum reinforcement applies only to systems with bonded prestressed reinforcement. The commentary indicates that the transfer of force between the concrete and prestressing steel, and abrupt flexural failure immediately after cracking, does not occur when the prestressing steel is unbonded.

## 4.2 CURRENT AASHTO PROVISIONS

AASHTO LRFD Bridge Design Specifications have unified provisions that apply to both prestressed and nonprestressed construction. To meet the minimum reinforcement requirements, the flexural resistance ( $M_r$ ) must satisfy Equation 3 or Equation 4:

$$M_r \geq 1.2M_{cr} \quad \text{Equation 3}$$

$$M_r \geq 1.33M_u \quad \text{Equation 4}$$

where  $M_{cr}$  is the cracking moment and  $M_u$  is the factored moment from the applicable load combination. The cracking moment is to be determined using Equation 5:

$$M_{cr} = S_c (f_r + f_{cpe}) - M_{dnc} \left( \frac{S_c}{S_{nc}} - 1 \right) \geq S_c f_r \quad \text{Equation 5}$$

where:

$S_c$  is the section modulus for the extreme fiber of the composite section where tensile stress is caused by externally applied loads;

$f_r$  is the modulus of rupture of the concrete;

$f_{cpe}$  is the compressive stress in the concrete due to effective prestress forces only (after allowance for all prestress losses) at the extreme fiber of the section where tensile stress is caused by externally applied loads;

$S_{nc}$  is the section modulus for the extreme fiber of the monolithic or noncomposite section where tensile stress is caused by externally applied loads; and

$M_{dnc}$  is the total unfactored dead load moment acting on the monolithic or noncomposite section.

Where monolithic or noncomposite sections are designed to resist all loads, the designer is directed to substitute  $S_{nc}$  for  $S_c$  in the above equation for the calculation of  $M_{cr}$ . The modulus of rupture ( $f_r$ ) to be used in the above equation depends on the limit state being checked and the specified concrete strength. Literature is cited in which the modulus of rupture values typically range between  $7.5\sqrt{f'_c}$ (psi) and  $11.7\sqrt{f'_c}$ (psi) (ACI 318-92 1992; Walker and Bloem 1960; Khan et al. 1996). For determining minimum steel requirements the cracking moment is to be calculated using  $11.7\sqrt{f'_c}$ (psi). The Florida Department of Transportation (FDOT), however, allows the use of  $7.5\sqrt{f'_c}$ (psi) to calculate minimum reinforcement requirements (FDOT 2009). The rationale for using a higher modulus of rupture value for minimum steel requirements is that it is a strength limit state so the use of the upper bound value is justified and that the 20% margin

provided by Equation 3 could be lost by using a lower modulus of rupture value. These provisions are valid for specified concrete strengths up to 15,000 psi.

#### 4.3 CURRENT ACI PROVISIONS

ACI 318-08 2008 specifies the following for minimum reinforcement:

*Total amount of prestressed and nonprestressed reinforcement in members with bonded prestressed reinforcement shall be adequate to develop a factored load at least 1.2 times the cracking load computed on the basis of the modulus of rupture  $f_r$  specified in 9.5.2.3*

The cracking load, however, is not explicitly defined in the code as it is in AASHTO. In general, it is implicitly understood that the cracking load (or moment) is that force required to raise the extreme tension fiber stress to a value equal to the modulus of rupture.

#### 4.4 PARAMETRIC STUDY

The cracking in prestressed concrete can only be reached when the applied flexural tensile stress exceeds both the net compressive stress from the prestressing and the tensile strength of the concrete. Consequently, when bonded prestressing steel quantities are increased, the cracking moment increases. Depending on the shape of the cross section and ultimate strength requirements, in certain instances it is possible that a section can contain a large volume of bonded prestressing steel and yet not meet the minimum reinforcement requirement. This issue has been raised in previous publications (Kleymann et al. 2006, Freyermuth and Aalami 1997, Ghosh 1986).

To explore this anomaly, a parametric study was conducted on three different cross sections. The sections investigated were the Florida Bulb Tee 78 (FBT), a 4-ft wide by 8-in. deep hollow core (HC) slab, and a segmental box girder (SB). The FBT and HC were considered to be under positive bending (tension at bottom of section) and the box girder was considered to be under negative bending (tension at top of section).

The FBT was assumed to have a 7-in. deck and the HC contained a 2-in. topping. Concrete strength was assumed to be 6000 psi for the precast girder, hollow core, and segmental precast box. The concrete strength for both the bridge deck and topping for the hollow core was assumed to be 3500 psi. Prestress losses were assumed to be 25% after an initial strand stress of

$0.74f_{pu}$ . Prestressing strand was assumed to be 0.6-in. diameter Grade 270 strand for FBT and SB and 0.5-in. diameter strand for HC.

Figure 8 shows the results of the study. The sections were compared by calculating the ratio of the nominal moment capacity ( $M_n$ ) to the cracking moment ( $M_{cr}$ ). This was done for varying areas of prestressing steel ( $A_{ps}$ ). Mild steel was not considered in this study. The area of prestressing steel was normalized by the precast area of concrete in flexural tension ( $A_{ct}$ ).  $A_{ct}$  is that portion of the cross section between the flexural tension face and center of gravity of the gross section. The nominal cracking moment was calculated using strain compatibility and the cracking moment was calculated using Equation 5.

Two plots are shown for each section that correspond to the tensile strength of concrete used to calculate the cracking moment. The plots show both ACI 318 modulus of rupture requirement of  $7.5\sqrt{f'_c}$ (psi) and AASHTO requirement of  $11.7\sqrt{f'_c}$ (psi). The spans were assumed to be 25 ft for HC, 140 ft for FBT, and 140 ft for SB.

As prestressing steel is added, the plots quickly rise above the minimum steel requirement of 1.2, indicating that the requirement is met (ignoring the phi factor). Because the cracking moment increases at a slightly greater rate than that of the moment capacity, each plot eventually declines with the addition of more prestressing. FBT has the greatest margin above the 1.2 mark while SB has the least. In general, the use of bonded prestressing steel in quantities sufficient to cause a decrease in the moment ratio is beyond that needed for strength and serviceability. In some cases, however, strength or serviceability requirements for large bonded prestressing quantities may make satisfying the minimum reinforcement requirement impossible.

Oladapo 1968 conducted a similar parametric study by varying the level of prestress, eccentricity, and tensile strength of the concrete. As found in the present study, increasing the level of prestress moved the curve further away from the minimum requirements. Increasing the eccentricity decreased the range in which the requirement was met. Varying the tensile strength of concrete only caused large variations in the curve for relatively low values of the reinforcement ratio. It was recommended that the curves developed be used to provide bounds for minimum and maximum reinforcement amounts.

For sections with relatively small compression zones and large tension zones, such as box girders in negative bending, the tensile strength of the concrete has a much greater effect relative to the precompression than it does in sections with large compression flanges. This is seen in the

plot where the difference between the two curves for SB in negative bending is much greater than that of HC or FBT. Consequently, as the amount of prestressing steel is increased the cracking moment increases at a faster rate than the moment capacity, due to the overriding effect of the tension zone.

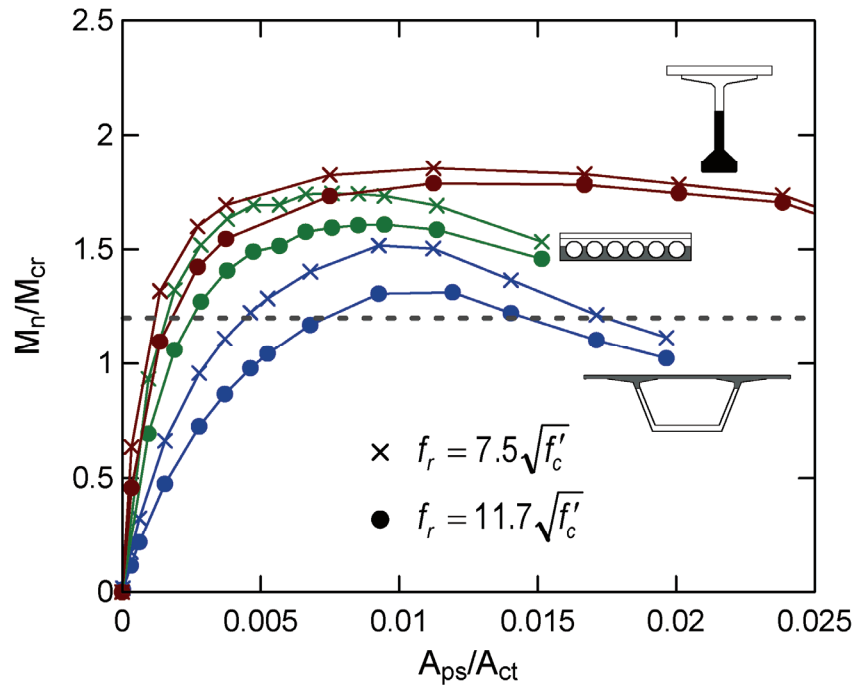


Figure 8. Results from parametric study

This parametric study points out the dilemma presented by requiring that the cracking moment be calculated directly to satisfy the minimum reinforcement requirements. It has been shown here that, in some cases, two minimum reinforcement requirements can be calculated. Rather than refine the calculation of the cracking moment, the next section proposes an equation that implicitly includes the cracking moment and prestress in its formulation, thereby avoiding the possibility of having two possible minimum reinforcement requirements.

#### 4.5 PROPOSED PROVISIONS

Leonhardt 1964 proposed a minimum steel requirement for prestressed concrete that is based on providing sufficient steel area to resist net tensile concrete stresses that occur just prior to cracking. This avoids the quandary of defining and calculating cracking moment. Furthermore, this approach is applicable to both nonprestressed and prestressed concrete.

To illustrate the approach used by Leonhardt, consider a rectangular section prestressed with a single tendon as shown in Figure 9a. The stress diagram associated with the effective prestress is shown adjacent to the cross section, which represents the stress state caused by the prestressing. The effective prestress in the prestressing steel ( $f_{se}$ ) is shown. The compressive stress in concrete ( $f_{pe}$ ) due to effective prestress forces at extreme tension fiber-as caused by external loads-is also shown. The stress state caused by applied service moments can be superimposed on the prestressing stress state. If sufficient moment is applied, the net stress in the bottom fiber will equal zero. This moment is defined as the decompression moment ( $M_{dec}$ ). Considering the materials, methods, and designs currently used it can be shown that the change in stress in the prestressing steel caused by the decompression moment is negligible. In fact, with typical long-term losses, it is practically impossible for the steel stress to reach the original jacking stress. Allowable stresses typically imposed on the prestressing steel during stressing ensure that the effective stress state is at an acceptable and consistent level even with the full decompression moment applied. Indeed, stress in the steel increases significantly (as moment is increased) only after the section has cracked.

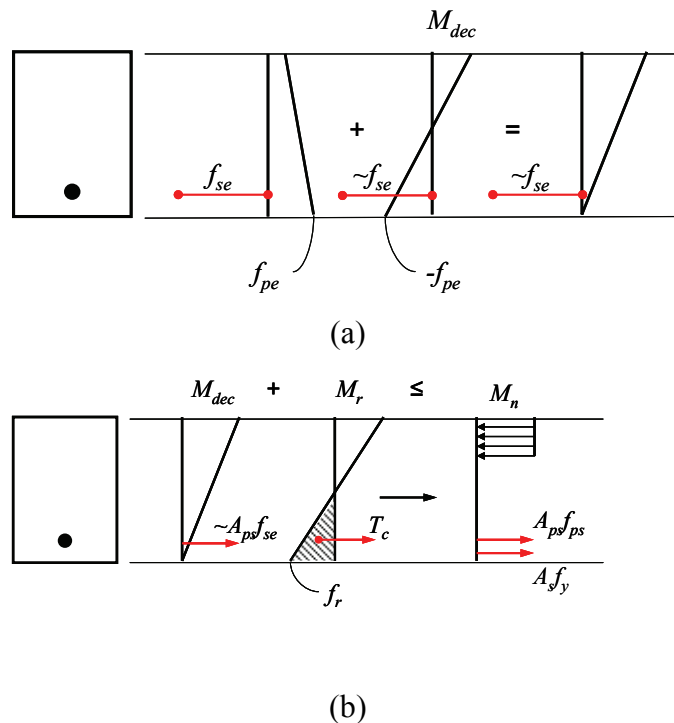


Figure 9. Stress state of section at decompression

The consideration of minimum reinforcement is a safety issue. The decompression moment, however, can be considered a service condition. Consequently it is useful to review the ACI commentary, which gives the original rationale for minimum reinforcement in nonprestressed members:

*The provision for a minimum amount of reinforcement applies to flexural members, which for architectural or other reasons, are larger in cross section than required for strength. With a very small amount of tensile reinforcement, the computed moment strength as a reinforced concrete section using cracked section analysis becomes less than that of the corresponding unreinforced concrete section computed from its modulus of rupture. Failure in such a case can be sudden.*

Although not explicitly stated, it is presumed that the minimum reinforcement limits for prestressed concrete, which are based on  $M_{cr}$ , are based on the same principle - to ensure sufficient reinforcement to prevent collapse when the section cracks. It is worthy to note that this provision was originally intended for large sections containing small amounts of nonprestressed reinforcement.

Figure 9b shows the same section as moment is increased beyond decompression to reach the rupture strength of the concrete in the extreme tension fiber. Leonhardt's approach suggests that the strength of the prestressed reinforcement ( $f_{pu}$ ) beyond the effective prestress be used to resist the tensile force generated in the concrete when taken beyond decompression. Perhaps a more rational and slightly more conservative approach is to consider the stress in the prestressing steel at capacity ( $f_{ps}$ ) rather than the ultimate strength. This approach can be expressed in terms of the required tensile forces show in the figure:

$$A_{ps}f_{ps} + A_s f_y \geq T_c + A_{ps}f_{se} \quad \text{Equation 6}$$

where;

$A_{ps}$  is the area of prestressing steel in flexural tension zone,

$A_s$  is the area of nonprestressed longitudinal tension reinforcement,

$f_{ps}$  is the stress in prestressing steel at nominal flexural strength,

If the reinforcement areas are collected on one side of the equation:

$$A_{ps}(f_{ps} - f_{se}) + A_s f_y \geq T_c \quad \text{Equation 7}$$

This equation ensures sufficient area of reinforcement such that the tensile force associated with the incremental change in steel stress from the effective prestress ( $f_{se}$ ) to the stress associated with ultimate flexural capacity ( $f_{ps}$ ) combined with the nonprestressed reinforcement yield strength ( $f_y$ ) are greater than the tensile force generated in the concrete just prior to cracking ( $T_c$ ).

The magnitude and location of the tensile force resultant in the concrete ( $T_c$ ) is important. When the section in tension is rectangular, then the resultant location is 2/3 of the depth of the tension stress block. If the section is irregular, that location will vary. To simplify the calculations it is assumed that the stress distribution is linear and that the area under the tension stress block is rectangular. Consequently, the tension force when the stress in the extreme tension fiber reaches the flexural tensile strength ( $f_r$ ) can be approximated by:

$$T_c \approx \frac{1}{2} A_{ct} f_r \quad \text{Equation 8}$$

Altering Equation 8 to make  $f_r$  a function of  $f'_c$  results in Equation 9, where  $\alpha$  is the numeric relation between the modulus of rupture and square root of the compressive strength: Currently, ACI 318 uses  $\alpha = 7.5$  while AASHTO uses  $\alpha = 11.7$  when concerning minimum reinforcement. AASHTO uses other values for  $\alpha$  for deflection calculations and shear calculations.

$$T_c \cong \frac{1}{2} A_{ct} \alpha \sqrt{f'_c} \quad \text{Equation 9}$$

The minimum area of prestressing steel required to satisfy the criterion established above can be determined by satisfying Equation 7. If the factor of 1.2 currently used in ACI and AASHTO is applied, Equation 7 becomes:

$$A_{ps}(f_{ps} - f_{se}) + A_s f_y \geq 1.2T_c$$

Equation  
10

Substituting Equation 9 into the above equation gives;

$$A_{ps}(f_{ps} - f_{se}) + A_s f_y \geq 1.2\left(\frac{1}{2} A_{ct} \alpha \sqrt{f'_c}\right)$$

Equation 11

This equation can be used as a general minimum requirement for either prestressed or nonprestressed reinforcement, or both. If the minimum area of bonded prestressing steel is desired, then  $A_{ps,min}$  can be substituted for  $A_{ps}$  and the equation rearranged as follows:

$$A_{ps,min} \geq \frac{0.6\alpha\sqrt{f'_c}A_{ct} - A_s f_y}{(f_{ps} - f_{se})}$$

Equation 12

Perhaps the greatest deviation of the proposed requirement from the current requirement is that it provides a minimum steel based only on the section geometry, concrete tensile strength as a function of concrete strength, and the available tensile capacity of the steel. With the current requirement, a designer must have some arbitrary value of prestressed steel in the section to be able to determine capacity ( $M_n$ ) and cracking moment ( $M_{cr}$ ). Once the designer chooses a value a check is made on the minimum requirement. The proposed requirement allows the designer to calculate a minimum area of steel that is independent of the amount of prestressing steel that is otherwise required by the design. Most of the reinforcement/prestressing needed to satisfy the minimum steel requirement must be placed close to the tension face.

#### 4.6 COMPARISON BETWEEN PROPOSED AND CURRENT PROVISIONS

The three cross-sections used in the previous parametric study were used to compare the proposed minimum steel provisions with those currently in AASHTO. They included a 78-in. deep Florida bulb tee (FBT), 8-in. deep hollow core slab (HC), and a segmental box girder (SB). These sections were chosen to represent the boundaries of the range of construction types and configurations likely to be used in bridge construction.

Comparing the current and proposed provisions is awkward because the current provisions are based on cracking moment, which changes when the amount of bonded

prestressing steel changes. On the contrary, the proposed minimum steel requirements do not depend directly on the cracking moment and therefore will be constant for any given cross section and set of material properties. As a compromise, the graphs shown in Figure 10 through Figure 12 were developed.

The first step to create the plots for the proposed provisions was to calculate the nominal moment capacity ( $M_n$ ) for each section using varying numbers of prestressing strand. The moment capacity was calculated using strain compatibility. In addition, cracking moment ( $M_{cr}$ ) was calculated using Equation 5 for each quantity of strand used to calculate  $M_n$ . Incorporating a phi-factor of 1.0, the minimum steel requirement for each section was determined as the lowest number of strands required to satisfy Equation 3. As pointed out in the parametric study, this approach is appropriate for most sections. In some cases, however, such as the box girder, as strand is added, the ratio will drop below 1.2 as illustrated in Figure 8. Beyond this point, it is impossible for the section to meet the minimum steel requirement. The plots for the proposed provisions were developed by calculating the minimum area of steel ( $A_{s,min}$ ) using Equation 12. This value remains constant regardless of the quantity of bonded prestressing steel used.

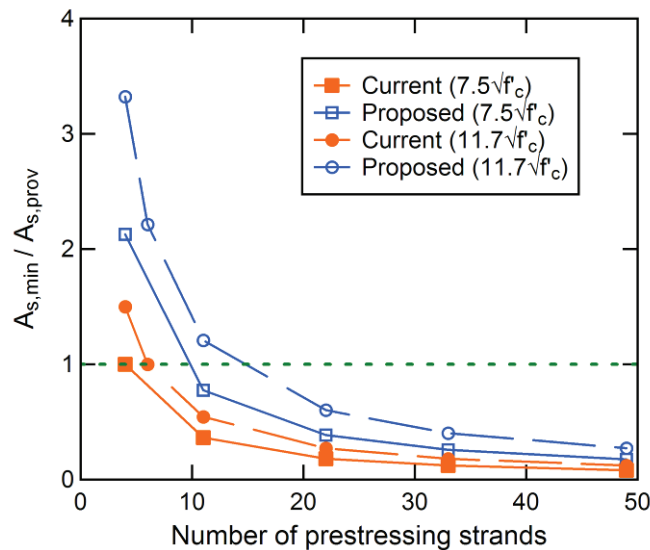


Figure 10. Comparison of proposed minimum reinforcement requirement for FBT

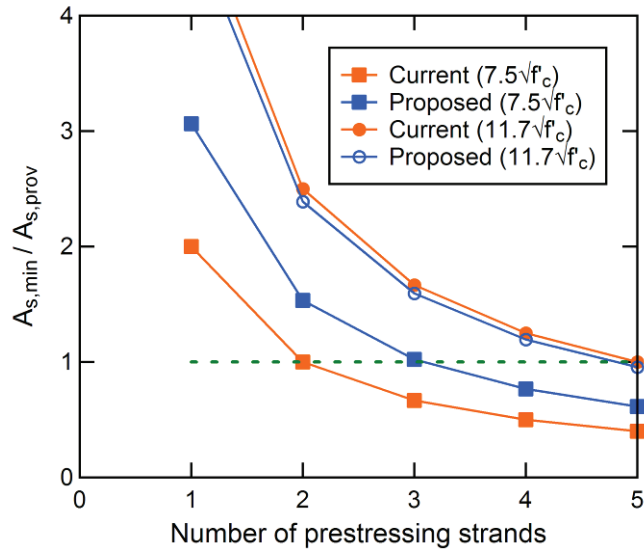


Figure 11. Comparison of proposed and current minimum requirement for HC

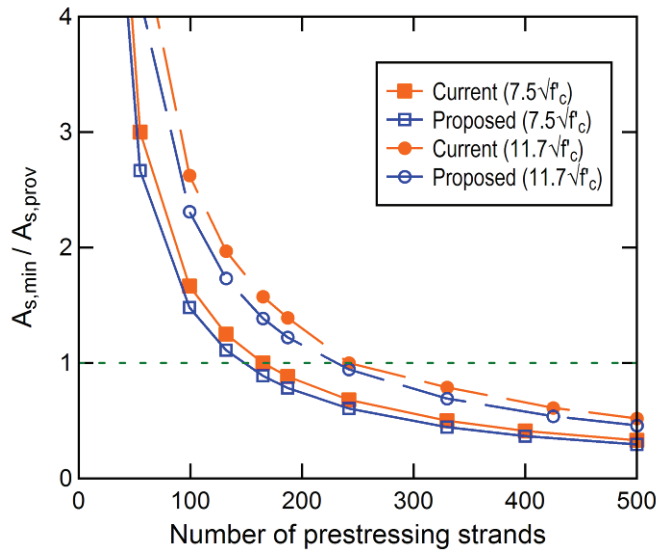


Figure 12. Comparison of proposed and current minimum requirement for SB under negative bending

Calculating the minimum reinforcement using the existing provisions required that the dead load moment carried by the precast section be determined separate from other superimposed loads (Equation 5). Unfortunately, this precludes the comparison of the minimum steel requirements on a section basis, since the relative moments will depend on span and self weight. Consequently, a typical span and girder spacing was chosen. Furthermore, no other

strength or serviceability requirements were considered. As a result, the plots may include impractically low and/or high quantities of strand. The total prestress losses were arbitrarily chosen as 25 percent.

When the quantities of bonded strand required to satisfy strength and serviceability are less than the minimum bonded strand requirement, the  $A_{ps}/A_{prov}$  ratio that is greater than one. When the strength and serviceability requirement for bonded strand is greater than the minimum bonded strand requirement, then the ratio drops below one. Most of the plots indicate that the proposed provisions require slightly more bonded prestressing steel than the current provisions. Practically, the numbers of strands required are quite low relative to the quantity required for service and strength requirements. One area of concern is the hollow core slab where the existing requirements are met with two strands and the proposed requirements are met with three. This is the result of the method of analysis where the provided area of steel was rounded to the nearest number of whole strands. The proposed revisions do not generally require 50% more minimum prestressing.

Perhaps the biggest contributor to the difference in minimum steel requirement is the modulus of rupture. For both the FBT and HC sections, nearly twice the number of strands are required when  $\alpha = 11.7$  than when  $\alpha = 7.5$ . In the SB girder, approximately 150 are required for  $\alpha = 7.5$  while 250 are required for  $\alpha = 11.7$ . Chapter 8 discusses section cracking and modulus of rupture.

## 5 INVERTED TEE TESTS

Two inverted tees (ITS and ITO) were designed and constructed to demonstrate the validity of the proposed minimum reinforcement requirements. The inverted tees were constructed at a precast concrete plant. FDOT personnel onsite provided quality control support by taking material samples and observing construction. Constructed beams were shipped to the FDOT Structures Laboratory in Tallahassee, FL for testing. Beams were tested in three-point bending with a single concentrated load placed at midspan. Beams were loaded twice: first to visible cracking, and then reloaded to failure.

### 5.1 DESIGN

The two test inverted tees were designed to allow for demonstration of beam behavior under load for a section with the minimum amount of reinforcement and maximum amount of reinforcement. For the inverted tee, the minimum and maximum amounts of reinforcement were governed by the typical strand patterns used by the FDOT.

Both inverted tees were 16-ft long with the cross section dimensions shown in Figure 13. The same stirrup and confinement arrangement was used for both specimens, which is detailed in Appendix A. The FDOT standard confinement details were used at the ends of the beams. Both beams contained two bonded 9/16-in. 270 ksi ASTM A416 seven-wire strands (Figure 14). Eight 3/4-in. diameter PVC pipes were installed in each specimen to serve as single-strand conduits to post-tension ITO at a later date. ITO was post-tensioned to increase the cracking moment but without the associated bonded prestressing. This was done in lieu of pretensioning to avoid damaging the specimen during prestress transfer. The post-tensioning process is described in a later section and the strand stressing log is detailed in Appendix A.

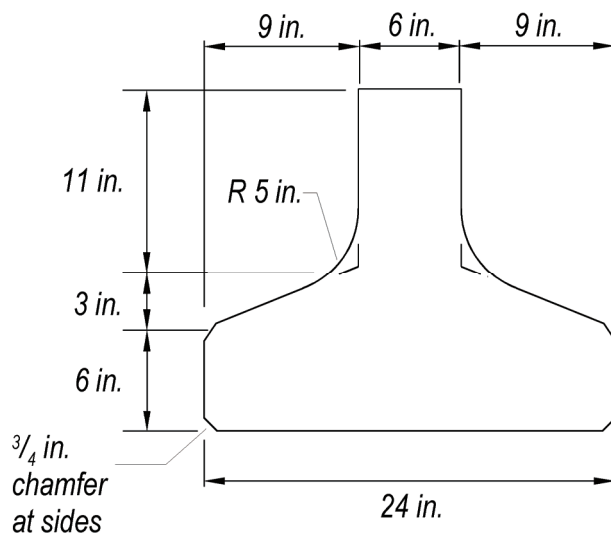


Figure 13. Cross section dimensions for inverted tees

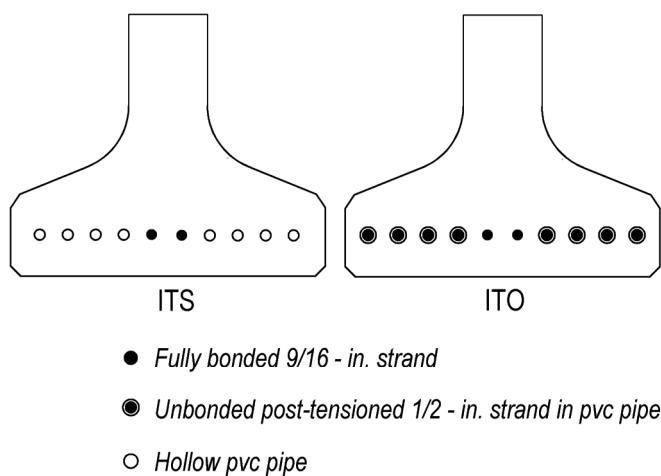


Figure 14. Prestressed steel layout for inverted tees

The concrete used to construct the beams was designed to have a minimum transfer strength of  $f'_{ci} = 3500$  psi and 28-day strength  $f'_c = 6000$  psi. The concrete mixture contained 3/8-in. diameter granite aggregate. Details of the mixture design are given in Appendix A. The average compressive strength from three 6 x 12-in. cylinder tests at 1 day was 5930 psi. The average compressive strength from three 6 x 12-in. cylinder tests at 28 days was 8410 psi.

## 5.2 CONSTRUCTION AND MATERIAL PROPERTIES

The two inverted tee specimens were constructed at the same time in the same bed with three other inverted tees that were for another project according to the schedule given in Appendix A. The specimens were constructed using steel formwork for the standard FDOT inverted tee shape (Figure 15). Plywood bulkheads were used to cap the end of the beam forms and to hold strand and PVC pipe in position. The PVC pipe was slipped onto the inactive strands in the specimens prior to stressing. These strands were removed from the PVC during detensioning for transport. Complete data on stressing and detensioning are included in Appendix A. During casting beams were consolidated internally and the top surface was troweled. When the formwork was removed, burlap was used to cover the beams and remained in place until prestress transfer, which occurred six days after casting.



Figure 15. Prestressing strand and reinforcement cage during form placement. Casting bed for inverted tees

Post-tensioning was conducted 100 days after casting the specimens. The average 28-day strength was 8410 psi. Eight 0.5-inch diameter strands were threaded through PVC pipe and stressed individually with a monostrand jack (Figure 16) at the FDOT Structures Laboratory in Tallahassee, Florida. Final strand elongation was measured to determine anchorage seating loss. A load cell (Figure 17) was also used in conjunction with the pressure dial gage from the jack to verify the applied stress to the strand. A chair anchorage configuration was employed at the live end to allow the stressed strands to be detensioned with a torch (Figure 18).



Figure 16. Monostrand jack used to post-tension ITO



Figure 17. Load cell to verify applied pressure

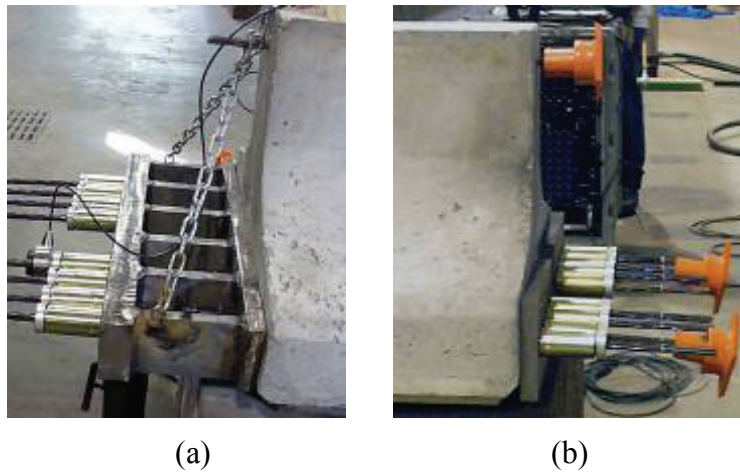


Figure 18. Anchorages for ITO (a) live end (b) dead end

### 5.3 TEST SETUP AND PROCEDURES

The specimens were setup with a center-to-center span of 15 ft and loaded at a single point at midspan applied under displacement control with a hydraulic actuator (Figure 19). Midspan loading was chosen over four-point bending to force the initial flexural crack to occur at midspan. The load rate was 0.02 inch/min.

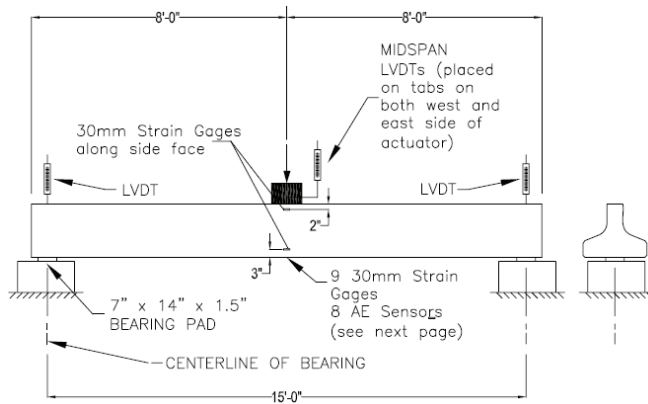


Figure 19. Test setup for inverted tee test.

Each girder was loaded until a visible crack had formed. The crack was marked, the load was removed, and two strain gages were applied directly adjacent to the crack as shown in Figure 18. The data taken from these gages during the second loading were used to estimate the effective prestress in each of the specimens. The entire procedure is explained in Section 5.6. During the second loading the beam was loaded to failure to determine the nominal moment capacity.

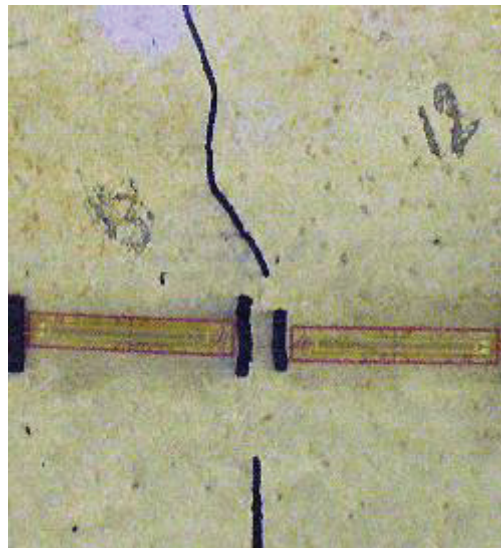


Figure 20. Gages placed adjacent to first visible crack

#### 5.4 INSTRUMENTATION

Strain, AE feature data, load, and displacement were monitored throughout the tests. Four LVDTs were used to monitor deflection during testing. Two were placed at midspan adjacent to the load point and one was placed over each bearing to measure the support displacement. Load was recorded in conjunction with both strain data and AE feature data.

The AE equipment utilized in this research was the commercially available DISP-16 channel AE System from Physical Acoustics Corporation. The piezoelectric sensors used were model R3I-AST integral preamp sensor. AE sensors were attached to the concrete surface using hot glue. They were placed on the bottom of the beam in a staggered array that was centered on the midspan and load point (Figure 21). The concept was to use the sensors to detect both distributed cracking and structural cracking using feature data and source location.

Thirty-mm long strain gages were placed end-to-end on the bottom surface of the concrete as shown in Figure 21. These gages were used in conjunction with the AE data to characterize cracking.

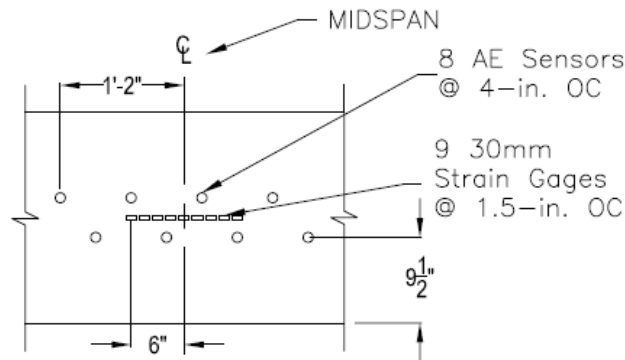


Figure 21. Layout of strain gages and AE sensors

#### 5.5 RESULTS AND DISCUSSION

The load-deflection plot for ITS is shown in Figure 22, which indicates linear behavior up to the appearance of the first crack at approximately 31 kip. The crack was marked and the beam was unloaded to allow the application of the two strain gages. As loading resumed, the behavior was linear up to the previous load where the girder stiffness decreased significantly. The post-cracking behavior was approximately bilinear until the compression zone crushed at 57 kip and 1.5 in. of deflection (Figure 23).

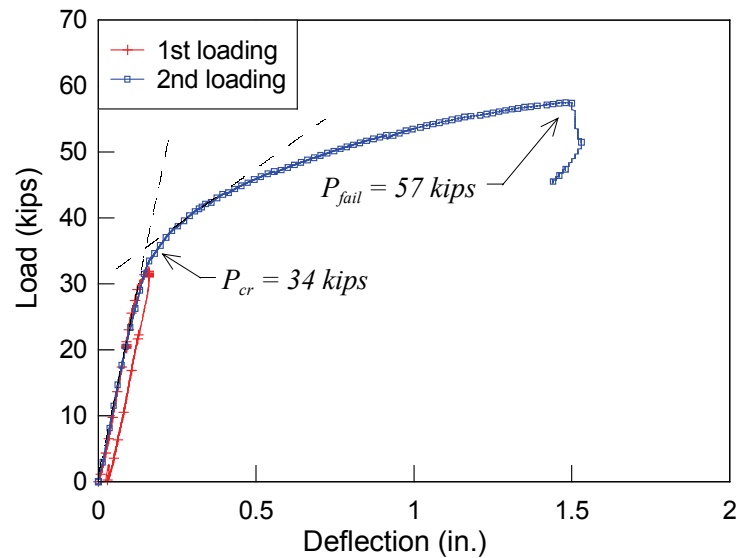


Figure 22. Load-deflection of ITS for initial and final loadings



Figure 23. Failure of the compression zone for ITS

The load-deflection plot for ITO is shown in Figure 24, which indicates linear behavior up to the appearance of the first crack at approximately 70 kip. The crack was marked and the beam was unloaded to allow the application of the two strain gages. As loading resumed, the behavior was linear up to the previous load where the girder stiffness decreased significantly. Although the post-cracking behavior did show a decrease in stiffness, the secondary branch of the curve was short relative to that of ITS. The ultimate capacity of ITO was 106 kip with an ultimate deflection of 0.7 in.

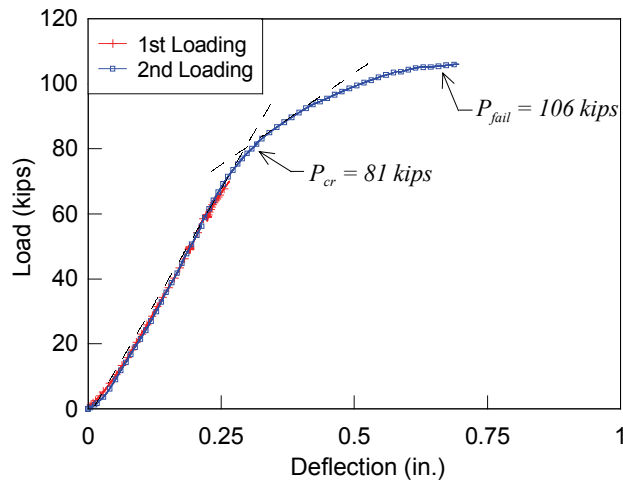


Figure 24. Load-deflection of ITO for initial and final loadings

### 5.6 EFFECTIVE PRESTRESS

The effective prestress was needed to calculate the cracking moment and was determined using the crack opening load from cracks that were formed during the initial loading of both specimens. Figure 25 shows a plot of the strain data from both gages applied adjacent to the first visible crack on ITS. When the initial cracking load was removed, the prestressing forced the crack closed and returned the beam section to full uncracked section properties. The decompression load is defined as the average of the two loads at which the strain load curve reaches a plateau. For ITS, this average is 10.9 kip. Theoretically, this is the load at which the crack just begins to open and the net stress at the extreme tension fiber is zero. To calculate the effective prestress force, the compression caused by the prestress force and its eccentricity are equated to the tensile stress caused by the decompression load using uncracked gross section properties. The resulting effective prestress forces for ITS and ITO were 70.0 kip and 252 kip. The detailed procedure is given in Appendix A.

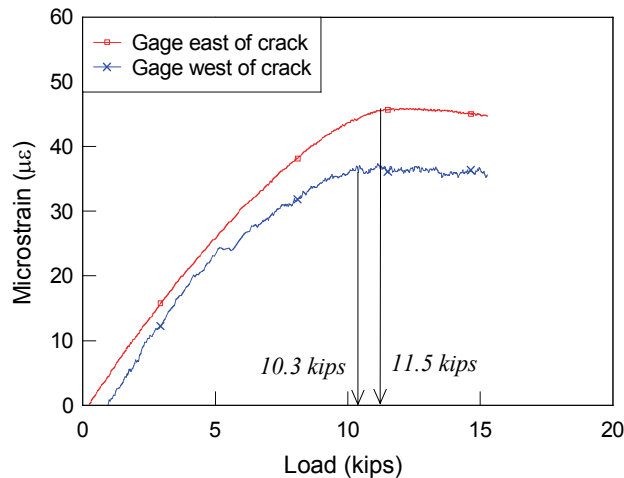


Figure 25. Strain/load data from gages placed adjacent to first visible crack

### 5.7 STRAIN AND AE RESULTS

In general, the use of AE during structural testing requires that cyclic loading be used. This allows evaluation of the Kaiser effect and the Felicity effect to determine if structural damage is occurring. The Kaiser effect can be used to determine the previous load level of the structure and the Felicity effect can be used to determine if the previous loading has caused structural damage. Furthermore, previous work (Hearn and Shield 1997) has indicated that the Kaiser effect may not be strictly applicable for prestressed concrete beams. The IT tests covered in this chapter, however, focused on minimum reinforcement requirements. Consequently, the tests were conducted in two cycles. The first was to crack the section and apply the decompression strain gages and the second was to load the section to failure. Nevertheless, AE data were collected during testing to determine if increased AE activity was associated with visual observation of structural cracking and with strain data. Figure 26 shows measured strain and AE event energy as the load is increased to cracking. Note that these results also indicate that the Kaiser effect is not necessarily applicable since this girder had not seen load prior to this test and AE events did not occur until the load reached approximately 22 kip. In addition, strain data were linear up to approximately this same level indicating linear elastic behavior. It is at this load level, however, that both AE event energy begins to accumulate and the load-strain plot becomes nonlinear. This is likely the result of the formation of distributed microcracks in the concrete causing a softening effect at the surface near the strain gage and also an accumulation of AE event data. Structural (visible) crack formation is marked by a sudden increase in both strain

and event energy at approximately 30 kip, which is slightly less than the load at which cracking was observed visually. Figure 27 shows similar results for ITO.

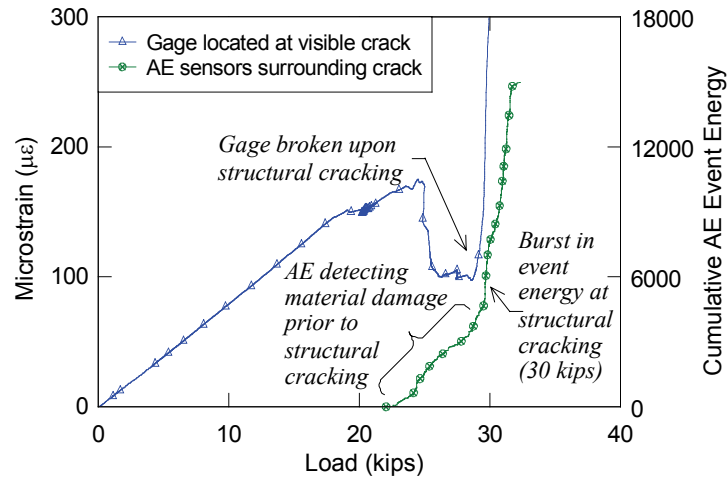


Figure 26. AE and strain results for ITS

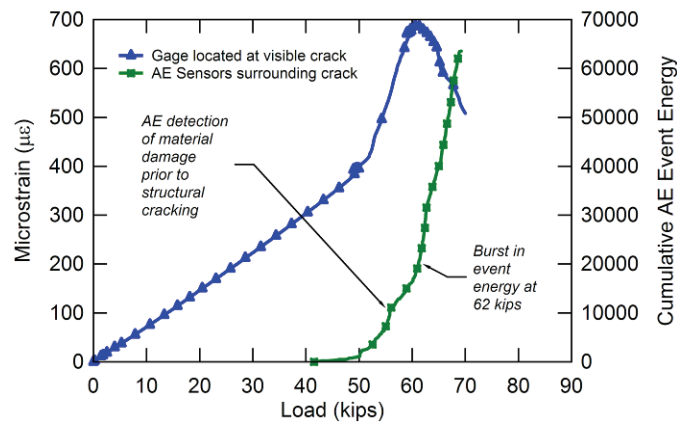


Figure 27. AE and strain results for ITO

### 5.8 CRACKING MOMENT

Table 1 presents a summary of the testing results for both IT specimens. An elastic stress analysis of the extreme tension fiber on the specimen was conducted to determine the calculated cracking moments shown in the table. The first value ( $f_r$ ) used the average results of the modulus of rupture test conducted the day after IT were tested, which was 857 psi. The cracking moment was calculated as the total moment required to cause a net tensile stress in the extreme tension fiber equal to  $f_r$ . Likewise, similar calculations were conducted for the two typical methods of estimating the concrete tensile strength based on the design concrete strength of  $f'_c = 6000$  psi.

These calculated moments are compared to the experimental cracking moments that were determined from the test data. The P- $\Delta$  value was determined from the load-deflection plot as the load at the bend in the curve. The AE value used the results of the AE event data to determine the point at which structural cracking occurred. Finally, the moment at which cracking was observed is given. The AE data appear to provide the earliest indication of cracking. Yet, the crack in ITS became visible nearly simultaneously with the AE indication, while in the ITO a crack is not sighted until the load is 12% greater than that at which the AE signals crack formation. As might be expected from the subjective nature, using the load-deflection plot to determine cracking moment provides higher estimates than either visual inspection or AE.

Table 1. Summary of cracking, capacity, and ductility results for IT tests.

ID	Calculated $M_{cr}$ (kip-ft)			Experimental $M_{cr}$ (kip-ft)			$M_{exp}$ (kip-ft)	$M_{exp}/M_{cr}$	$\Delta_{ult}/\Delta_{cr}$
	$f_r$	$7.5\sqrt{f'_c}$	$11.7\sqrt{f'_c}$	P- $\Delta$	AE	Visual			
ITS	121	96	125	135	120	123	221	1.77	8.8
ITO	250	221	249	311	241	270	394	1.40	2.4

The table also demonstrates how the lightly prestressed section (ITS) met the minimum requirement with a greater margin (1.77) than the heavily prestressed section (1.40). Furthermore, ITS displayed considerably more deflection ductility between cracking and ultimate failure. This indicates that the minimum reinforcement should not be based directly on the ratio of moment capacity to cracking moment for prestressed concrete.

## 6 PILE TESTS

Ten three-point flexure tests were performed on ten pile cut-offs. The pile cut-offs were from a bridge construction project that was evaluating the use of supplementary cementitious materials (SCM) to improve durability of piles in a marine environment. A series of highly reactive SCMs were employed in the concrete used to produce the piles including fly ash (FA), ultra-fine fly ash (UFA), ground granulated blast furnace slag (BFS), metakaolin (MET), and silica fume (SF). Two piles were obtained for each of the SCMs employed.

The piles were tested in flexure so that the cracking moment could be estimated using several techniques. One of the two piles from each SCM group was tested monotonically and the other was tested cyclically. Strain on the tensile surface in the midspan of the pile, strain throughout the depth of the pile at midspan, midspan deflection, applied load, and AE activity were all monitored during the testing.

### 6.1 DESIGN

Pile design was based on standard FDOT drawings from the State Structures Design Office. The selected strand pattern for the 24-in. bridge pile was 20 0.5-in. diameter special low relaxation GR270 seven-wire strands evenly distributed around the perimeter (Figure 28). Each strand was prestressed to approximately 34.0 kip according to the structural plans. Piles were designed with 3-in. of clear cover over the spiral ties as required by FDOT for piles in marine environments. The specified concrete strength  $f'_c$  was 6,000 psi at 28-days. The design also called for a minimum compressive strength of 4,000 psi at the time of prestress transfer. Pile construction documents are given in Appendix B.

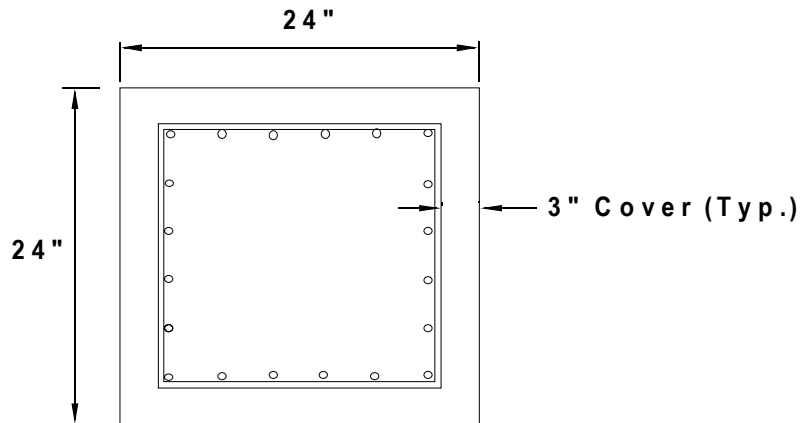


Figure 28. Cross Section of Piles

## 6.2 CONSTRUCTION AND MATERIAL PROPERTIES

Prestressing strand was pulled using standard plant practice and according to FDOT specifications. Elongation and force were monitored and recording accordingly. Immediately after the piles were cast, burlap was applied to the exposed surface and a sprinkler maintained moist curing conditions for three days as required by FDOT for piles in a marine environment. After curing and when the concrete reached sufficient compressive strength, the strands were torch-cut to transfer the prestress. The results of the material testing are shown in Table 2.

Testing was conducted in accordance with the following standards:

1. ASTM C 39 – Compressive Strength of Cylindrical Concrete Specimens
2. ASTM C 78 – Flexural Strength of Concrete
3. ASTM C 469 – Static Modulus of Elasticity and Poisson’s Ratio of Concrete in Compression

Table 2. Summary of materials testing results

Mixture	Compressive strength (psi)				Modulus of rupture (psi)	Modulus of elasticity (ksi)
	7 days	28 days	91 days	364 days	28 days	365 days
UFA	4,950	7,560	7,550	N/A	889	N/A
FA	5,900	7,790	8,000	9,080	857	5,183
SF	6,720	8,050	8,860	9,840	1,218	5,242
BFS	5,090	7,570	10,060	10,610	1,262	5,208
MET	5,740	6,550	7,580	9,290	933	4,767

After the piles were driven, the unneeded portion of the pile was saw cut and removed. Cut-off lengths ranged from 26 to 28 ft. Although the exact method of removal is not known, inspection of the ends of the cut-offs indicated that the saw was passed around the pile perimeter to sever the prestressing strands (Figure 29). After this cut was made it is believed that the crane was used to break the remaining concrete at the saw cut. This may have caused cracking in some of the piles, which may have affected the results of the cracking tests.

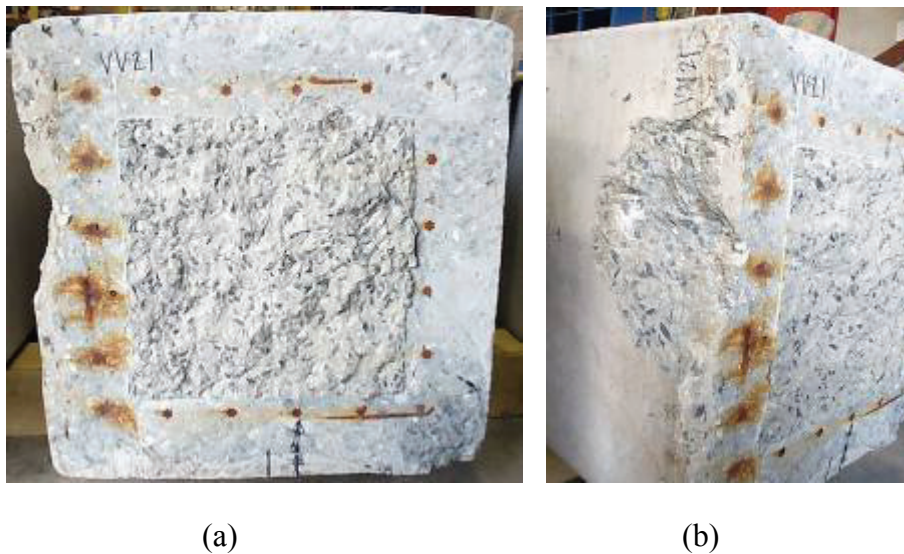


Figure 29. Evidence of pile damage a)end view b)side view

### 6.3 TEST SETUP AND PROCEDURES

All piles were tested in three-point bending as shown in Figure 30. Since specimen lengths ranged from 26 to 28 feet the test setup was arranged to provide the same center-to-center span for all tests. Three-point bending was used to ensure flexural cracks formed at midspan first. The load rate was 0.02 inch/min.

Two procedures were used to load the specimens. One specimen from each mixture design was loaded monotonically up to 100% of the estimated cracking load. Cracking load was estimated using the AASHTO method for calculating prestress losses and the modulus of rupture and averaged to approximately 65 kip for all specimens. Typically, the piles cracked at a lower load than was estimated. Cracks were located, marked, and measured. The pile was then unloaded and strain gages were applied adjacent to a selected crack. Load was reapplied to a level approximately 10% greater than the previous load to reopen the crack(s). This procedure

was used to estimate the effective prestress in the tendon. The remaining five specimens were cyclically loaded to 20%, 40%, 60%, 80% and 100% of the estimated cracking load. This was done to observe the Kaiser and Felicity effect if evident.

Load was applied using a hydraulic actuator at midspan at a load control rate of 10 kip/min for all tests. For both the monotonic and cyclic load tests load was held when cracks were first visible to mark crack patterns and measured crack widths.

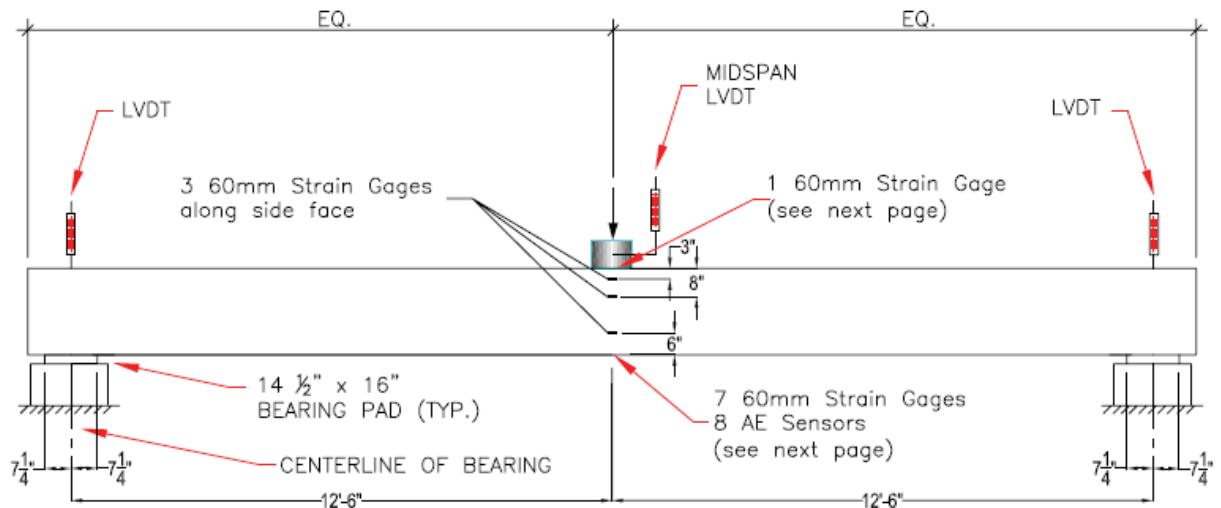


Figure 30. Test setup for pile

#### 6.4 INSTRUMENTATION

Strain, AE feature data, load, and displacement were monitored during testing. Details of the strain gage and AE sensor layout are shown in Figure 31 and Figure 32. The strain gage and AE arrangements are similar to those used on the Inverted Tee tests reported in Chapter 5. See Section 5.4 for further discussion.

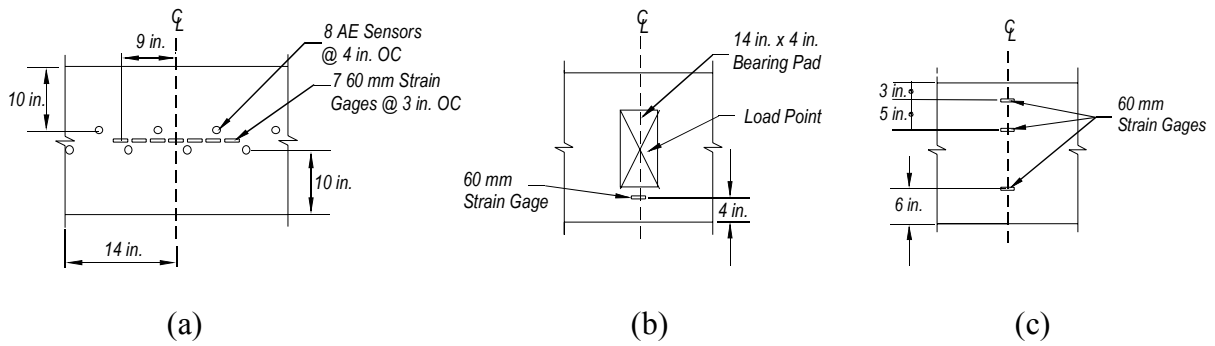


Figure 31. Strain gage and sensor layout at midspan along the a) bottom of the pile b) top of the pile and c) elevation of the pile.

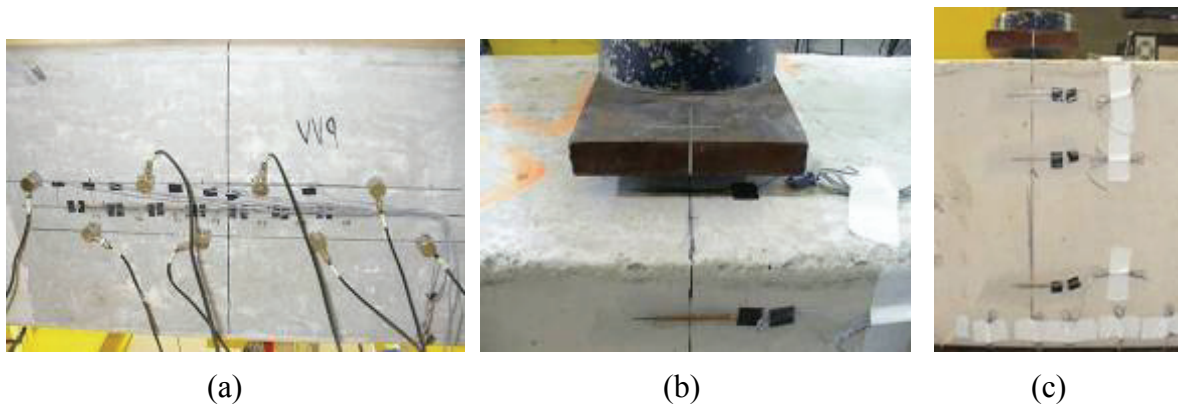


Figure 32. Photographs of strain gage and sensor layout at midspan along the a) bottom of the pile b) top of the pile and c) elevation of the pile.

Four LVDTs were used to monitor deflection during testing. Two were placed at midspan adjacent to the load point and one was placed over each bearing to measure the support displacement. Load was recorded in conjunction with both strain data and AE feature data.

## 6.5 RESULTS AND DISCUSSION

Figure 33 shows the load-deflection plot for the monotonically loaded FA specimen, which was typical for all of the monotonic load tests. Initially, the pile responded linearly up to nearly 52 kip. At a load of approximately 23 kip the midspan deflection was 0.1 in. Calculated deflection for the same load, assuming linear elastic behavior gave a midspan deflection of 0.098 in., only 2% different than the measured value. As load was taken beyond 52 kip the stiffness began to decrease indicating cracking had occurred. Loading was terminated when cracking was identified visually.

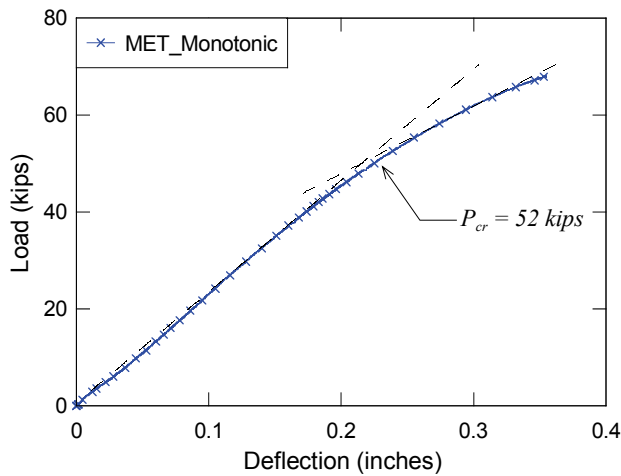


Figure 33. Typical load-deflection behavior of piles loaded monotonically

Figure 34 shows the load-deflection curve for the cyclically loaded MET pile, which was typical of the other piles tested cyclically. The first three curves appear to project along the same slope once the load exceeds the maximum load of the previous cycle. As with the companion monotonically loaded specimen, the linear behavior appears to cease after reaching approximately 56 kip. The plot illustrates that for the 80% loading cycle, the curve no longer appears to project the same slope as was maintained in the previous cycles. This is even more apparent for the 100% loading cycle, as the slope continually decreases. Loading was terminated when cracking was identified visually.

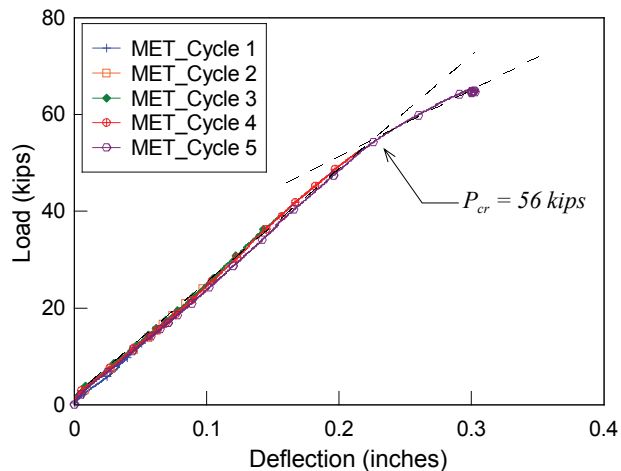


Figure 34. Typical load-deflection behavior of piles loaded cyclically.

Both Figure 33 and Figure 34 show that the cracking load was determined using the intersection of best fit lines from above and below the point at which the plot changes slope. The change in stiffness, however, was much less abrupt than that of the inverted tee tests. In addition, the piles were not taken to ultimate load capacity. Consequently, some subjectivity was required in choosing the points to include when fitting the lines. The cracking moments of each pile determined using this technique are shown in Figure 35. The variance between monotonically and cyclically loaded cracking moments never exceeded 10%.

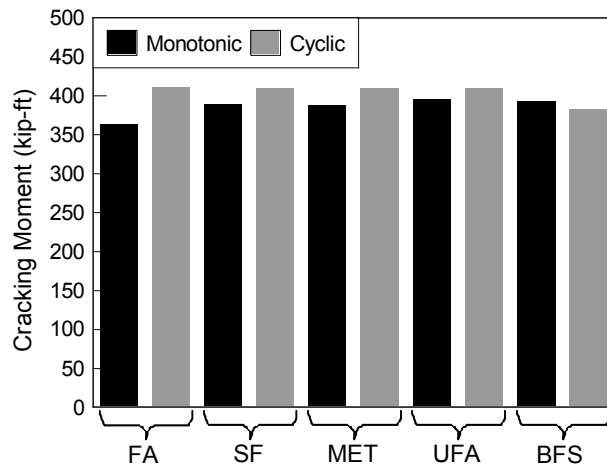


Figure 35. Measured cracking moment from load-deflection data

## 6.6 EFFECTIVE PRESTRESS

The strain gage data were used to indirectly determine the effective prestress force in the monotonically loaded piles and cyclically loaded piles. In some cases, because the cracks formed between existing strain gages, additional gages were not added to measure crack opening load. The results of these analyses are shown in Figure 36. The measured losses vary by as much as 15 percent.

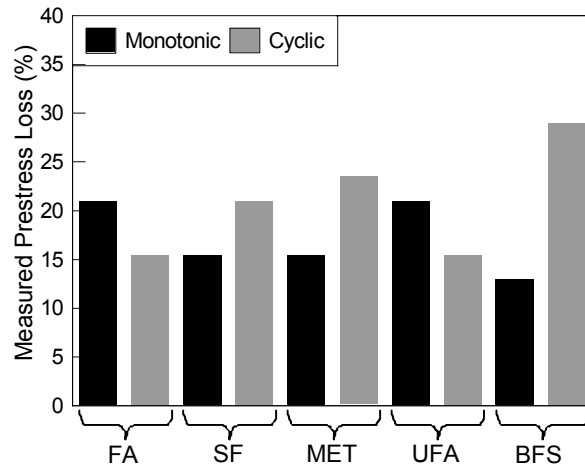


Figure 36. Measured percent prestress loss

### 6.7 STRAIN AND AE RESULTS

Figure 37 shows the strain gage and AE sensor layout used during the pile testing. During the flexural test, a primary flexural crack was identified and located visually. The AE data from the two sensors adjacent to the primary flexural crack were then selected and analyzed for events. The cumulative event energy for each cycle was then compared load and to the strain data from the gage closest to the primary crack.

Figure 38 shows the results of this analysis for MET. Five strain load plots are shown for the gage closest to the crack for load cycles at 20, 40, 60, 80, and 100% of estimated cracking load. The load-strain plot remains linear for both of the first two cycles. Furthermore, no AE events were detected during these cycles. During the third cycle, however, the plot shows some deviation from linear in conjunction with the occurrence of AE events. No visible cracking, however, was detected. This indicates that distributed microcracking is being detected in the concrete by both the strain gage and the AE sensors. During the fourth cycle, the load strain plot deviates from linear at a much lower load, indicating decompression. AE events, however, were detected when the load was above the 30 kip mark but below the maximum load reached during the previous cycle, which indicates a breakdown of the Kaiser effect (Felicity effect) and a high probability that damage had occurred. Had AE events not been detected until the load reached the previous peak of 40 kip, then this would have been an indication that microcracking had not initiated. This same phenomenon was noted by Hearn and Shield 1997 during testing of

pretensioned concrete girders. These results suggest that as with concrete in direct tension, distributed microcracking occurs early in the loading and progresses until sufficient damage has accumulated to result in the formation of a single structural crack. This idea is explored more in Chapter 8 where the range over which this damage occurs is quantified.

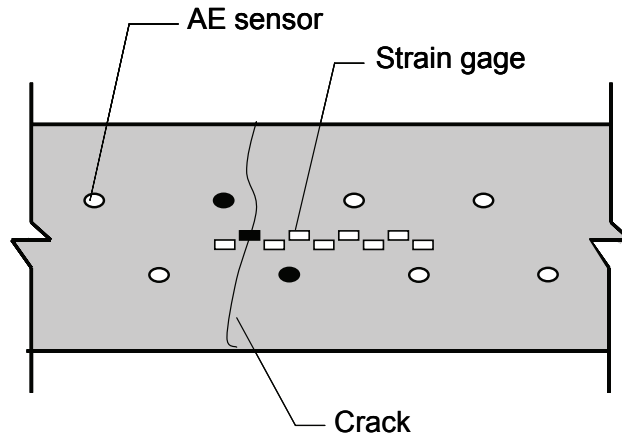


Figure 37. Gage and sensors utilized for data analysis

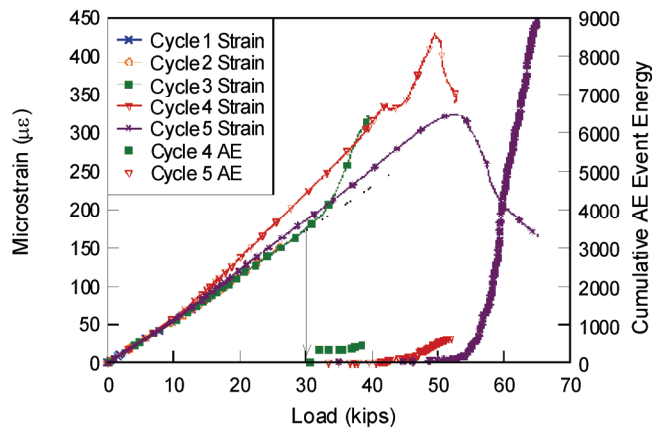


Figure 38. Felicity effect and distributed microcracking in specimen MET

## 7 PRETENSIONED GIRDER TESTS

Pretensioned concrete girders with custom section dimensions were constructed to evaluate cracking behavior with variations in prestressing strand size and quantity. The span-to-depth ratio of the girders was selected to be similar to that of standard AASHTO sections, which are used in Florida bridges. Six precast pretensioned girders were constructed at a precast concrete plant. FDOT personnel onsite provided quality control support by taking material samples and observing construction. Constructed beams were shipped to the FDOT Structures Laboratory in Tallahassee, FL for testing. Girders were tested in three-point bending with a single concentrated load placed at midspan. Girders were loaded cyclically to measure the progression of microcracking and structural cracking.

### 7.1 DESIGN

Girders were 18-ft long and had the cross section dimensions shown in Figure 39. The stirrup and confinement steel arrangement is detailed in Appendix C. The girders were prestressed with ASTM A416 seven-wire strand. B6S, B6M and B6L contained 0.6-in. diameter strand and B5S, B5M and B5L contained 0.5-in. diameter strand in the patterns shown in Figure 40. The girders with the 0.6-in. diameter strands were constructed in the same bed at the same time. The same applies to the girders containing the 0.5-in. diameter strands. The debonding shown in the figure allowed the three girders to be constructed at the same time with the same prestressing pattern.

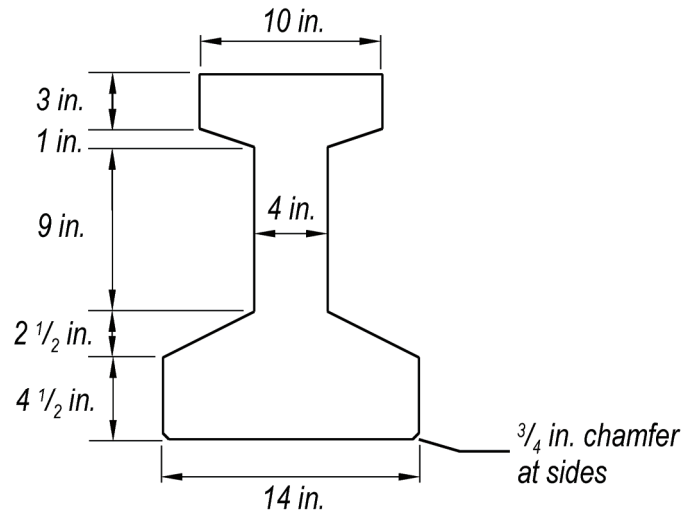


Figure 39. Cross section dimensions of all test girders

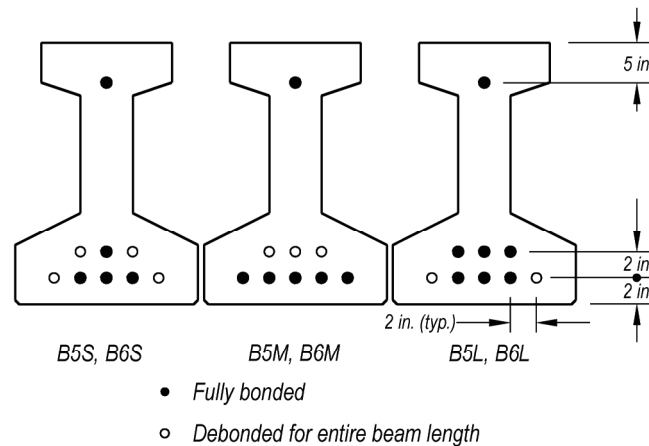


Figure 40. Strand layouts for girders containing 0.5-in. and 0.6-in. strand

## 7.2 CONSTRUCTION AND MATERIAL PROPERTIES

Three girders with the same size strand (B5x) were cast in the same bed and using the same tendon for ease of construction (Figure 41). The remaining three (B6x) were cast and tensioned in the same fashion. The 0.5-in. and 0.6-in. prestressing strands were initially stressed to 50% and 74% of the ultimate strength (270-ksi), respectively. The dates of strand stressing, casting, and detensioning are given in Table 3. More detail on the detensioning sequence and release strengths are given in Appendix C.



Figure 41. Girder construction.

All girders were consolidated internally with vibrators. To ensure an adequate connection between each girder and its top slab, the top slab was intentionally roughened. The design transfer strength,  $f'_{ci}$ , was 3500 psi. The compressive strength at release for the B5x and B6x girders was 3900 psi and 5370 psi, respectively. The specified compressive strength at 28-days,  $f'_c$ , was 6000 psi. The tested 28-day compressive strength for the B5x and B6x girders was 9750 psi and 8840 psi, respectively.

Table 3. Construction and testing schedule.

Girders	Strand Stressed	Concrete Cast	Strand Detensioned	Deck Cast	Tested
B5S	9/29/2008	9/30/2008	10/1/2008	12/22/2008	1/27/2009
B5M	9/29/2008	9/30/2008	10/1/2008	12/4/2008	1/26/2009
B5L	9/29/2008	9/30/2008	10/1/2008	12/22/2008	1/26/2009
B6S	10/02/2008	10/02/2008	10/6/2008	12/4/2008	1/21/2009
B6M	10/02/2008	10/02/2008	10/6/2008	12/4/2008	1/21/2009
B6L	10/02/2008	10/02/2008	10/6/2008	12/22/2008	1/26/2009

Girders B5S, B5M, and B5L were cast in pour from a single mixing batch. Similarly, girders B6S, B6M, and B6L were also cast from a single mixing batch. The mixture contained 90% of granite aggregate equal to or less than 3/8 in. with no aggregates exceeding 0.5 in. More detail on the mixture design can be found in Appendix A (the same mixture design was used for the inverted tee beams). For each pour nine 6 x 12 in. cylinders for compressive strength and modulus of elasticity testing were taken. Additionally, the producer cast 4 x 8 in. cylinders for

release strengths and 28-day compressive strength tests for quality control purposes. Five 4 x 4 x 12 in. beams from each pour were cast for modulus of rupture (MoR) testing.

Table 4 shows the cylinder and beam test results at release and at 28-days. Each value is the average of three tests. The design called for a release strength of 3500 psi, which was reached within one day of casting. The B6x girders, however, were not released until four days after casting due to construction scheduling. Notice in the table that the average 28-day compressive strength for the B6x girders completed on the 6 x 12 in. cylinders was less than the release strength. It is believed there was a problem with the testing device when the cylinder breaks were completed and that the producer tests conducted at 28-day age are a better estimate of the compressive strength. Mill certificates and test data for the strand are in Appendix C.

Table 4. Results for compressive strength and modulus of rupture tests (psi).

Girders	6 x 12 in. cylinders			4 x 8 in. cylinders (Durastress)		4 x 4 x 12 in. MoR	
	Release	28 day	Test day	Release	28 day	28 day	Test day
B5x	3900	8400	7940	3980	9750	680	850
B6x	5370	n/a*	8071	4902	8840	590	817

\*Problem with testing device

A FDOT Class II concrete deck (Figure 42 and Figure 43) was cast on each girder ( $f'_c = 4500$  psi) after delivery to the FDOT Structural Research Center. The decks for B6S, B6M and B5M were cast on 12/4/2008 and the decks for B5S, B5L and B6L were cast on 12/22/2008. Nine 6 x 12 in. cylinders were cast on each of the pour dates for material testing.

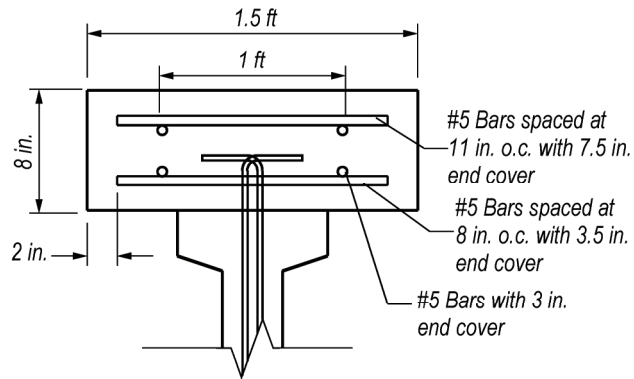


Figure 42. Deck dimensions and reinforcement layout

To facilitate the deck pour, steel forms with wooden endblocks (Figure 44) were attached to the girders. Concrete was transported to the girder with a hopper, which was supported and maneuvered by an overhead gantry crane. After placement, the concrete was internally vibrated to ensure adequate consolidation (Figure 45). The finished girders ready for testing are shown in Figure 46.



Figure 43. Bridge deck reinforcement prior to casting



(a)

(b)

Figure 44. Deck construction a) Steel forms, and b) wood bulkhead



Figure 45. Deck concrete placement and vibration.



Figure 46. Finished girder specimens ready for testing.

### 7.3 TEST SETUP AND PROCEDURES

The specimens were tested with a center to center span of 17 ft and loaded at midspan with a hydraulic actuator (Figure 47). Midspan loading was chosen over four-point bending to force the initial flexural crack to occur at midspan. Beam bearing was on 1.5-in. thick steel plate and roller to ensure a consistent span length. Load was applied at the rate of 10 kip/min. The girders were cyclically loaded to 30%, 60%, 90%, and 110% of the estimated cracking moment for each girder. Incrementally loading allowed for the Kaiser and Felicity effects to be observed.

When a visible crack was first detected, the load was held constant while the crack was marked. Two additional gages were added to the bottom surface of the girder on each side of the crack to determine the load required to open the crack.

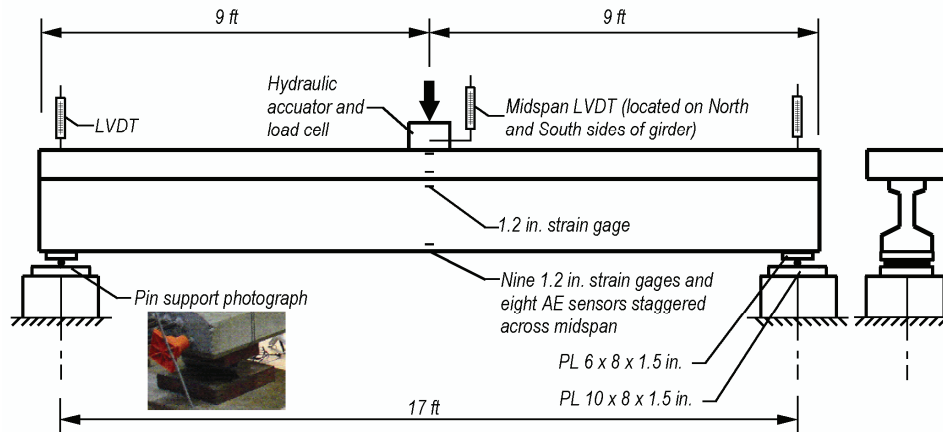


Figure 47. Pretensioned girders test setup.

#### 7.4 INSTRUMENTATION

Prestress losses were monitored using vibrating wire strain gages (VWSG). Gages were installed at midspan and at the centroid of the tendon, which varied as shown in Figure 48. To ensure each VWSG remained at the center of gravity of the tendon, cable loop clamps and cable ties were used to attach the VWSG to threaded rod support bars as shown in Figure 49 and Figure 50. Support rods were attached perpendicular to the prestressing strand with cable ties. Figure 51 shows the cable connected to the embedded VWSG spooled atop the girder at midspan.

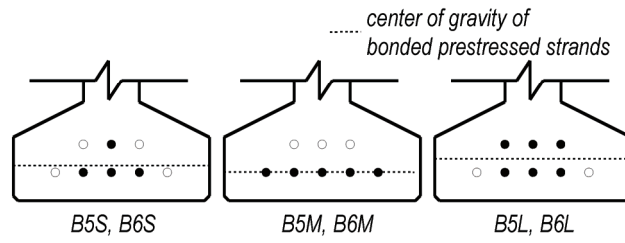


Figure 48. Centroid of prestressing steel and corresponding VWSG setup

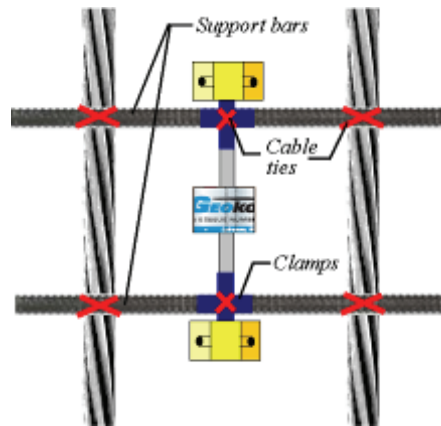


Figure 49. VWSG placement setup



Figure 50. VWSG installation at midspan (arrow) of girder



Figure 51. VWSG cable coil at midspan

Readings were taken with both a single channel readout box (Figure 52a) and a four channel data logger (Figure 52b). The data logger allowed readings to be taken from each of the three girders during detensioning without having to switch connections among the specimens. The data logger logged readings from the VWSGs every 10 seconds. The readout box displayed readings for a single channel and was used as a check on the data logger's initial and final readings.



(a) (b)

Figure 52. VWSG a) readout box b) data logger

Strain, AE feature data, load and displacement were monitored during load testing. Four LVDTs were used to monitor deflection during testing. Two were placed at midspan and one at

each of the supports (Figure 47). Load was recorded in conjunction with both strain data and AE feature data. Figure 53 shows the strain gage and AE sensor arrays, which were similar to those used in the IT and pile tests. The center of both the strain gage and AE sensor arrays are located at midspan.

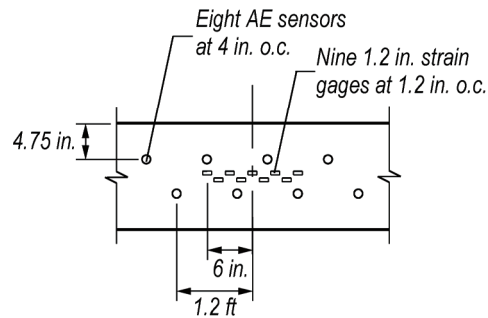


Figure 53. Strain gage and AE sensor layout along girder bottom.

## 7.5 RESULTS AND DISCUSSION

Typical load-deflection behavior observed for the B5x girders is shown in Figure 54. A visible crack was first observed during cycle 3. This cracking was associated with a loss in stiffness as indicated by a relatively sudden slope change. Prior to cracking, the load-deflection plots were linear. A cracking load of 48 kip was determined as the intersection of the bilinear curves as was done with the IT and piles. Cracking was first visually noted at 51 kip.

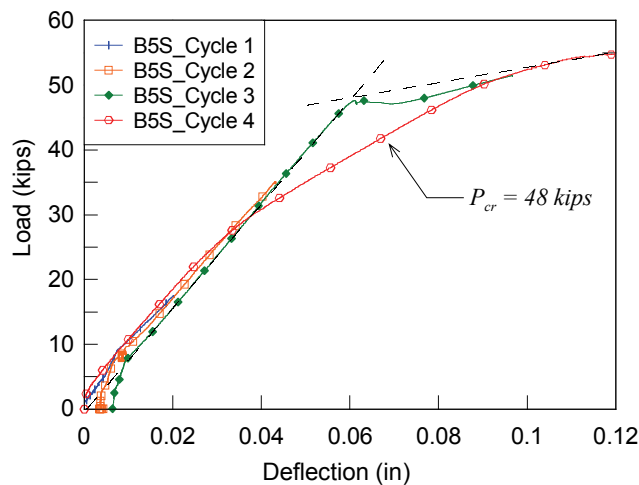


Figure 54. Typical Load-deflection behavior (B5S)

A plot typical of girders reinforced with 0.6 inch strand is given in Figure 55 for B6S. For girders with 0.6 inch strand the change in slope at structural cracking is more gradual than it was for those with 0.5 inch strand. This is likely due to the greater area of prestressing steel and larger prestressing force used in B6S, B6M and B6L.

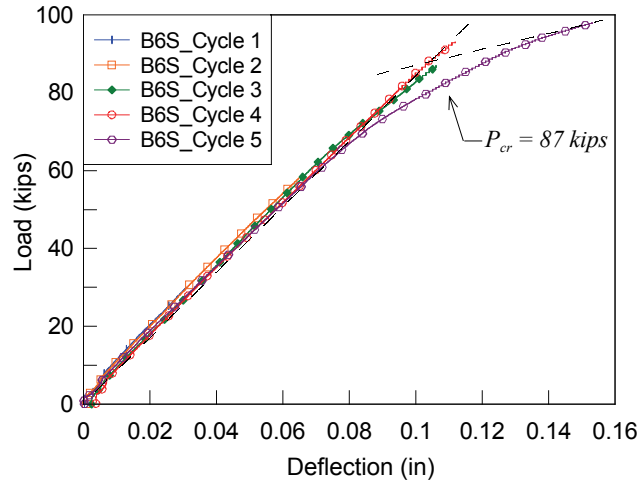


Figure 55. Typical Load-deflection behavior (B6S)

Figure 56 shows the cracking moments determined from the load-deflection plot and cracking noted visually. The cracking moment is the total moment present when the crack is first detected. This includes the self weight of both the precast girder and cast-in-place deck and the superimposed load from the hydraulic jack. This was done to determine how closely load-deflection results supported visual observation. Load-deflection cracking moment and visual cracking moment show close agreement. Generally, the visible cracking moment is slightly larger than the cracking moment determined from the load deflection plot. The chart also shows that as the area of strand and effective prestress increase, the cracking moment increases.

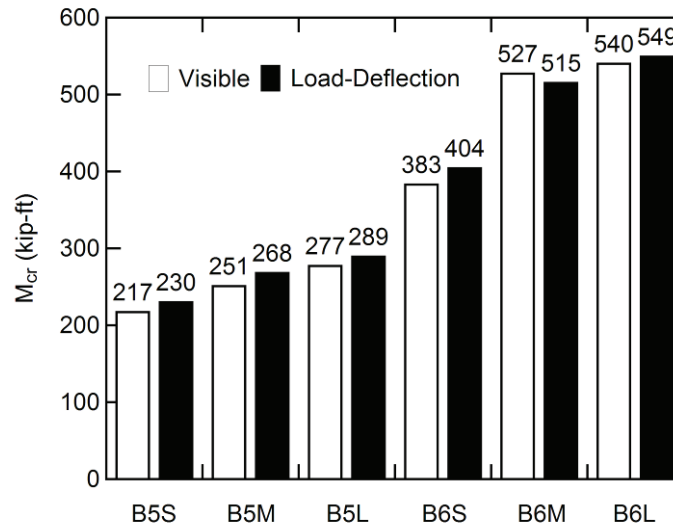


Figure 56. Measured cracking moment from load-deflection data and visual documentation

## 7.6 EFFECTIVE PRESTRESS

VWSG readings were taken prior to, during, and after detensioning to measure the compressive strain in the concrete caused by the prestressing on the section at the time of detensioning, which will also allow an estimate of elastic losses resulting from shortening. VWSG readings were also taken just prior to testing to estimate the time-dependent losses that occurred since prestressing the girders.

Strain readings were taken both before and after detensioning for both sets of girders. In addition, continuous readings were taken of the B6x girders through the detensioning process (Figure 57). The section with the largest prestress force (B6L) had the largest strain followed by B6M and B6S, respectively. The short term losses measured with the VWSG are given in Table 5. The change in tendon stress was calculated based on the differential strain readings and Young's modulus of the strand. The percentages reported in the table are relative to the initial prestress, which was  $0.5f_{pu}$  and  $0.74f_{pu}$  for B5x and B6x, respectively. Elastic losses were calculated using the PCI method (Zia et al. 1979) for estimating losses and are presented for comparison.

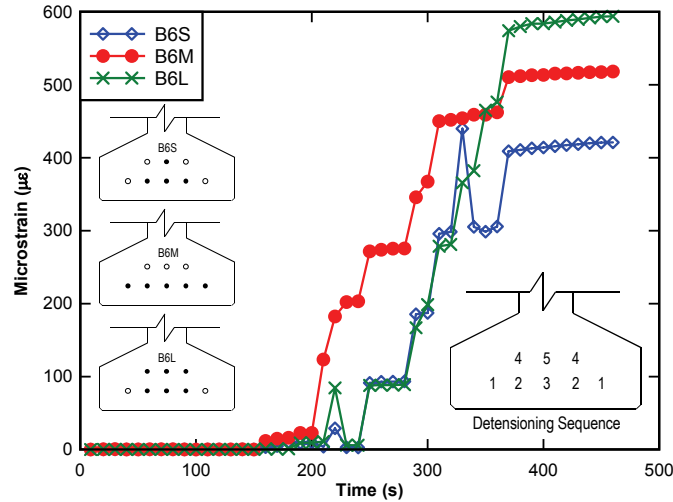


Figure 57. VWSG readings during prestress transfer to girders prestressed with 0.6-in. strand

Table 5. Measured short-term prestress loss from VWSG (% of initial prestress)

Girder	Measured	Calculated	Measured/Calculated
B5S	4.2	4.6	0.92
B5M	6.6	6.4	1.03
B5L	7.1	6.8	1.04
B6S	6.0	6.3	0.95
B6M	7.4	7.5	0.99
B6L	8.5	8.7	0.98

The total losses at the time of the load test were estimated from the strain gage data in a similar manner as the elastic losses. The change in strain measured by VWSG from just prior to release to just prior to load testing were measured and converted to stress, which is presented as a percentage of the initial prestress in Figure 58 as VSWG. The age indicates the number of days from prestress release to testing. For comparison, the losses calculated using the decompression method are also shown. While the B6x specimens provide comparable results between the VWSG and decompression measurements, the B5x specimens do not. Of the three B6x specimens, B6L shows the highest loss at 16.9% with a slight trend downward as the prestressing force is reduced. This downward trend continues for the VWSG readings on B5x. The decompression measurements, however, show a marked increase in loss as the prestress force is decreased.

It is not clear why the VWSG measurements gave such different results from the decompression measurements for B5x. The decompression test is an indirect measurement of the

prestress force and requires some subjectivity in determining the load required to open the crack. Furthermore, the crack opening is assumed to correspond with a zero stress state in the bottom fiber where gross section properties are then used to calculate a theoretical crack opening. Conversely, VWSG are a direct measure of the strain in the concrete at the centroid of the tendon. Long term and short term changes in the strain of the concrete are reflected directly in the strain readings from the strain gages. The only assumption required is that of perfect bond between the prestressing strand and concrete. If the concrete is uncracked, then the strain in the concrete and steel are likely to be the very close. Consequently, the VWSG were the preferred method of measuring losses in this research and the values obtained from this method were used for further analysis. As an added confirmation, the losses were estimated using the PCI method (Figure 59). These values are for the life of the structure, which is why they are larger than those of the I girder at an approximate age of 100 days. The trend of the calculated losses, however, follows that of the VWSG rather than that of the decompression test, lending further confidence in the VWSG data.

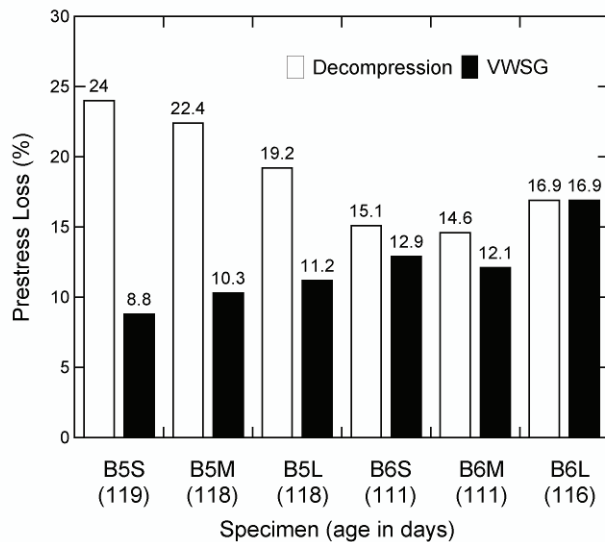


Figure 58. Measured total prestress loss as a percentage of the initial prestress.

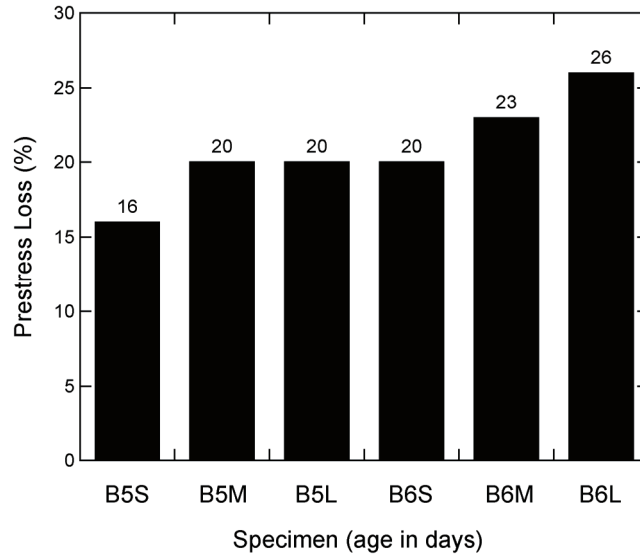


Figure 59. Estimate losses using PCI method.

### 7.7 STRAIN AND AE RESULTS

Similar to the results of the pile tests, onset of strain nonlinearity and the occurrence of the Felicity Effect occurred at similar load levels during cyclic testing. The nonlinearity combined with the Felicity Effect was an indication that microcracking had initiated. The same method that was used for both the piles and girders. For the three girders prestressed with 0.5-inch strand, AE energy was minimal until the onset of strain nonlinearity and the subsequent load cycle revealed the Felicity Effect (Figure 60). For the three more heavily prestressed girders with 0.6-inch strand, energy was observed during all load cycles. The Felicity Effect, however, consistently occurred during the loading cycle after strain nonlinearity was first observed (Figure 61).

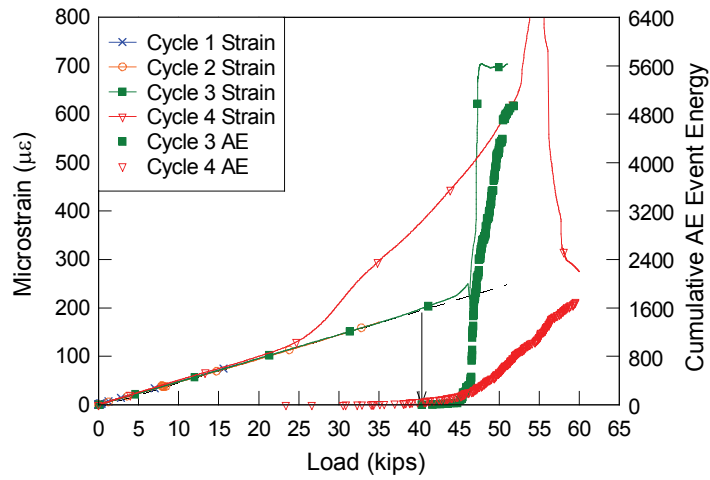


Figure 60. Microstrain and AE Energy vs Applied load for B5S

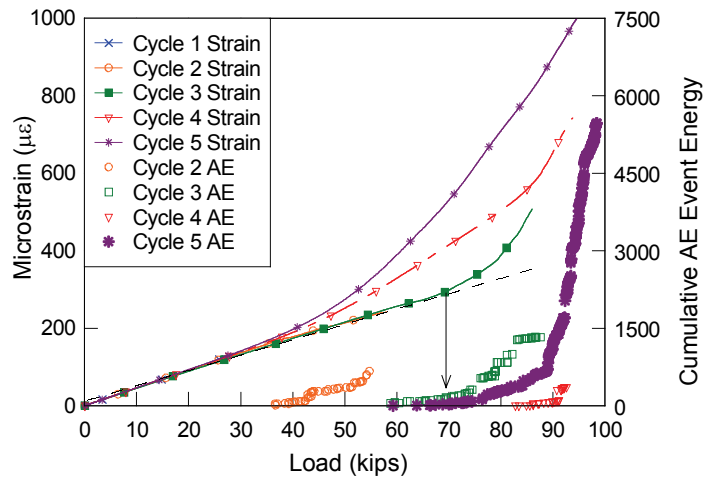


Figure 61. Microstrain and AE Energy vs. Applied load for B6S

## 8 MICROCRACK ACCUMULATION

In Chapter 6 flexural tests of pile cut-offs from a construction project were reported. Five of the ten tests were conducted using cyclic loading. This ensured that both strain and AE data detected the initiation of microcracking in the piles. In Chapter 7 flexural tests on six girders with the same cross section but varying prestressing force and steel quantities were also covered. The behavior for both the piles and girders was similar; the load-strain behavior of the concrete in the precompressed tensile zone was initially linear. When sufficient net tension was applied, the strain data indicated a softening of the concrete due to initiation of microcracking. AE activity increased markedly at these same stress levels, confirming the distributed damage in the concrete caused by the microcracking. Ultimately, as sufficient microcracking accumulated, a single or multiple visible structural cracks formed. As noted previously, the stress range over which the microcracking accumulated varied among the specimens. Determining the extent of microcrack accumulation and how it varies between girders with varying parameters is the focus of this chapter.

Figure 62 shows strain and AE data from test B5S. The net extreme fiber stress ( $f_t$ ) in the bottom of the girder or pile was calculated from the applied load (including self weight) assuming elastic theory. This stress was then reduced by the measured effective compressive prestress determined from the VWSG data for the girders and the decompression test data for the piles. The calculated stress was then normalized by the square root of the average cylinder strength of that specimen on the day of testing ( $f'_c$ ).

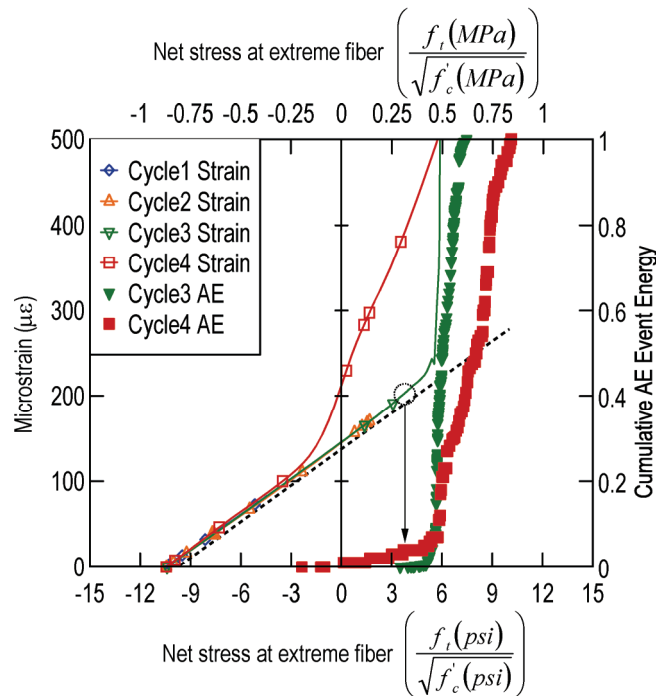


Figure 62. Plot to show how onset of material damage was determined (B5S)

Using these plots, two distinct stress levels were determined for each specimen (plots included in Appendix D). One was the stress level associated with initiation of microcracking and was determined by using the onset of strain nonlinearity and accumulation of AE event energy. The other stress was associated with structural cracking and was defined as the stress the intersection of the bilinear load-deflection curves and visual detection of cracking.

The onset of strain nonlinearity usually occurred during the cycle prior to the observation of the Felicity effect in the AE event data. For the lightly prestressed girders (B5x), AE event energy typically did not begin accumulating prior to the cycle where strain nonlinearity was first observed. For the heavily prestressed girders (B6x) and piles, some instances of relatively low energy events were noted during earlier loading cycles, but were not considered indicative of microcracking because subsequent load cycles exhibited the Kaiser effect. Figure 62 shows that the onset of strain nonlinearity (circled) occurred in conjunction with the rise of AE cumulative energy (also circled). The simultaneous occurrence of increased AE activity with the initiation of strain nonlinearity is believed to indicate the beginning of material damage. For this particular girder (B5S), no AE energy was noted prior to the load cycle where strain nonlinearity was

detected. For the cycle following this onset, AE event energy began accumulating prior to the previous maximum stress reached during the prior cycle, demonstrating the Felicity effect (material damage). In instances where girders or piles had a relatively greater effective prestress, AE energy was observed in early load cycles but upon reloading did not indicate any material damage had occurred by demonstrating the Kaiser effect.

Structural cracking was determined for both the piles and girders as the net stress level at the intersection of the load-deflection curves. For the girders, this stress level was in reasonable agreement with the stress level at which a crack was visually detected. These data were not documented for the piles. The vertical line at a stress of  $6.1\sqrt{f'_c}$  is the stress level of structural cracking by the load-deflection approach.

Figure 63 graphically illustrates the stress at initiation of microcracking and at the formation of a structural crack. The difference between the initiation of microcracking and structural cracking is the stress range over which microcracking is accumulating until sufficient cracking has occurred to coalesce into a single structural crack. The results of this analysis are shown in Table 6. The microcracking accumulation was calculated using the bilinear intersection of the load-deflection curve for the girders and piles. The table also includes the measured stress accumulation from the visible cracking load for the girders as additional verification of the load-deflection approach measurements.

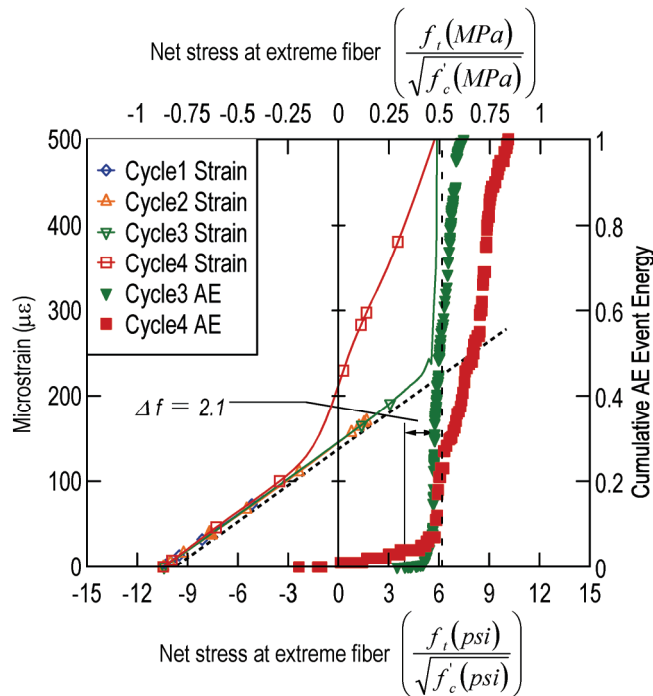


Figure 63. Stress range of material damage through structural cracking (B5S)

For the girders, the net stress determined as structural cracking from the load-deflection data was slightly less than that determined from the noted onset of visible cracking for all B5 girders and B6S. This might be due to the fact that load-deflection curves have been found to have a sharper bilinear intersection than heavily prestressed sections (Warwaruk et. al., 1962), causing the net structural cracking stress to be more easily discerned from the load-deflection plots than by visual detection. For more heavily prestressed sections, like B6M and B6L, the net structural cracking stress determined from visual observation was observed at a lower stress than what was determined from the load-deflection curves, indicating a longer, more rounded load deflection response.

The results shown in the table are presented graphically in Figure 64. The y-axis is the normalized net stress on the bottom fiber of the specimen. The top of the plot shows the specimen designation and the bottom of the plot shows the initial precompression in the bottom fiber in terms of the specified concrete strength. The piles have relatively low prestress values. The piles, however, were concentrically prestressed so the precompression did not vary across the height of the cross section as it did with the girders. Each bar in the plot represents either a

pile or girder specimen in which the bottom of the bar is the stress at which microcracking was initially detected and the top of the bar is the stress at which structural cracking formed. The length of the bar is then the stress range over which the microcracking accumulates prior to a single crack forming.

Table 6. Results of microcracking and structural cracking analysis on girders and piles ( $f_t/\sqrt{f'_c}$ (psi)).

ID	Microcracking initiation	Structural cracking by load-deflection approach		Structural cracking by visible cracking approach																			
		Stress	Stress range	Stress	Stress range																		
B5S	4.0	6.1	2.1	7.1	3.1																		
B5M	2.5	5.4	2.9	6.8	4.3																		
B5L	2.5	6.2	3.7	7.2	4.7																		
B6S	1.9	7.6	5.7	9.3	7.4																		
B6M	-0.1	12.1	12.2	11.1	11.2																		
B6L	-0.1	14.0	14.1	12.6	12.7																		
VV22 BFS	-2.8	6.6	9.4	n/a	n/a																		
VV18 SF	-1.5	7.9	9.4	n/a	n/a </tr <tr> <td>VV30 MET</td> <td>2.6</td> <td>10.1</td> <td>7.5</td> <td>n/a</td> <td>n/a</td> </tr> <tr> <td>VV4 UFA</td> <td>0</td> <td>9.4</td> <td>9.4</td> <td>n/a</td> <td>n/a</td> </tr> <tr> <td>VV10 FA</td> <td>0</td> <td>8.9</td> <td>8.9</td> <td>n/a</td> <td>n/a</td> </tr>	VV30 MET	2.6	10.1	7.5	n/a	n/a	VV4 UFA	0	9.4	9.4	n/a	n/a	VV10 FA	0	8.9	8.9	n/a	n/a
VV30 MET	2.6	10.1	7.5	n/a	n/a																		
VV4 UFA	0	9.4	9.4	n/a	n/a																		
VV10 FA	0	8.9	8.9	n/a	n/a																		

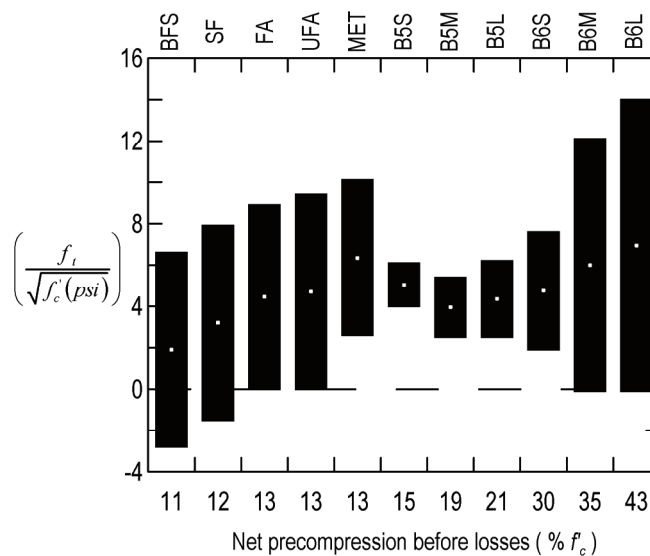


Figure 64. Stress range over which microcracking occurs prior to structural cracking

The piles all had similar precompression and similar damage ranges though the microcrack initiation stress varied. The stress range for the girders, however, increased markedly as the precompression increased. Similarly, the stress at structural cracking increased while the microcracking initiation stress decreased as the precompression increased. This may be due to the technique used to determine the effective prestressed force. For the girders, the effective prestress values using the decompression method were typically lower than those measured by the VWSG (Figure 58). If the measured prestress force reported in Figure 36 overestimated the force, then the microcracking stress would increase proportionately for each pile. Another possible reason for the relatively lower microcrack initiation stresses when compared to those of the girders is that some cracking may have occurred during the removal of the piles. No visible cracks, however, were noted prior to the pile tests indicating that significant microcracking may have already taken place.

There are little data in the literature that report both initiation of microcracking and structural cracking loads to provide a comparison with the results of the present work. Kaplan 1963, however, published both the initiation of microcracking and ultimate capacity results for modulus of rupture beam tests conducted to compare the effect of aggregate volume. Based on an assumed concrete strength of 3000 to 4000 psi, the reported stress ranges ranged from  $3\sqrt{f'_c}$  (psi) to  $4\sqrt{f'_c}$  (psi), which agrees with the stress ranges for the B5x girders. B6x girders, however, with the larger effective prestressing have considerably larger stress ranges. The prestressing appears to decrease the microcracking initiation stress and also to distinctly increase the structural cracking stress. One possible explanation is that the larger sustained compressive stress and attendant creep strain retards the early growth of microcracks due to drying. Microcracks that have already formed may also be blunted or even closed by the creep strains. McNeely and Lash 1963, however, concluded that precompression had no effect on the modulus of rupture of the concrete. Their tests consisted of precompressing 3 x 3 x 14.5 in. beams by 1000 and 2000 psi for 7 and 28 days. Following this period, the precompression was removed and the beams were tested in flexure. When compared to the control beams, no significant effect on the modulus of rupture values was noted. The tests in the present work, however, were conducted on deeper sections that had precompression levels from 2200 to 3200 psi. It's not clear how these differences might influence the effect of the microcracks.

Another explanation for the difference in stress range between the B5x and B6x girders is the restraint provided by the bottom bonded prestressing strands. Both B5M and B6M, however, contained five prestressing strands in the same level. Yet, the stress range for B6M was nearly twice that of B5M.

Differential drying shrinkage strains can cause large tensile strains to occur at the surface of the concrete. For pretensioned girders, this is particularly true of the bottom of the girder. The bottom of the girder is exposed to drying shrinkage only after the prestressing has been released and the girder has cambered. This exposes precompressed concrete to the drying shrinkage tensile strains that can seriously impair the precompression applied by the prestressing. Although this is generally understood not to penetrate too deeply into the concrete (Samaha and Hover 1992), it is apparent that their presence has affected the microcracking behavior of the girders in the present research.

McGinnis and Pessiki 2007 conducted core tests to determine stresses in existing concrete members. They evaluated the effect of differential drying shrinkage on the stresses at the surface of the girder and also concluded that the drying shrinkage stresses dissipate over time. Hossain and Weiss 2006 and McLaskey et al. 2007, however, have measured AE from concrete undergoing drying shrinkage, and found that microcracking is occurring in the regions which are undergoing restrained drying shrinkage. This microcracking is not likely to be reversible unless sufficient moisture is present to allow autogenous healing to occur over time.

Drying shrinkage can also be restrained by reinforcement. B5S and B6S have three strands in the bottom; B5M and B6M have five; and B5L and B6L have four. For both the B5 and B6 specimens, as the number of bottom strands increased from 3 to 5, the microcracking stress decreased a proportional amount, indicating that the drying shrinkage is restrained less in the 3-strand specimen than the 5-strand specimen. This behavior is reflected in the microcracking initiation stress. The specimens with 3 strands in the bottom had microcracking initiate at a higher stress than those of the specimens with 4 or 5 strands in the bottom.

In recent years, considerable work has been conducted on the durability of concrete that has sustained microcracking damage from compressive stresses (Samaha and Hover 1992 is one early example). These studies have confirmed an increase of permeability in concrete in which microcracks have formed due to compressive loading. No studies, however, have been found that have examined the microcracking of precompressed concrete that is routinely stressed into

net tension, such as the precompressed tensile zone of pretensioned concrete girders. The work in this research has shown that the stress range over which microcracking occurs is relatively sensitive to the level of precompression in the concrete. The durability implications of the magnitude of this stress range are not clear.

AASHTO recommends that the minimum reinforcement requirements be calculated using  $11.7\sqrt{f'_c}$ (psi). FDOT, however, allows the use of  $7.5\sqrt{f'_c}$ (psi) for Florida bridges. The structural cracking stress for the test girders ranged from approximately  $6\sqrt{f'_c}$ (psi) to  $14\sqrt{f'_c}$ (psi). Minimum reinforcement requirements typically control when the quantity of bonded prestressing required for strength and serviceability is low. This will, in turn result in a low effective prestress force. Girders with lower effective prestress values had structural cracking occur at lower stresses ( $6.1\sqrt{f'_c}$ (psi) to  $7.6\sqrt{f'_c}$ (psi)) than those of the girders with heavier prestressing ( $12.1\sqrt{f'_c}$ (psi) and  $14\sqrt{f'_c}$ (psi)). Similarly, the piles, which had lower effective prestress at the extreme tension fiber, were found to reach structural cracking at  $6.6\sqrt{f'_c}$ (psi) to  $10.1\sqrt{f'_c}$ (psi).

Modulus of rupture data have been used to provide justification for increasing the minimum reinforcement requirements from 7.5 to 11.7 in AASHTO. MoR strengths are generally higher than direct tension strengths because of the strain gradient. As the extreme fiber in a MoR test reaches the allowable tensile strength, two things are happening. One is that the concrete at the extreme fiber is undergoing microcracking as measured in the present research. The other is that the areas that are under higher stresses are stiffened by the concrete in the areas that have lower tensile stress-and less microcracking. This behavior results in a higher apparent tensile strength for MoR than for direct tension. Consequently, cracking strength is also a function of the strain gradient.

For members in service, the strain gradient is between that of the modulus of rupture and a direct tension test. Figure 65 illustrates the effect of the member depth and applied moment or tension on the stress state at the extreme fiber in tension. For modulus of rupture specimens that are typically four to six inches in depth, the strain gradient is steep relative to that of the much deeper girders used in this research or those used as bridge girders. The extreme case is an element under direct tension where the entire cross section is under tension without the beneficial effect of areas that are under less tension.

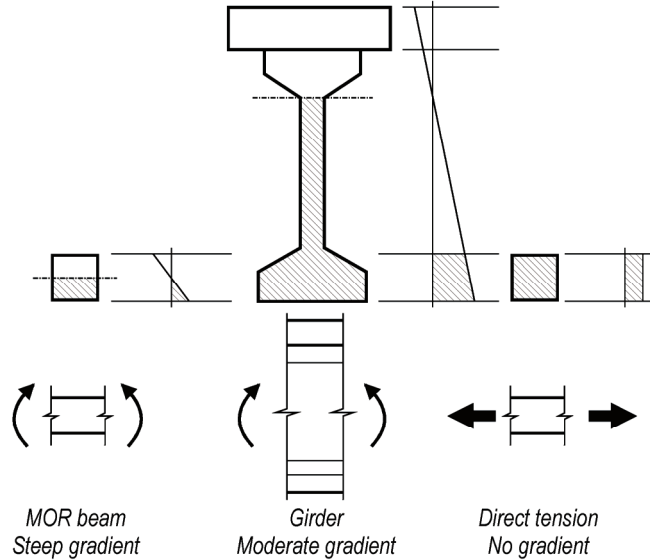


Figure 65. Effect of strain gradient on cracking moment.

The strain gradient effect can be seen when comparing the modulus of rupture test results shown in Table 7 to the results in Table 6 from the pile and girder tests. Table 7 shows the results of the modulus of rupture tests for the girders at 28-day and on the day of flexural testing normalized by the square root of the compressive strength results from those same times. The only results available for the piles are the 28-day tests. The girders with lower effective prestress values had structural cracking occur at lower stresses ( $6.1\sqrt{f'_c}$ (psi) to  $7.6\sqrt{f'_c}$ (psi)) than indicated by the test day results from Table 7. Similarly, the piles were found to reach structural cracking at  $6.6\sqrt{f'_c}$ (psi) to  $10.1\sqrt{f'_c}$ (psi), yet the modulus of rupture values ranged from  $9.7\sqrt{f'_c}$ (psi) to  $14.5\sqrt{f'_c}$ (psi).

Table 7. Coefficients for modulus of rupture and cylinder tests from girder concrete.

ID	MoR (psi)/ $\sqrt{f'_c}$ (psi)	
	28-day	Test day
B5x	7.4	9.5
B6x	6.6	9.0
BFS	14.5	n/a
SF	13.6	n/a
FA	9.7	n/a
UFA	10.2	n/a
MET	11.5	n/a

For fully prestressed sections AASHTO limits the tensile stresses in the precompressed tensile zone to  $3\sqrt{f'_c}$ . This value is at the lower end of the microcracking stress range for the I-girders. Based on the results of this testing it is recommended that this provision be retained in the design specifications for severe exposure conditions. The effect of service microcracking on the durability of the concrete is not clear.

## 9 SUMMARY AND CONCLUSIONS

This report presents research on the evaluation of service flexural stresses and cracking moment in prestressed concrete members and on the minimum reinforcement requirements that are currently controlled by the flexural cracking moment. A parametric study was conducted on hollow core, Florida bulb tee, and segmental box girders to evaluate the current minimum steel provisions. New minimum reinforcement provisions were then derived based on recommendations by Leonhardt 1964. These reinforcement provisions were then compared to the existing ACI and AASHTO provisions using the sections from the parametric study. Two inverted tee sections were constructed and tested to evaluate the existing minimum reinforcement requirements. Ten precast, pretensioned pile cut offs from an FDOT construction project were salvaged and tested to determine cracking moment and to evaluate cracking behavior. Half of the piles were loaded monotonically to cracking and half were loaded cyclically to cracking. Cyclic loading was used in conjunction with AE monitoring and strain gage data to determine the initiation of microcracking. Structural cracking was determined using visual identification combined with interpolation from the load deflection plot. Six precast, pretensioned I-girders were constructed and tested cyclically to determine cracking moment and evaluate cracking behavior. The following are significant findings from this research:

- Current minimum reinforcement requirements can, in some cases, result in quantities that are practically unattainable when considering the contribution of bonded prestressing steel. New minimum reinforcement requirements were derived and compared to existing reinforcement requirements.
- In both the pile and girder tests, two levels of cracking were identified: microcracking and structural cracking.
- As the girders were loaded, microcracking was found to occur at lower net stresses (zero to  $4\sqrt{f'_c}$  (psi)) than would be calculated from the estimated modulus of rupture and precompression. Some of the pile specimens indicated microcracking when the section was still under net compression. This microcracking was detected using a combination of AE and strain gage data and is thought to be the result of differential drying shrinkage, which may cause irreversible microcracking near the surface of the concrete. The current AASHTO

provisions limiting tensile stress (to no more than  $3\sqrt{f'_c}$ (psi)) in harsh environments appear to be adequate in light of the girder test results. The durability implications of this microcracking and the stress range over which it occurs, however, are not clear.

- Using the strain gage data from the extreme tension fiber, the Felicity effect (related to the AE) was confirmed to be an indication of microcracking in the precompressed tensile zone.
- Structural cracking for the girders and piles occurred at tensile stresses that ranged from approximately  $6\sqrt{f'_c}$ (psi) to  $14\sqrt{f'_c}$ (psi) and  $6.1\sqrt{f'_c}$ (psi) to  $10.1\sqrt{f'_c}$ (psi), respectively. The ranges for the specimens that had lower effective prestressing were generally lower than the respective modulus of rupture values

## 10 RECOMMENDATIONS

The following equation is recommended for use in calculating the minimum reinforcement requirements for prestressed concrete. This equation was derived based on recommendations by Leonhardt 1964 and is intended to be universally applicable to all structural concrete. It has not, however, been compared systematically to the existing requirements and so is not recommended for use with nonprestressed concrete. Based on the analysis presented in Chapter 8 and the successful use  $7.5\sqrt{f'_c}$  (psi) under previous AASHTO and current ACI 318 design requirements, the minimum reinforcement requirements shown below were derived using  $\alpha = 7.5$ . Equation 13 was derived for units of psi and Equation 14 for units of ksi.

$$A_{ps,min} \geq \frac{4.5\sqrt{f'_c}A_{ct} - A_s f_y}{(f_{ps} - f_{pe})} \quad \text{Equation 13}$$

$A_{ps,min}$  is the minimum required area of bonded prestressing steel in flexural tension zone (in.<sup>2</sup>),

$A_s$  is the area of nonprestressed longitudinal tension reinforcement (in.<sup>2</sup>),

$A_{ct}$  is the portion of the gross cross-section under tension from the applied moment (in.<sup>2</sup>),

$f'_c$  is the specified concrete strength (psi),

$f_{se}$  is the effective prestress in the prestressing steel (psi),

$f_{ps}$  is the stress in prestressing steel at nominal flexural strength (psi),

$f_y$  is the specified yield strength of the nonprestressed flexural reinforcement (psi).

$$A_{ps,min} \geq \frac{0.15\sqrt{f'_c}A_{ct} - A_s f_y}{(f_{ps} - f_{pe})} \quad \text{Equation 14}$$

$A_{ps,min}$  is the minimum required area of bonded prestressing steel in flexural tension zone (in.<sup>2</sup>),

$A_s$  is the area of nonprestressed longitudinal tension reinforcement (in.<sup>2</sup>),

$A_{ct}$  is the portion of the gross cross-section under tension from the applied moment (in.<sup>2</sup>),

$f_c$  is the specified concrete strength (ksi),

$f_{se}$  is the effective prestress in the prestressing steel (ksi),

$f_{ps}$  is the stress in prestressing steel at nominal flexural strength (ksi),

$f_y$  is the specified yield strength of the nonprestressed flexural reinforcement (ksi).

## 11 FUTURE RESEARCH

As indicated in the report, the durability implication of the microcracking in the precompressed tensile zone of girders is not clear. Differential drying shrinkage is an issue on structural elements of most any size. If sufficiently massive, differential thermal strains will also develop. In general, the differential shrinkage and temperature strains will be transverse to the concrete surface, which will result in microcracking that is perpendicular to the surface.

Microcracking has been confirmed to be caused by both compressive and tensile strains. Furthermore, sufficient microcracking increases the permeability of the concrete, which will reduce the durability of prestressed concrete bridge elements placed in aggressive environments. In particular, piles and other elements placed in proximity of salt water. In the interest of long-term durability of concrete susceptible to microcracking, research should be conducted on the effect that microcracking has on the permeability of the concrete.

Minimum steel reinforcement requirements are intended to prevent a catastrophic failure in a flexural member when the strength of the reinforcement is less than the tensile strength of the concrete. The requirements were originally intended for use when a section size is disproportionately large due to architectural or other functional reasons rather than strength. Experimental validation of minimum steel reinforcement requirements, however, is difficult. When a structural crack forms, the section properties and stiffness change abruptly. The mass of the member and load cause a dynamic effect that is difficult to capture when using displacement controlled test equipment. Experimental work that captures the load control behavior of the structural system would provide much needed validation of minimum steel reinforcement requirements.

## 12 REFERENCES

AASHTO. (2007). *AASHTO LRFD bridge design specifications, 4th edition with 2007 interim revisions*. American Association of State Highway and Transportation Officials, Washington, D. C.

Abels, P. W., and Hu, C. H. (1971). "Flexural microcracking in unreinforced concrete beams." *ACI Journal*, 68(10), 779-787.

ACI 318-08. (2008). *Building code requirements for structural concrete and commentary*. American Concrete Institute, Farmington Hills, MI.

ACI 318-63. (1963). *Building code requirements for reinforced concrete*. American Concrete Institute, Detroit, MI.

ACI 318-83. (1986). *Building code requirements for reinforced concrete*. American Concrete Institute, Detroit, MI.

ACI 318-92. (1992). *Building code requirements for structural concrete and commentary*. American Concrete Institute, Farmington Hills, MI.

ACI 318-95. (1995). *Building code requirements for structural concrete and commentary*. American Concrete Institute, Farmington Hills, MI.

ACI Committee 501. (1936). "Building regulations for reinforced concrete." *ACI Journal-Proceedings*, 32(3), 407-444.

ACI-ASCE Committee 323. (2004). "Landmark series: tentative recommendations for prestressed concrete." *Concrete International*, 26(3), 95-131.

ASTM E1316. (2009). *Standard terminology for nondestructive examinations* ASTM International, West Conshohocken, PA.

Bureau of Public Roads. (1954). *Criteria for prestressed concrete bridges*. U. S. Government Printing Office, Washington, D. C.

Carrasquillo, R. L., Slate, F. O., and Nilson, A. H. (1981). "Microcracking behavior of high strength concrete subject to short-term loading." *ACI Journal*, 78(3), 179-186.

Evans, R. H., and Marathe, M. S. (1968). "Microcracking and stress-strain curves for concrete in tension." *Materials and Structures*, 1(1), 61-64.

FDOT. (2009). *Structures design guidelines*. Florida Department of Transportation, Tallahassee, FL.

Freyermuth, C. L., and Aalami, B. O. (1997). "Unified minimum flexural reinforcement requirements for reinforced and prestressed concrete members." *ACI Struct.J.*, 94(4), 409-420.

Ghosh, S. K. (1986). "Exceptions of precast prestressed concrete members to minimum reinforcement requirements." *PCI Journal*, 31(6), 74-91.

Guo, Z., and Zhang, X. (1987). "Investigation of complete stress-deformation curves for concrete in tension." *ACI Mater.J.*, 84(4), 278-285.

Hearn, S. W., and Shield, C. K. (1997). "Acoustic emission monitoring as a nondestructive testing technique in reinforced concrete." *ACI Mater.J.*, 94(6), 510-519.

Hossain, A. B., and Weiss, J. (2006). "The role of specimen geometry and boundary conditions on stress development and cracking in the restrained ring test." *Cement and Concrete Research*, 36(1), 189-199.

Hsu, T. T. C., Slate, F. O., Sturman, G. M., and Winter, G. (1963). "Microcracking of plain concrete and the shape of the stress-strain curve." *ACI Journal*, 60(2), 209-224.

Kaplan, M. F. (1963). "Strains and stresses of concrete at initiation of cracking and near failure." *ACI Journal*, 60(7), 853-880.

Khan, A. A., Cook, W. D., and Mitchell, D. (1996). "Tensile strength of low, medium, and high-strength concretes at early ages." *ACI Mater.J.*, 93(5), 487-493.

Kleymann, M., Girgis, A., Tadros, M. K., and Vranek, C. J. (2006). "Open forum problems and solutions - minimum reinforcement in flexural members." *PCI Journal*, 146-148.

Labuz, J. F., Cattaneo, S., and Chen, L. (2001). "Acoustic emission at failure in quasi-brittle materials." *Construction and Building Materials*, 15(5-6), 225-233.

Leonhardt, F. (1964). *Prestressed concrete design and construction*. Wilhelm Ernst & Sohn, Germany.

McGinnis, M. J., and Pessiki, S. (2007). "Differential shrinkage effects in the core-drilling method." *Magazine of Concrete Research*, 59(3), 155-164.

McLaskey, G. C., Glaser, S. D., and Grosse, C. U. (2007). "Integrating broad-band high-fidelity acoustic emission sensors and array processing to study drying shrinkage cracking in concrete." *Sensors and Smart Structures Technologies for Civil, Mechanical, and Aerospace Systems 2007*, SPIE, San Diego, CA, .

McNeely, D. J., and Lash, S. D. (1963). "Tensile strength of concrete." *ACI Journal*, 60(6), 751-761.

Nielsen, J., and Griffin, D. F. (1977). "Acoustic emission of plain concrete." *Journal of Testing and Evaluation*, 5(6), 476-483.

Oh, B. H., Kim, K. S., and Kim, E. J. (2000). "Identification of cracking damages of concrete structures using acoustic emission." *SP-193: Repair, Rehabilitation, & Maint of Conc Struct, & Innovations in Design & Constr: Proc 4th Intl Conf (Seoul Korea-2000)*, American Concrete Institute, 195-210.

Oladapo, I. O. (1968). "Relationship between moment capacity at flexural cracking and at ultimate in prestressed concrete beams." *ACI Journal*, 65(10), 863-875.

Ridge, A. R., and Ziehl, P. H. (2006). "Evaluation of strengthened reinforced concrete beams: Cyclic load test and acoustic emission methods." *ACI Struct.J.*, 103(6), 832-841.

Samaha, H. R., and Hover, K. C. (1992). "Influence of microcracking on the mass transport properties of concrete." *ACI Mater.J.*, 89(4), 416-424.

Shah, S. P., and Chandra, S. (1968). "Critical stress, volume change, and microcracking of concrete." *ACI Journal*, 65(9), 770-781.

Smadi, M. M., and Slate, F. O. (1989). "Microcracking of high and normal strength concretes under short- and long-term loadings." *ACI Mater.J.*, 86(2), 117-127.

Sturman, G. M., Shah, S. P., and Winter, G. (1964). "Microcracking and inelastic behavior of concrete." *Proceedings of International Symposium on Flexural Mechanics of Reinforced Concrete*, 473-499.

Walker, S., and Bloem, D. L. (1960). "Effects of aggregate size on properties of concrete." *ACI Journal*, 32(3), 283-298.

Zia, P., Preston, H. K., Scott, N. L., and Workman, E. B. (1979). "Estimating prestress losses." *Concrete International*, 1(6), 32-38.

# APPENDIX A – INVERTED TEE DATA

B:279

APPROVED  
Dis. TRACT'S  
MATERIALS & RESEARCH

*Carole Murray*

ISSUED: *J. Fitzgerald*  
REVIEWED: B. PRICE  
DATE: 10/15/04  
MIX NO.: 05-1014

## CONCRETE MIX DESIGN

CONCRETE SUPPLIER: DURASTRESS  
ADDRESS: 11325 COUNTY ROAD 44 EAST LEESBURG, FLORIDA 34788  
PLANT LOCATION: LEESBURG TELEPHONE NO: 352/787-1422  
FDDT ASSIGNED PLANT NO.: 11-013 PROJECT NO: 24252315201  
DATE: 10/14/04 *23134025201*

CLASS CONCRETE: V SPECIAL (6000PSI)

## SOURCE OF MATERIALS

COARSE AGGREGATE:	ANDERSON COLUMBIA	GRADE:	78	S.G.(SSD):	2.710
FINE AGGREGATE :	FLORIDA ROCK	F.M.:	2.11	S.G.(SSD):	2.630
PIT NO.(COARSE) :	GA-555	TYPE:	CRUSHED GRANITE		
PIT NO.(FINE) :	36-491	TYPE:	SILICA SAND		
CEMENT :	SUWANEE AMERICAN (BRANFORD)	SPEC:	AASHTO M-85 TYPE II		
AIR ENTR.ADMIX :	DARAVAIR 1000	W.R. GRACE	SPEC: AASHTO M-154		
1ST ADMIX :	WRDA 50	W.R. GRACE	SPEC: AASHTO M-194 TYPE D		
2ND ADMIX :	ADVA 540	W.R. GRACE	SPEC: AASHTO M-194 TYPE F		
3RD ADMIX :	----	SPEC:	----		
FLY ASH :	ISG	FERNANDINA BEACH	SPEC: ASTM C-618 CLASS F		

HOT WEATHER MIX DESIGN 4 X 8 COMPRESSIVE STRENGTH 10740 PSI

CEMENT (Kg) LBS	775	SLUMP RANGE	:	5.50 TO 8.50 (mm)IN
COARSE AGG (Kg) LBS	1750	AIR CONTENT	:	1.0 % TO 5.0 %
FINE AGG (Kg) LBS	896	UNIT WEIGHT (WET):	145.1	(Kg/M3)PCF
AIR ENT ADMX (ML) OZ	3.0	W/C RATIO(PLANT):	0.35	(Kg/Kg)LBS/LB
1ST ADMIXTURE (ML) OZ	23.0	W/C RATIO (FIELD):	0.35	(Kg/Kg)LBS/LB
2ND ADMIX (ML) OZ	47.0	THEO YIELD	:	27.00 (M3)CU FT
3RD ADMIX (ML) OZ	0.0			
WATER (ML) GAL	39.30			
WATER (Kg) LBS	327.4			
FLY ASH (Kg) LBS	170			

CC:  
D. M. E. 5  
D. M. E. 1 & 7  
TEST FILE

PRODUCER TEST DATA  
CHLORIDE CDNT : 0.209 (kg/m3)LB/CY  
SLUMP : 7.50 (MM)IN  
AIR CONTENT : 2.90 %  
TEMPERATURE : 97 DEG (C)F  
COMPRESSIVE STRENGTH (MPA)PSI  
28 -DAY- 10410 -DAY-  
-DAY- -DAY-

PRODUCTION: PLEASE NOTIFY CHRISTINA O'NEILL PRIOR TO CASTING PH. (813)205-0348

**END ELEVATION**  
STRANDING NOT SHOWN FOR CLARITY

**END CROSS SECTION**  
STRANDING NOT SHOWN FOR CLARITY

**STRAND PATTERN & SHIELDING**

**BILL OF EMBED MATERIALS**  
FOR ONE MEMBER ONLY

BAR	SIZE	D.S. I.D. #	QTY.	LENGTH	REMARKS
BAR D	3	RE-BAR 3	24	2'-10"	SEE DIAGRAM
BAR K	4	RE-BAR 4	30	2'-2"	SEE DIAGRAM
BAR N	3/8"	270 STRAND	11	16' ± 5"	STRAIGHT
STRAND	9/16"	270 STRAND	11	16' ± 6"	STRAIGHT
PVC	3/4"		8	16'	STRAIGHT

**HANDLING & DUNNAGE DIAGRAM FOR INVERTED-T**  
TYP. EA. END OF ALL BEAMS

**ELEVATION**

**BENDING DIAGRAMS**  
ALL #3 BARS SHALL BE BENT AROUND A 1/4" DIA. PIN  
ALL #4 BARS SHALL BE BENT AROUND A 2" DIA. PIN  
NOTE: ALL DIMENSIONS ARE CUT TO OUT

**DETECTONING SEQUENCE**

**END SECTION**  
VIEWED IN THE DIRECTION OF STATIONING  
STRANDING NOT SHOWN FOR CLARITY

**END ELEVATION OF BEAM**

**SHIELDING LEGEND**

**INVERTED-T BEAM**

**BILL OF EMBED MATERIALS**  
FOR ONE MEMBER ONLY

MARK	WEIGHT	QTY.	LENGTH	BAR. P. #	BAR. P. # DIM	NOT RECD.	NOT RECD.
IT-S	4,000 #	1	16'			NOT RECD.	NOT RECD.
IT-OR	4,000 #	1	16'			NOT RECD.	NOT RECD.

**U F SSB**

REV.      DESCRIPTION      DATE      BY      CK

**DURA-STRESS Inc.**  
STRUCTURAL PRESTRESSED AND ARCHITECTURAL PRECAST CONCRETE PRODUCTS  
P.O. BOX 460778    LEESBURG, VA 20152    703-441-0778  
FAX: (552) 781-1222    TEL: (552) 781-0080

JOB NAME: \_\_\_\_\_  
LOCATION: \_\_\_\_\_  
ARCHITECT: \_\_\_\_\_  
ENGINEER: \_\_\_\_\_  
CONTRACTOR: \_\_\_\_\_  
PROJ. NO.: \_\_\_\_\_

DRAWING: \_\_\_\_\_  
CHK'D.: \_\_\_\_\_  
APPR.: \_\_\_\_\_  
DATE: \_\_\_\_\_  
RELEASED: \_\_\_\_\_

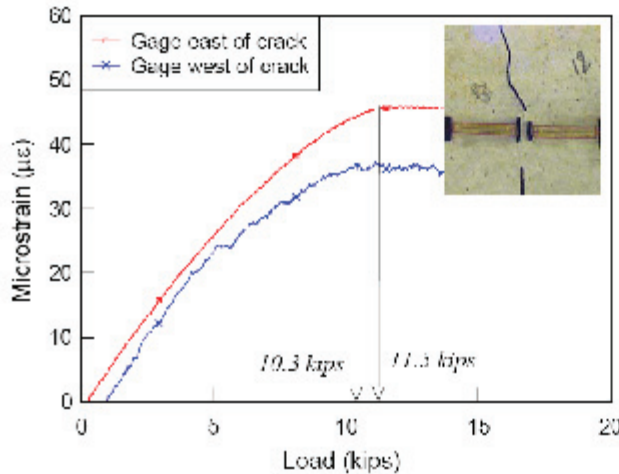
JOB NO.: \_\_\_\_\_

SHEET 4 OF 4

**Decompression Test to find effective prestress of IT\_S tested 12.11.2008**

UNITS...

kip := 1000lbf    psi := lbf ÷ in<sup>2</sup>    ksi := kip ÷ in<sup>2</sup>



*SPAN AND SECTION PROPERTIES...*

- $w_{dl} := 25 \frac{\text{kip}}{\text{ft}}$  (self-weight)
- $L := 15\text{ft}$  (span)
- $A := 240.69\text{in}^2$  (area)
- $y_t := 6.71\text{in}$  (centroid to bottom fiber)
- $I := 7.073 \times 10^3 \text{in}^4$  (moment of inertia)
- $e := 3.71\text{in}$  (prestress eccentricity)
- $r := \sqrt{I \div A}$  (radius of gyration)
- $S := I \div y_t$  (sxn modulus)

*DATA FROM DECOMPRESSION TESTS...*

$P_{dec} := 10.9 \cdot \text{kip}$  (average decompression load)     $x := 7.375\text{ft}$ (distance from crack position to nearest support)

*TOTAL MOMENT AT OBSERVED CRACK...*

$$M_{dl} := \frac{1}{2} \cdot [w_{dl} \cdot x \cdot (L - x)] \quad \text{(Self-weight moment where crack is located)}$$

$$M_{dec} := \frac{1}{2} \cdot (P_{dec} \cdot x) \quad \text{(Moment due to applied decompression load)}$$

$$M_t := M_{dl} + M_{dec} \quad \text{(Total moment where the crack is located)}$$

*EFFECTIVE PRESTRESS AND LOSS DETERMINATION...*

Stress level in prestressed concrete due to effective prestress force, self weight moment and applied moments.

$$f = \frac{-P_e}{A} \cdot \left( 1 + \frac{ey_t}{r^2} \right) + \frac{M_t \cdot y_t}{I}$$

Taking above equation and setting  $f = 0$  (decompression) and solving for  $P_e$ ...

$$P_e := [(M_t \cdot y_t \div I) \cdot A] \div \left[ 1 + \left[ \frac{(e \cdot y_t)}{r^2} \right] \right] \quad \mathbf{P_e = 70.051 \text{ kip}} \quad \text{(Measured effective prestress force)}$$

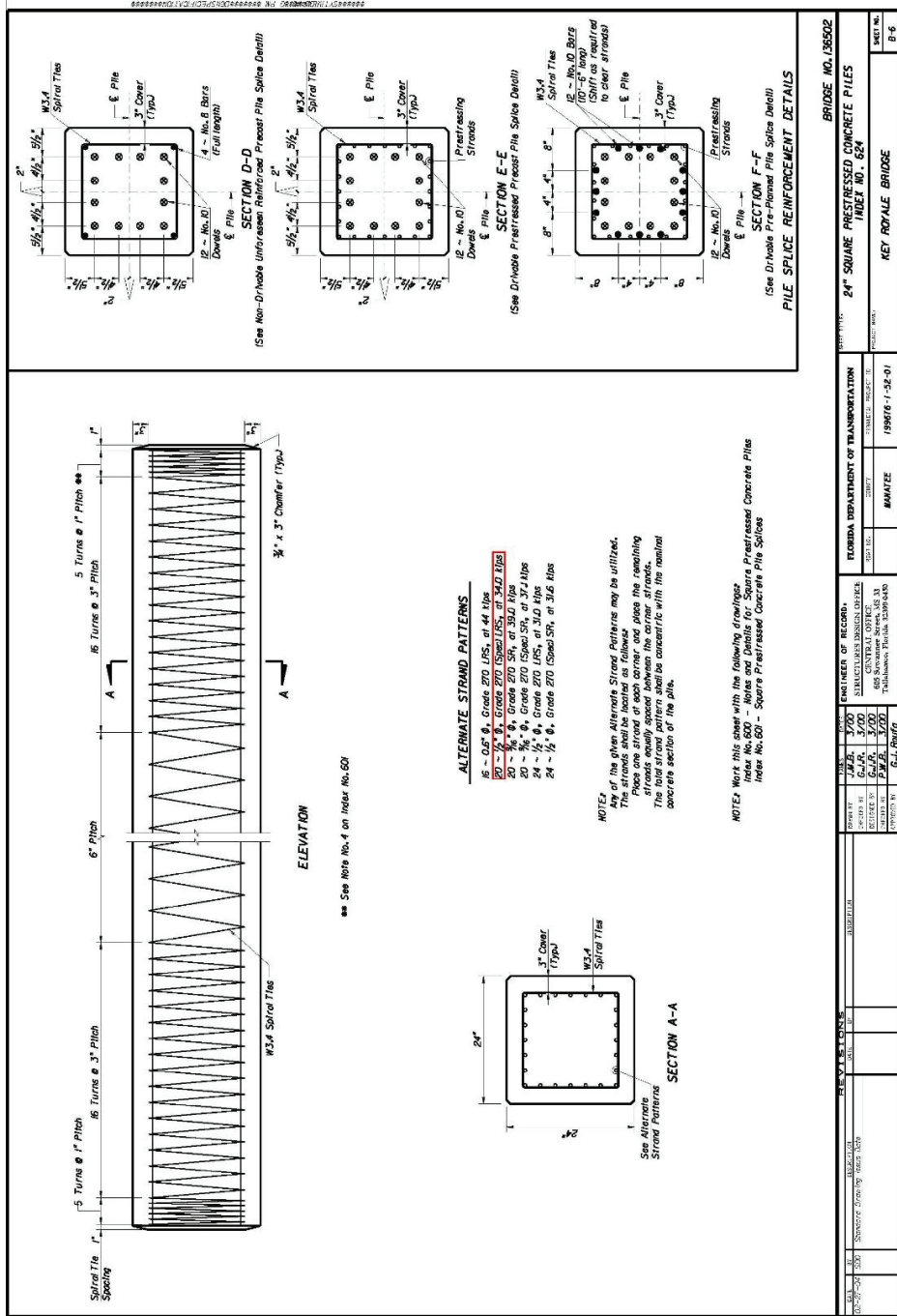
*BACK CALCULATION OF CRACKING MOMENT...*

$f_t := 840\text{psi}$  (from MoR test completed 12.12.2008)

$$M_{cr} := \frac{S \cdot P_e}{A} + P_e \cdot e + f_t \cdot S \quad \mathbf{M_{cr} = 121.01 \text{ kip} \cdot \text{ft}}$$

Cracking moment due to self weight and applied loads ( $P_e$  determined from decompression test)

# APPENDIX B – PILE DATA



BRIDGE NO. 13502		INDEX NO. 624		KEY ROYALE BRIDGE	
ENGINEER OF RECORD J.A.B. 3/70		ENGINEER OF RECORD G.A. 3/70		ENGINEER OF RECORD P.P. 3/70	
DESIGNED BY G.A. 3/70		DESIGNED BY P.P. 3/70		DESIGNED BY G.L. 6/11	
CHECKED BY G.L. 6/11		CHECKED BY G.L. 6/11		CHECKED BY G.L. 6/11	
APPROVED BY G.L. 6/11		APPROVED BY G.L. 6/11		APPROVED BY G.L. 6/11	
FLORIDA DEPARTMENT OF TRANSPORTATION CENTRAL OFFICE 800 BOYD AVENUE, SUITE 200 TALLAHASSEE, FLORIDA 32304-3000		STATE OF FLORIDA TRANSPORTATION DEPARTMENT TALLAHASSEE, FLORIDA 32304-3000		DATE 1987/6-1-56-01	
SHEET NO. 15-6		SHEET NO. 15-6		SHEET NO. 15-6	

DATE	10/4/2006		0
BED #	18N		2 @ 70' 4 @ 85'
JACK #			0
STRAND SIZE	1/2 SPECIAL TW 270 LR ASTM A416		0
COIL/PACK/REEL #	130146677942	130146677932	
	130246678379	130146678377	130146677930
	130246678996	130146678034	130246678434
	0	130246678462	130246678426
BED LENGTH (L)	6317.25	0	
STRAND SIZE (A)	0.167	0	
FINAL TEN. (P)	34000	0	
PRE TEN. (Pi)	5000	0	
M.O.E. (E)	29.00	0	

CORRECTION INFO.	
Number of cable #	20
Ambient temperature(al)	70
Abutment rotation (ar)	N/A
Live end seating (les)	0.28125
Dead end slippage (des)	0.1094
anchorage movement	0.5

ELONGATION  
 delta a.t (Plxdb/Pb)= 0  
 defl.(Pi x L)/(A x E) = 6.522  
 delta b.(PxL)/(Ax E) = 37.8278  
 delta bed shortning  
 (bs/2)+(bs/#strand)= 0.275

FORCE ADJUSTMENTS  
 Pb (P - Pi) = 29000  
 Pi( 0  
 Par (arxAxE)/(L)= 0  
 Ples(lesxAxE)/(L)= 215.615  
 Pdes no adj. required 0  
 Pbs (bsxAxE)/(L)= 210.8235  
 TOTAL FORCE ADJ. 426.4385  
 ADJUSTED FORCE = 29426.4385  
 JACKING FORCE = 34426

GROSS ELONG. 38.493  
 NET ELONG. 38 3/16

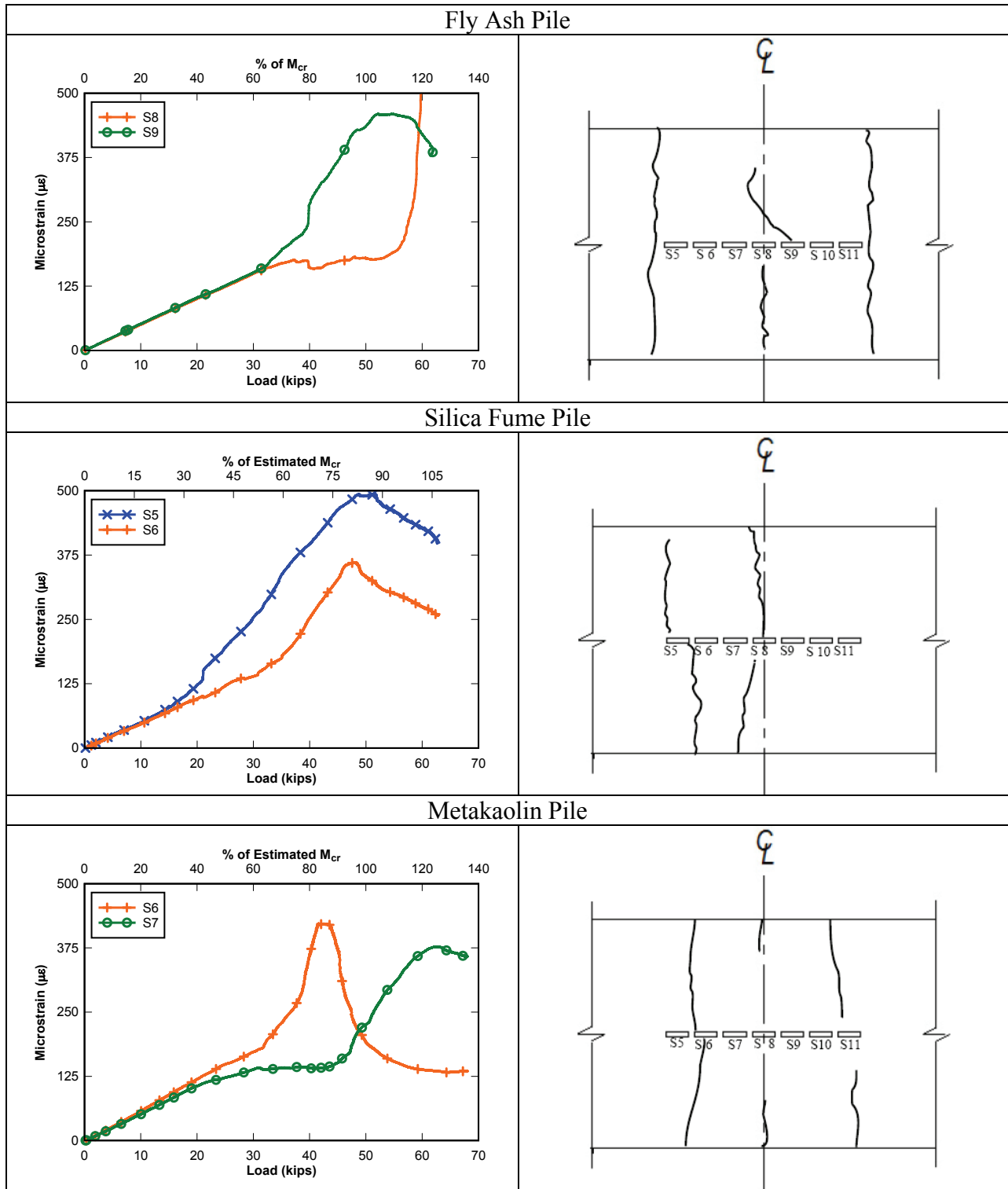
TOTAL ADJ. FORCE 34426

RANGE +2.5% 39 3/16  
 RANGE -2.5% 37 1/4

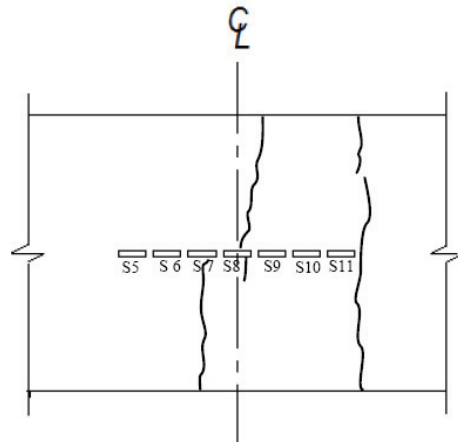
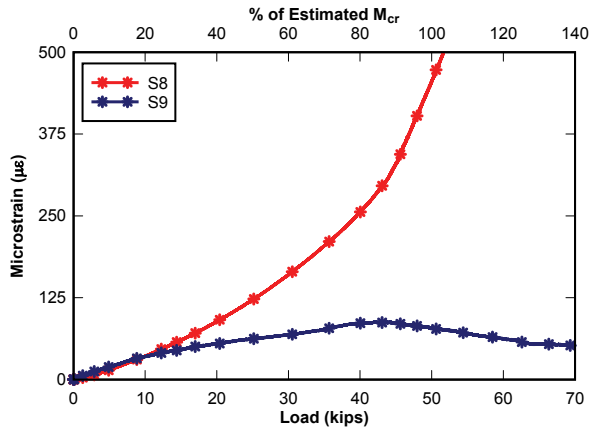
AASHTO MAX \* 36072  
 RANGE +2.5% = 35287  
 RANGE -2.5% = 33585

**18N**

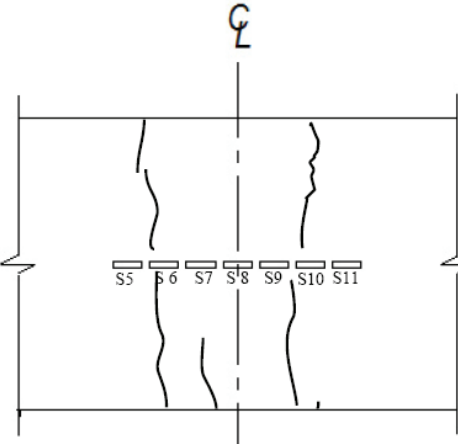
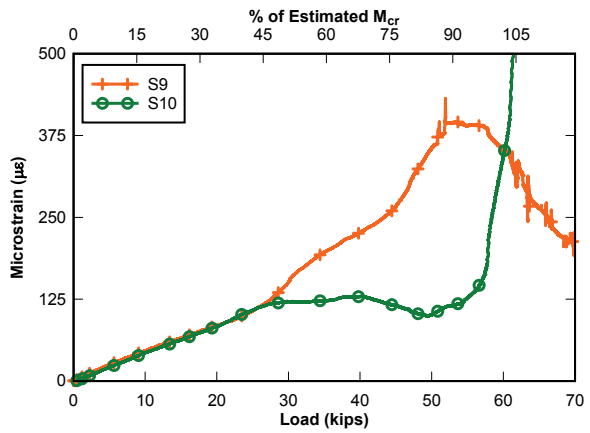
Load-strain plots and crack patterns for monotonically loaded piles.

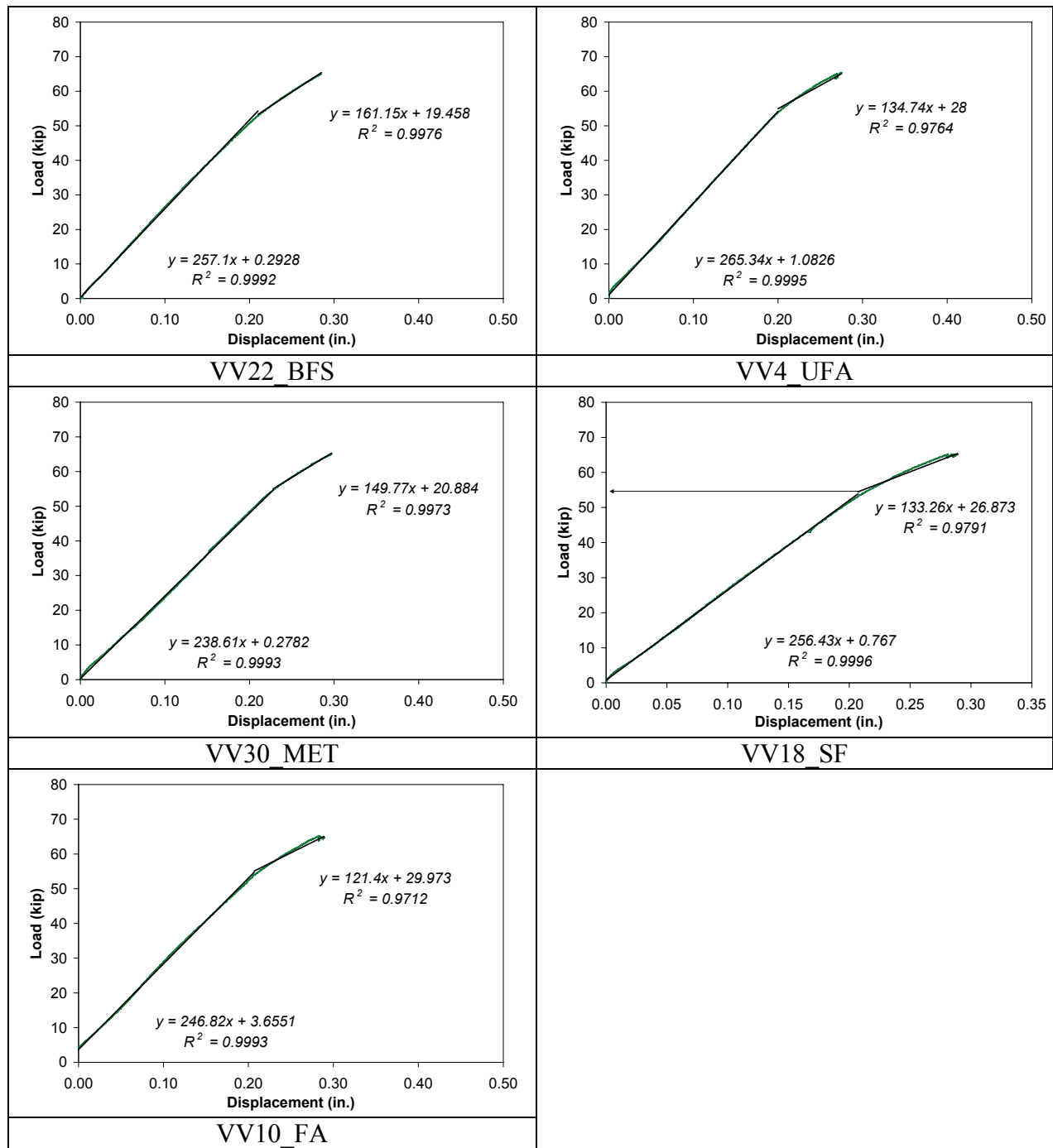


### Ultra-fine Fly Ash Pile



### Blast Furnace Slag Pile





## APPENDIX C – GIRDER DATA









INSTEEL WIRE PRODUCTS

MATERIAL CERTIFICATION

1 WIREMIL ROAD - SANDERSON, FL 32087

DURA STRESS INC
11325 COUNTRY ROAD 44
LISBON FL 34788

Bill of Lading: 0047823
Date: 05-AUG-08

Insteel Wire Products hereby certifies that the specimens taken from strand package(s) consisting of one or more of the following Lot/serial numbers were tested in accordance with and met the requirements of the applicable ASTM specification listed below. The attached test report(s) represent the result of such test(s).

1/2 7W 270 LR ASTM A416

Test Report Number 10052452

Lo/Serial Numbers

Heat Number/ Lot Number

- 130146891013
130146891014
130146891017
130146891022
130146891137
130146891138
130246891101

32305

Insteel Wire Products hereby certifies that the prestressing strand described above meets or exceeds the minimum bonding requirements as currently accepted in the NASP (North American Strand Producers) pull-out test and the Mustafafa block pull-out test.

Insteel Wire Products Company certifies that the use of this product conforms with Buy America Requirements set forth in 23 CFR Subpart D, Section 635.410, Buy America Requirements and Title 49 Transportation, Chapter VI - Federal Transit Administration, Department of Transportation Part 661 - Buy America Requirements - Surface Transportation Assistance Act of 1982, As Amended.

Order Number: 337257

Customer Purchase Order Number: 91462

Certification prepared by: [Signature]

NOTARY PUBLIC-STATE OF FLORIDA
RICHARD M. GRIFFIS
Commission #DD632879
Expires: MAR. 12, 2011
BONDING THROUGH ATLANTIC BONDING CO., INC.

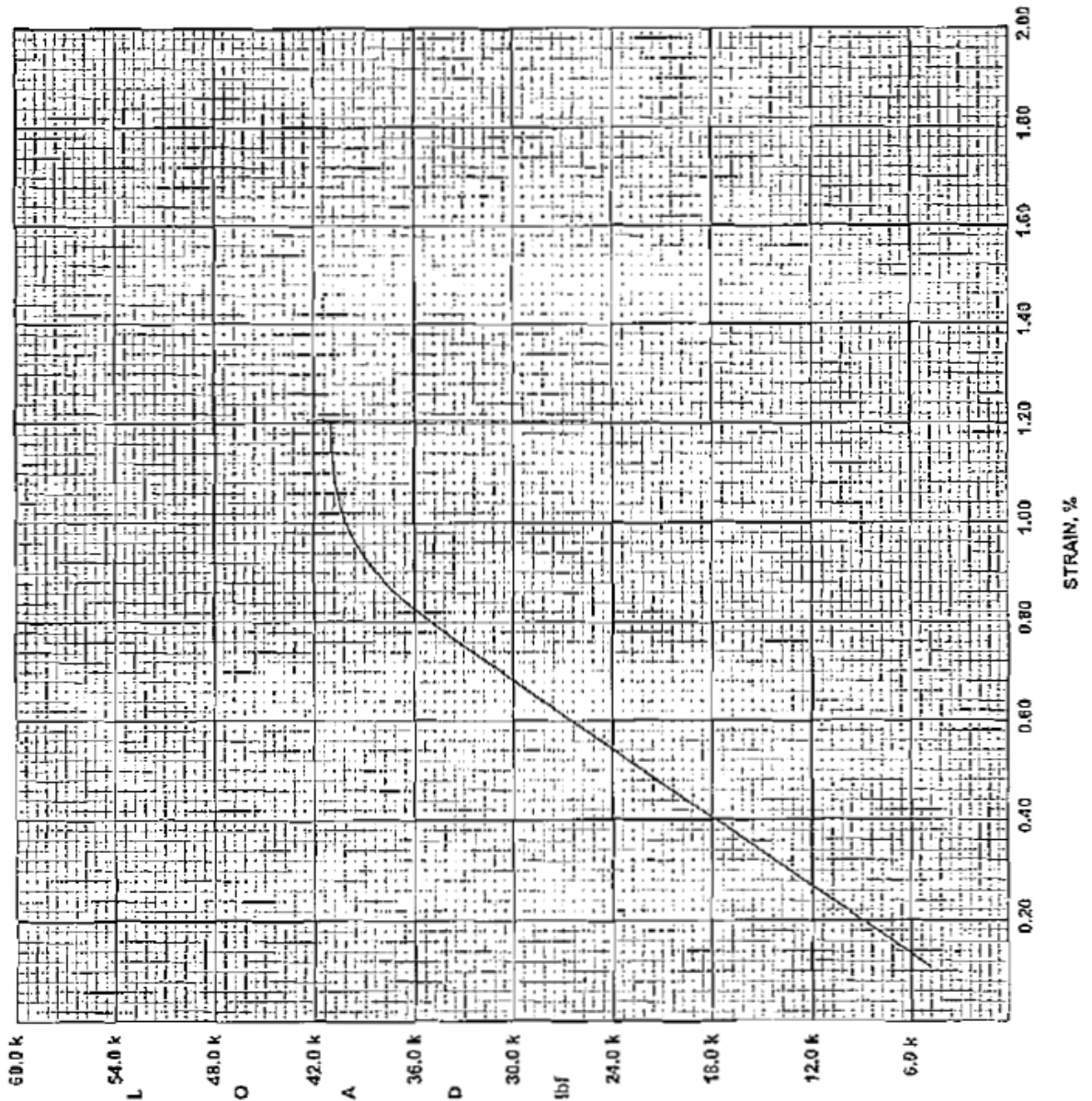
[Signature: Richard M. Griffis]

ENTERED

**Insteel Wire Products  
Prestressed Concrete Strand**

**1/2" 270 7W LOW RELAXATION**

Test Number:	10052452
Tested By:	CER
Ultimate Breaking Strength, lbf:	42427
Ultimate Breaking Strength, kN:	189
Load @ 1% Extension, lbf:	40071
Load @ 1% Extension, kN:	178
Ultimate Elongation, %:	4.95
Representative Area, in <sup>2</sup> :	0.153
Representative Area, mm <sup>2</sup> :	98.7
Actual Area, in <sup>2</sup> :	0.1520
Actual Area, mm <sup>2</sup> :	98.0934
Avg Modulus of Elasticity, Mpsi:	29.0
Avg Modulus of Elasticity, MPa:	199947.6
Reference:	





INSTEEL WIRE PRODUCTS

MATERIAL CERTIFICATION  
Sanderson Plant - Sanderson, FL 32087

DURA STRESS INC  
11325 COUNTRY ROAD 44  
LISSON FL 34788

Bill of Lading: QB48756  
Date: 26-SEP-08

Insteel Wire Products hereby certifies that the specimens taken from strand package(s) consisting of one or more of the following Lot/serial numbers were tested in accordance with and met the requirements of the applicable ASTM specification listed below. The attached test report(s) represent the result of such test(s).

.600 7W 270 LR ASTM A416

Test Report Number 10053352

Lot/Serial Numbers

Heat Number/ Lot Number

130146892418  
130146892419  
130146892420  
130146892422  
130146892423  
130146892426  
130146892427  
130146892428

33271

Insteel Wire Products hereby certifies that the prestressing strand described above meets or exceeds the minimum bonding requirements as currently accepted in the NASP (North American Strand Producers) pull-out test and the Moustafis block pull-out test.

Insteel Wire Products Company certifies that the use of this product conforms with Buy America Requirements set forth in 23 CFR Subpart D, Section 635.410, Buy America Requirements and Title 49 Transportation, Chapter VI - Federal Transit Administration, Department of Transportation Part 661 - Buy America Requirements - Surface Transportation Assistance Act of 1992, As Amended.

Order Number: 338713

Customer Purchase Order Number: 92314

NOTARY PUBLIC STATE OF FLORIDA  
BURNARD H. GARDNER  
Commission Expires: MAR 12, 2011  
FORMERLY TRISTAR HOLDINGS CO., INC.

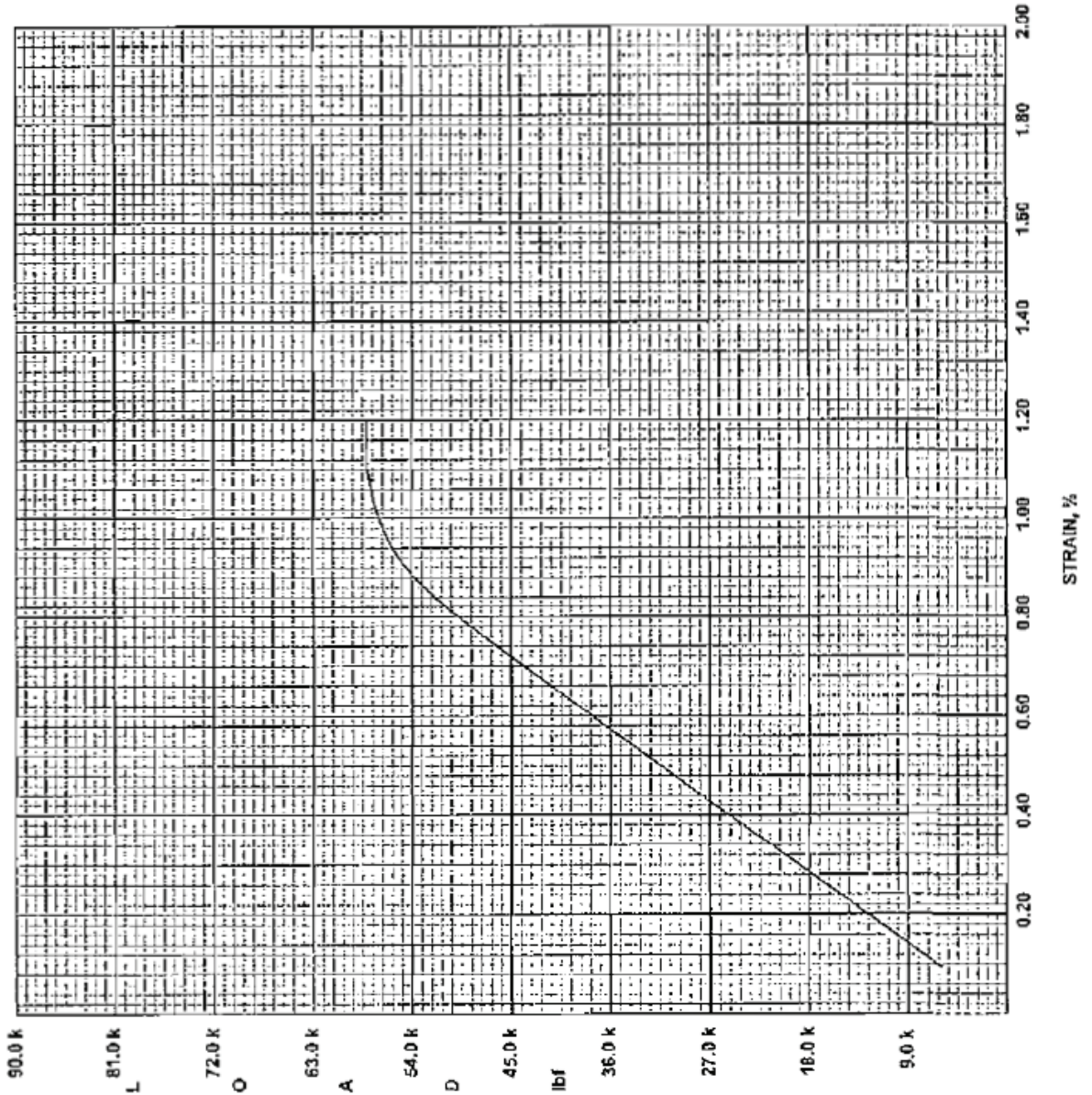
Certification prepared by:

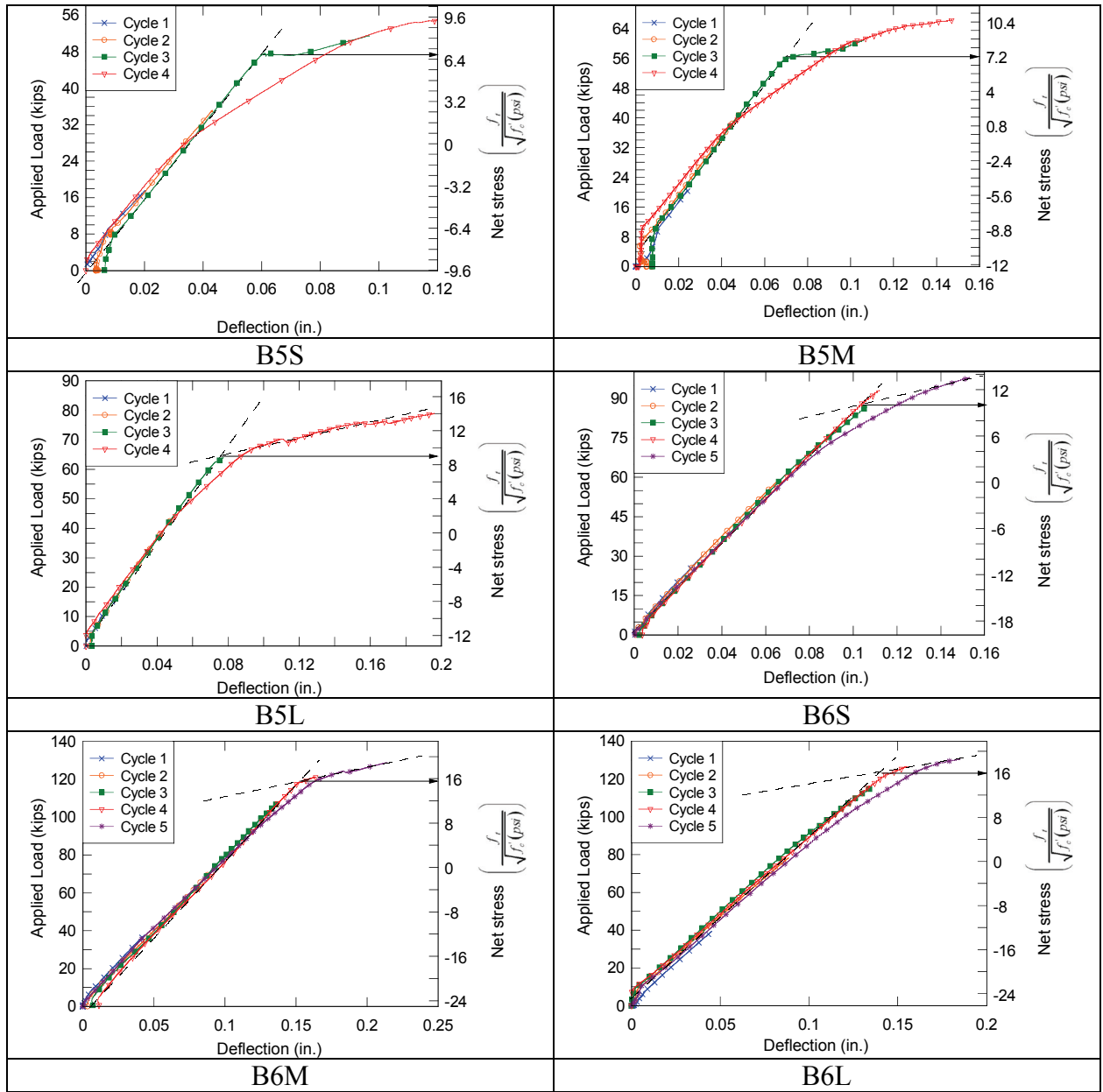
AXED

Insteel Wire Products  
 Prestressed Concrete Strand

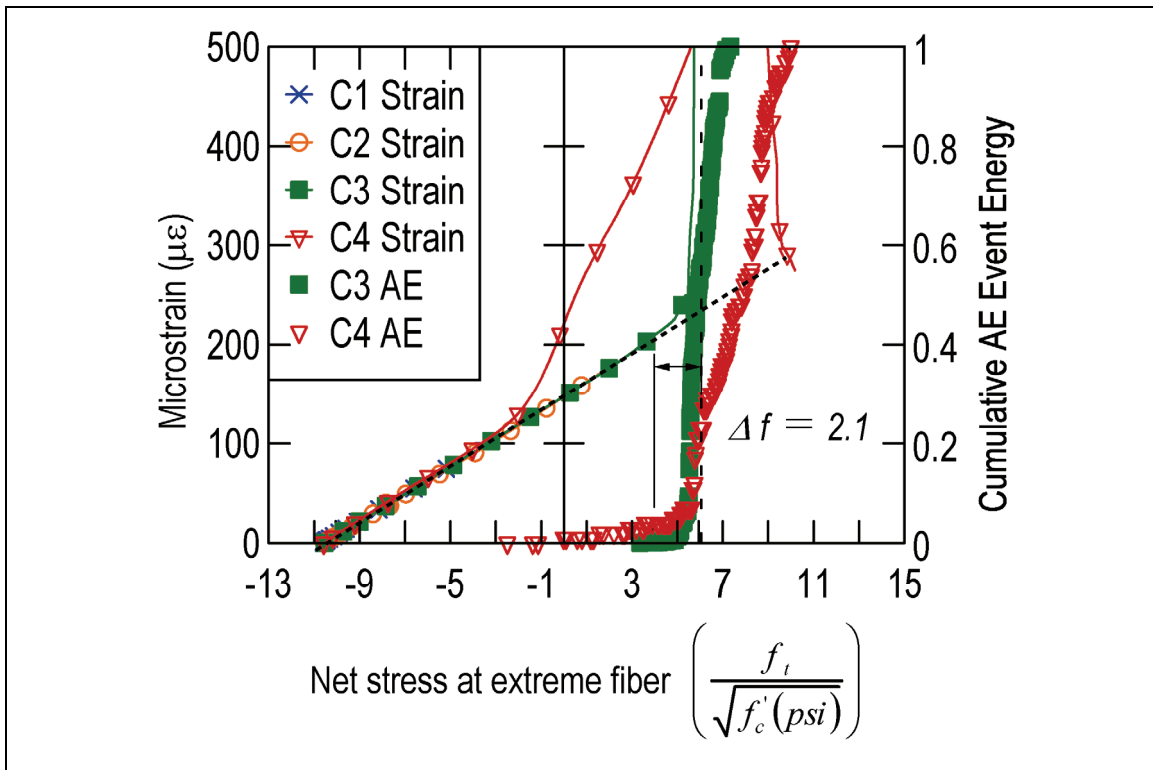
.600" 270 7W LOW RELAXATION

Test Number: 10053352  
 Tested By: CER  
 Ultimate Breaking Strength, lbf: 60480  
 Ultimate Breaking Strength, kN: 269  
 Load @ 1% Extension, lbf: 56965  
 Load @ 1% Extension, kN: 253  
 Ultimate Elongation, %: 4.95  
 Representative Area, in<sup>2</sup>: 0.217  
 Representative Area, mm<sup>2</sup>: 140  
 Actual Area, in<sup>2</sup>: 0.2189  
 Actual Area, mm<sup>2</sup>: 141.2139  
 Avg Modulus of Elasticity, Mpsi: 29.0  
 Avg Modulus of Elasticity, MPa: 199947.6  
 Reference:

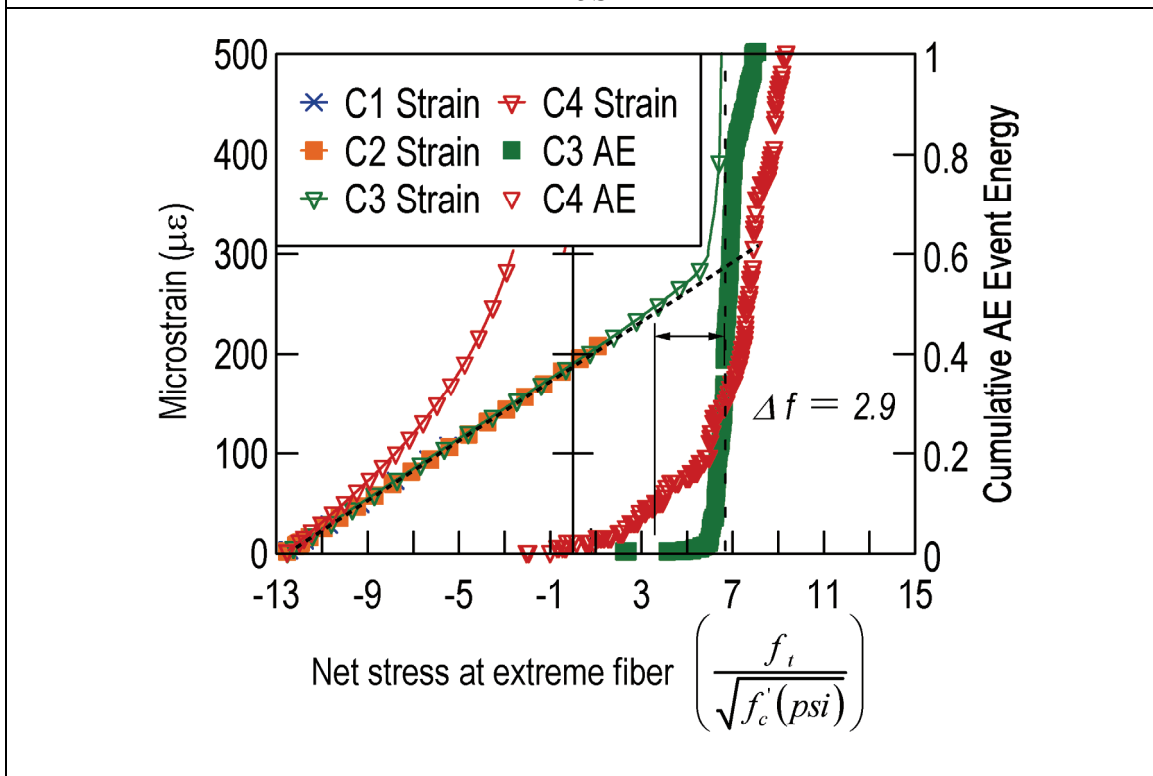




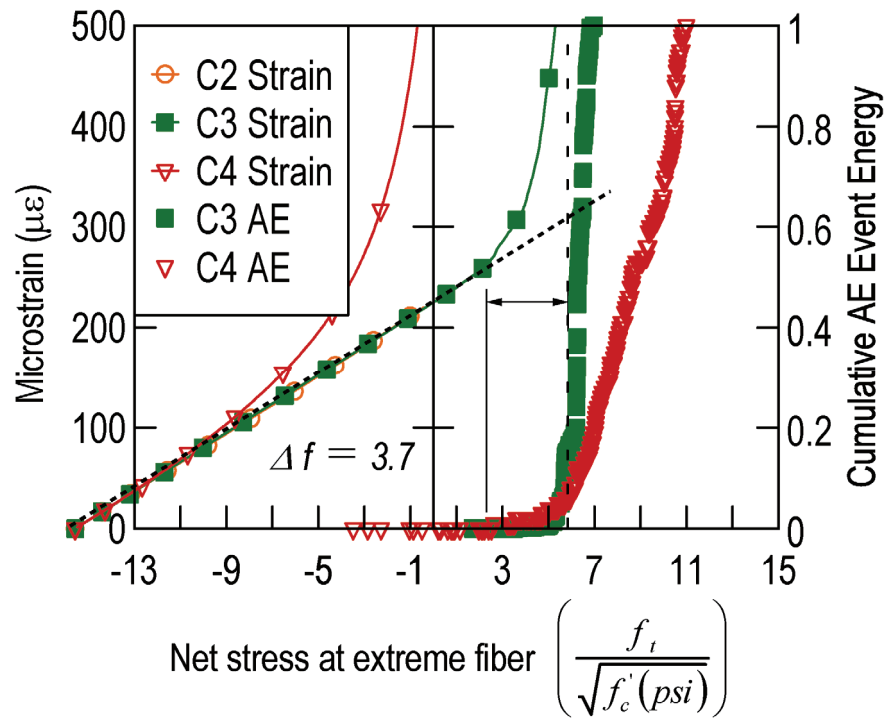
**APPENDIX D – ACCUMULATED DAMAGE ANALYSIS**



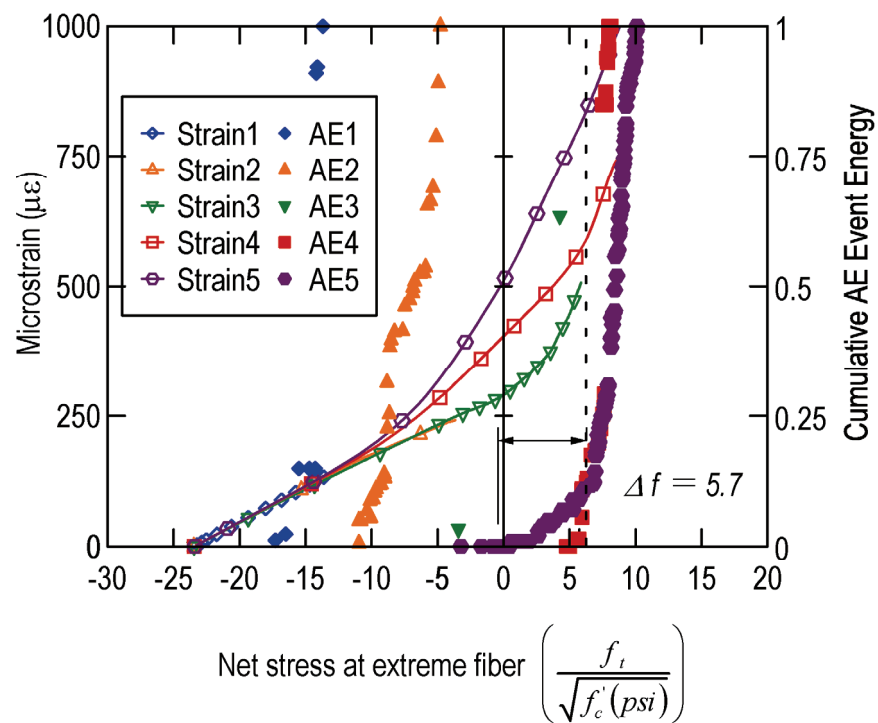
B5S



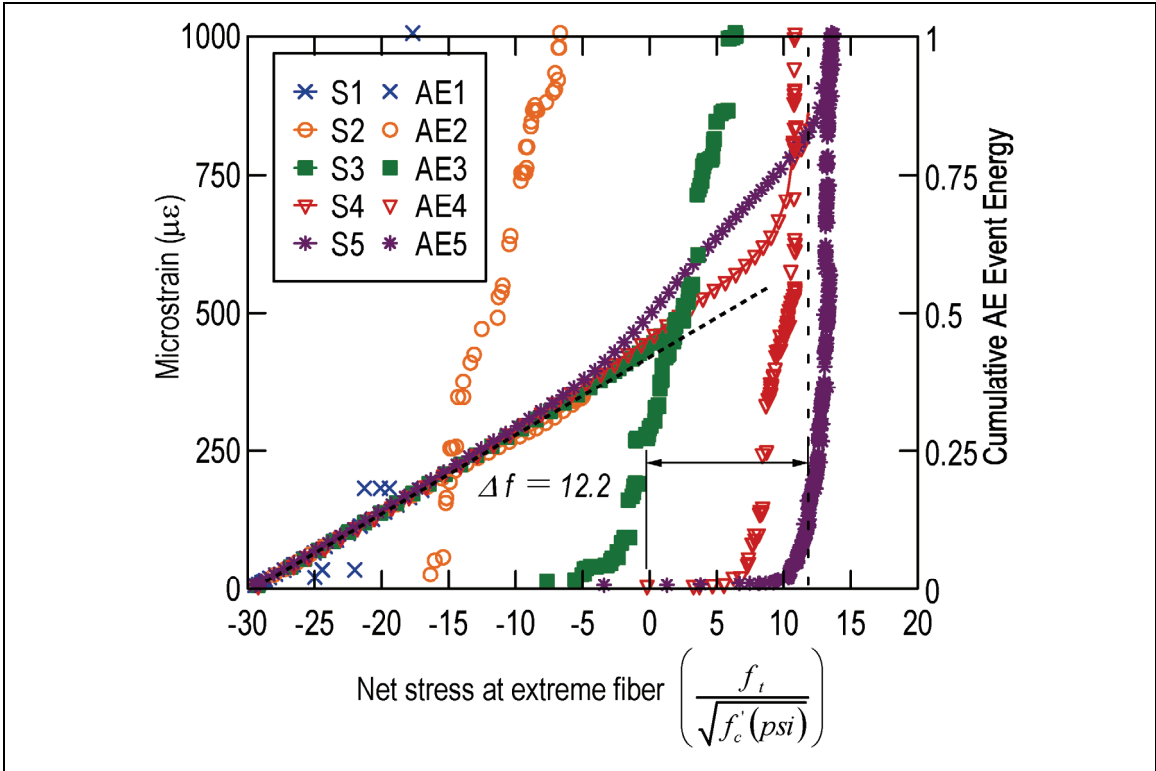
B5M



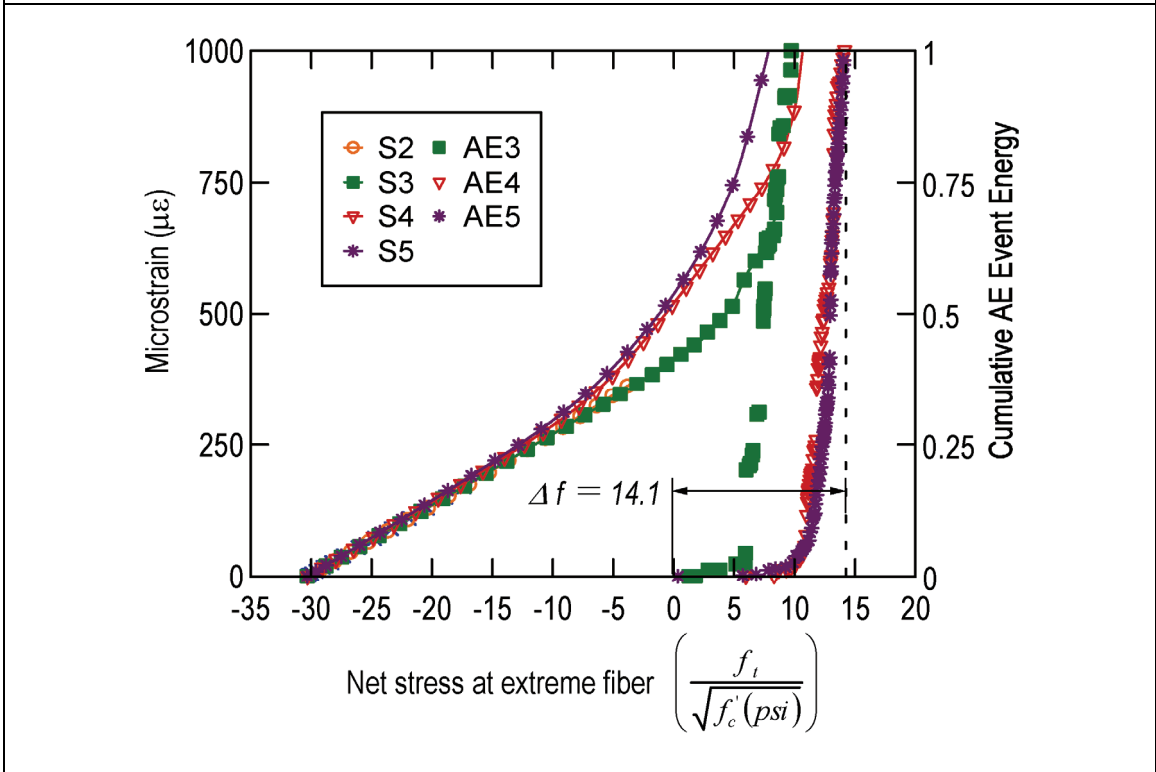
B5L



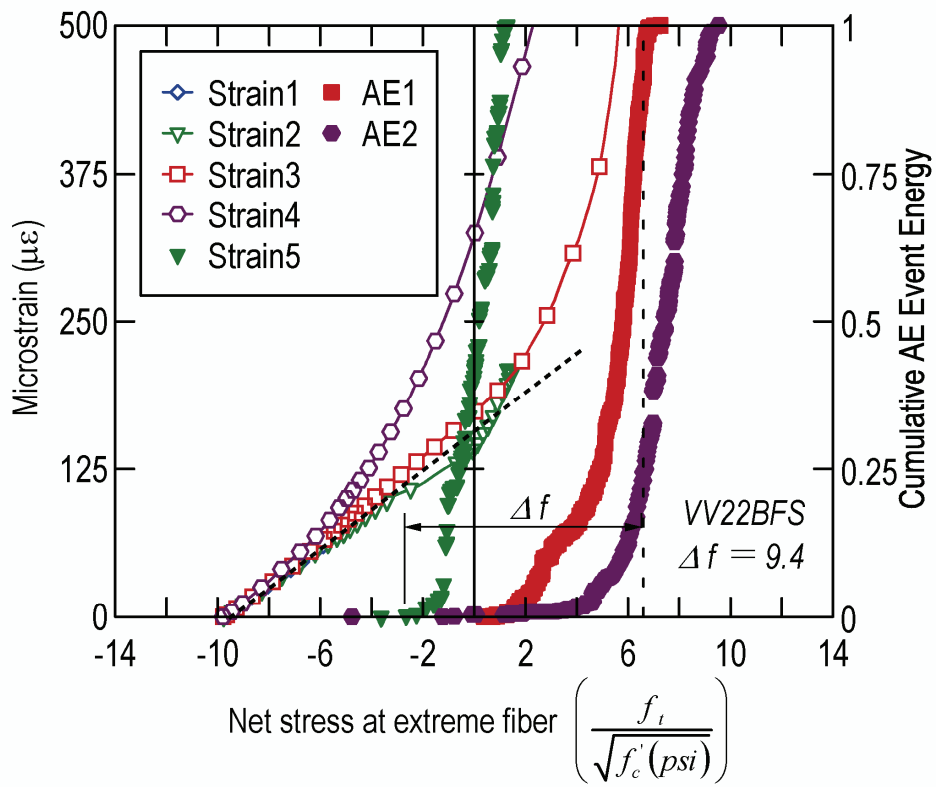
B6S



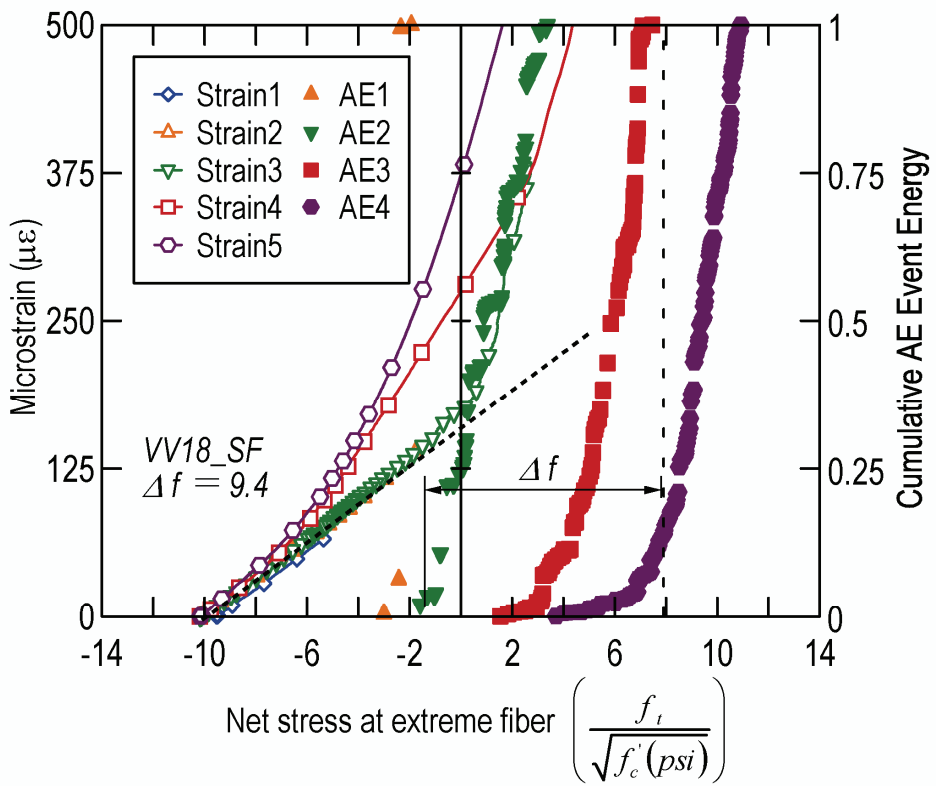
B6M



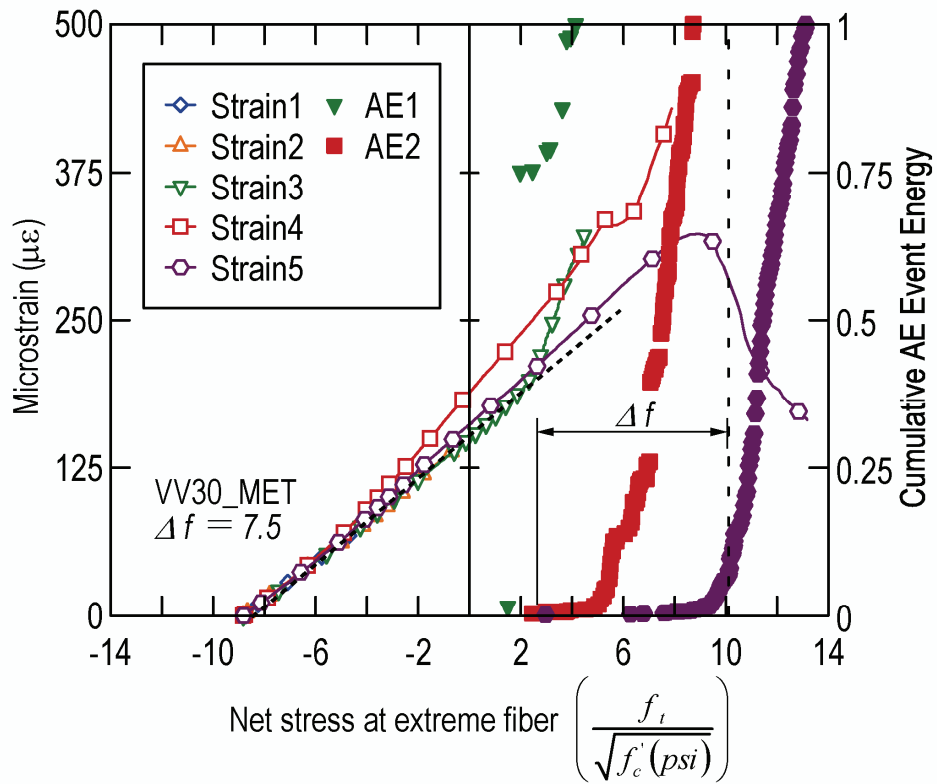
B6L



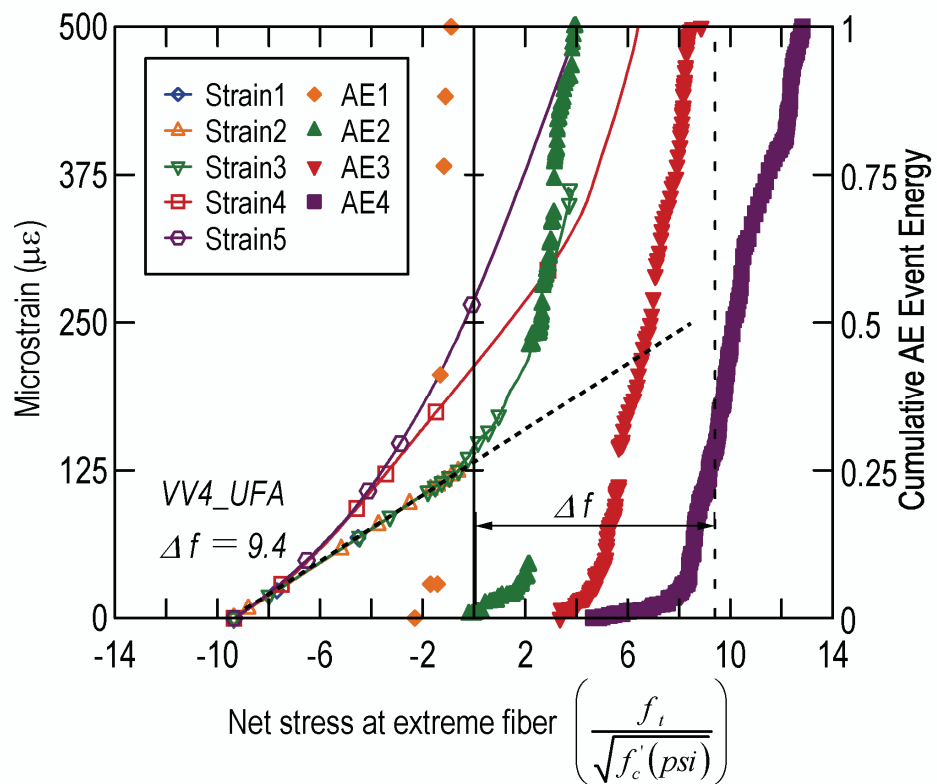
VV22 BFS



VV18 SF



VV30\_MET



VV4\_UFA

